# NATIONAL ADVISORY COMMITTEE FOR AERONAUTICS

**TECHNICAL NOTE 3785**

## HANDBOOK OF STRUCTURAL STABILITY

## PART V - COMPRESSIVE STRENGTH OF FLAT STIFFENED PANELS

By George Gerard

New York University


Washington
August 1957

TABLE OF CONTENTS

NATIONAL ADVISORY COMMITTEE FOR AERONAUTICS

TECHNICAL NOTE 3785

# HANDBOOK OF STRUCTURAL STABILITY

## PART V - COMPRESSIVE STRENGTH OF FLAT STIFFENED PANELS

By George Gerard

## SUMMARY

A generalized crippling analysis for short panels with formed or extruded stiffeners is presented. The analysis applies to monolithic panels. Criteria are given for riveted panels which indicate if the panels can be considered to behave in a monolithic manner. Riveted panels that are subject to interrivet buckling and wrinkling or forced crippling do not behave in this manner. Methods are presented for estimating the strength of such panels.

Intermediate-length and long stiffened panels are subject to other failure modes. Methods are given for estimating the column strength of panels. Various forms of column curves and direct-reading charts are considered. Theory and test data on optimum stiffened panels are presented for use in preliminary design studies.

In box types of construction, the rib and spar structures influence the compressive strength of the stiffened panel. The various factors which can be of importance are considered.

## INTRODUCTION

This part of the Handbook of Structural Stability is concerned with the compressive strength of flat stiffened panels both in the form of individual panels and as components of box structures under bending.

Considerations of the compressive strength of stiffened panels are governed to a large extent by the crippling or short-panel strength. This quantity is commonly determined experimentally on panels with an effective slenderness ratio in the neighborhood of 20. In this region, variations in length have a negligible effect upon the crippling strength.

In Part IV of this Handbook (ref. 1), a generalized crippling analysis was presented for individual formed and extruded elements. This

method of analysis is extended to panels with formed stiffeners in the section "Crippling Strength of Panels With Formed Stiffeners" and to panels with extruded stiffeners in the section "Crippling Strength of Panels With Extruded Stiffeners" herein. At the end of the last-named section, the pertinent results of the generalized crippling analysis are summarized.

The crippling analysis presented is valid for stiffened panels of monolithic construction such as machined, forged, and extruded panels and also for riveted panels if certain riveting requirements are satisfied. The strength of short riveted panels is discussed in the section by that name in terms of interrivet buckling and wrinkling or forced crippling.

By utilizing the methods of analysis presented in the above-mentioned sections, the short-panel strength may be estimated. For intermediate-length and long panels, consideration of additional failure modes is required as presented in the section "Column Strength of Stiffened Panels." Various types of column curves are discussed and direct-reading column charts for determining minimum-weight panel designs are reviewed.

For use in preliminary design studies, it is convenient to represent the envelope of all minimum-weight stiffened-panel designs in the form of optimum-panel curves. In the section "Optimum Stiffened Panels" optimum-panel theory and test data are reviewed and the results are summarized in terms of panel efficiency coefficients for hat, Y, and Z stiffener shapes. Finally, methods of generalizing the results on optimum panels of one material to panels of other materials are presented.

The use of stiffened panels in box construction, which is representative of wing and tail structures, requires the use of ribs or formers to subdivide the compression cover into panels of reasonable length. In the section "Stiffened-Panel Box Construction" strength and stiffness criteria for the supporting rib structures are presented. In addition to the ribs, the spar structure may contribute to the strength of the stiffened panel. A brief consideration of the pertinent factors is presented.

This survey was conducted under the sponsorship and with the financial assistance of the National Advisory Committee for Aeronautics.

## SYMBOLS

| | |
|---|---|
| A | area; for stiffened panel, area of stiffener plus area of sheet corresponding to stiffener spacing, sq in. |
| B | flexural rigidity per unit width, in-lb |

| | |
|---|---|
| $b$ | spacing, in. |
| $b_e$ | effective width, in. |
| $b_{ei}$ | effective width of skin corresponding to $\sigma_i$ from equation (10) |
| $C$ | shear rigidity per unit width, in-lb |
| $c$ | number of corners |
| $d$ | rivet diameter, in. |
| $d_e$ | effective rivet diameter, in. |
| $E$ | modulus of elasticity, psi |
| $\bar{E}$ | effective modulus, psi |
| $E_s$ | secant modulus, psi |
| $E_t$ | tangent modulus, psi |
| $e$ | end-fixity coefficient |
| $f$ | effective rivet offset, in. |
| $g$ | number of cuts plus flanges |
| $K$ | deflectional spring constant, lb/in. |
| $k$ | buckling coefficient |
| $k_w$ | coefficient in wrinkling mode |
| $L$ | column length or rib spacing, in. |
| $L'$ | effective column length, $L' = L/e^{1/2}$, in. |
| $m$ | slope |
| $N$ | loading per unit width, lb/in. |
| $p$ | rivet pitch, in. |
| $q$ | lateral pressure, psi |
| $R$ | radius, in. |

| | |
|---|---|
| $s$, $s_r$ | rivet strength, ksi |
| $t$ | thickness, in. |
| $\bar{t}$ | effective thickness, in. |
| $w$ | panel width or spar spacing, in. |
| $\alpha$ | crippling coefficient |
| $\alpha_p$ | panel efficiency coefficient |
| $\beta_c$ | crippling coefficient based on corners |
| $\beta_g$ | crippling coefficient based on cuts plus flanges |
| $\eta$ | plasticity-reduction factor for plates |
| $\bar{\eta}$ | cladding reduction factor |
| $\theta$ | rotational spring constant, torque per unit rotation |
| $\nu$ | Poisson's ratio |
| $\rho$ | radius of gyration, in. |
| $\sigma_{cr}$ | buckling stress, ksi |
| $\sigma_{cy}$ | compressive yield strength, ksi |
| $\sigma_e$ | Euler column stress, ksi |
| $\sigma_i$ | interrivet buckling stress, ksi |
| $\sigma_{pl}$ | proportional-limit strength, ksi |
| $\sigma_{20}$ | panel strength at $L'/\rho = 20$, ksi |
| $\bar{\sigma}$ | effective strength, psi |
| $\bar{\sigma}_{co}$ | effective panel strength, ksi |
| $\bar{\sigma}_{cy}$ | compressive yield strength in corner of formed section, ksi |
| $\bar{\sigma}_f$ | crippling strength, ksi |
| $\bar{\sigma}_{fr}$ | strength of a short riveted panel, ksi |

| | |
|---|---|
| $\bar{\sigma}_p$ | panel strength under lateral pressure, ksi |
| $\bar{\sigma}_w$ | strength of riveted panel in wrinkling mode, ksi |
| $\tau$ | plasticity-reduction factor |
| $\bar{\tau}$ | plasticity-reduction factor for optimum stiffened panels |

Subscripts:

| | |
|---|---|
| o | optimum |
| r | rivet or rib |
| s | skin or sheet |
| st | stiffener |
| w | stiffener web |
| av | average |

## CRIPPLING STRENGTH OF PANELS WITH FORMED STIFFENERS

Considerations of the compressive strength of stiffened panels can be conveniently divided into approximately three regions: Long panels which behave essentially as columns, short panels which are subject to crippling, and panels of intermediate length. The latter generally fail as a result of combined crippling and column behavior with torsional effects often evident.

In the present section, the crippling strength of stiffened panels with formed stiffeners is treated. The skin and stiffeners are assumed to be fastened together in such a manner that the panel can be considered to be monolithic from the standpoint of crippling strength. Riveting requirements to obtain monolithic behavior are considered in some detail in the section entitled "Strength of Short Riveted Panels."

The method of crippling analysis used for formed stiffened panels is an extension of the generalized crippling analysis presented in Part IV of this Handbook (ref. 1). Panels utilizing extruded stringers of complex cross section, such as Y-shapes, are considered in the section "Crippling Strength of Panels With Extruded Stringers."

## Generalized Crippling-Analysis Review

In reference 1, the crippling strength of a variety of formed sections with three or more corners was analyzed. It was shown that excellent correlation was obtained with the following formula:

$$\frac{\bar{\sigma}_f}{\sigma_{cy}} = \beta_c \left[ \frac{ct^2}{A} \left( \frac{\eta E}{\sigma_{cy}} \right)^{1/2} \right]^{0.85} \tag{1}$$

The coefficient $\beta_c$ depended somewhat upon the increased yield properties in the corners of the formed section. For materials such as 2024-T4 aluminum alloy formed to radius-thickness ratio $R/t = 3$, $\beta_c = 1.3$, for example.

In analyzing the crippling strength of stiffened panels which consist of formed Z- or hat sections attached to a flat sheet, certain additional considerations arise beyond those encountered in the analysis of the stiffener section alone. To avoid consideration of the method of attachment of sheet to stiffeners, it is assumed that the panel is monolithic. Rivet strength requirements to achieve this condition are presented in the section "Strength of Short Riveted Panels." The line of attachment of the stiffener to the sheet introduces, in effect, another corner. Therefore, in determining $c$ in equation (1) for the stiffened panel, some allowance is necessary for the attachment.

Secondly, the thickness of the formed stiffener $t_w$ may be different from that of the sheet $t_s$. Thus, in evaluating the parameter $t^2/A$ in equation (1) it is necessary to account for this difference in thickness.

## Z-Stiffened Panels

Test data on the crippling strength of flat stiffened panels with Z-section stiffeners were obtained from three different sets of data (refs. 2 to 4) listed in table 1. In the first set, there was a systematic variation in the parameter $t_w/t_s$. In the second set, nine different materials were used covering a wide range of $E$ and $\sigma_{cy}$ values. The third group covers potential-strength estimates of the highest obtainable crippling strength of a large group of riveted panels. The potential strength of a riveted panel corresponds essentially to the strength of a monolithic panel. In all tests, the slenderness ratio of the panel $L'/\rho = 20$, approximately. Furthermore, the Z-section stiffener had substantially the same physical properties as those of the sheet, except for the increased yield properties in the corners of the formed Z.

The data presented in figure 1 are based on the nominal values of the geometric parameters and on the compressive yield strength of the 2024S-T3 material, which was 43 ksi ± 7 percent. Although there was a wide variation in the $b_w/t_w$ and $b_s/t_s$ parameters, no systematic variation in the correlation was obtained by accounting for these parameters independently. Thus the data are presented in figure 1 without regard to these parameters.

In equation (1), one of the basic parameters used for formed sections is $ct^2/A$. In evaluating this parameter for a stiffened panel it is necessary to specify the manner in which the cross-sectional area A and the number of corners c are determined. Also, it is necessary to account for the $t_w/t_s$ variations.

The cross-sectional area of a stiffened panel is taken as the area of the stiffener plus the area of sheet corresponding to the stiffener spacing. For a Z-stiffened panel, the number of corners for the typical area element consisting of the Z stiffener plus sheet is three: Two for the Z and one for the rivet line. This method of determining c is arbitrary. Its justification lies in the fact that the $\beta_c$ values of equation (1) obtained in this manner are in close agreement with those obtained for multicorner formed sections.

To account for the $t_w/t_s$ variation in the most simple and direct manner, the parameter $ct^2/A$ for the formed element is replaced by $ct_wt_s/A$ for the stiffened panel. Again, this procedure is somewhat arbitrary. It is relatively simple to introduce some weighting factors which may result in a more realistic evaluation of the $ct^2/A$ parameter for stiffened panels. However, such factors lead to additional complexity and do not improve the correlation sufficiently to warrant their use.

By use of the procedures outlined above, the data shown in figure 1 for 2024-T3 aluminum-alloy panels were found to correlated within ±10-percent limits with equation (1). The value of $\beta_c = 1.26$ for Z-stiffened panels is in good agreement with the value of 1.30 established in reference 1 from test data on multicorner elements of 2024-T3 aluminum alloy formed to $R/t = 3$ at the corners. The slight difference in the two coefficients may be attributed to the fact that, in counting the number of corners, no increase in yield strength occurs at the rivet line as does occur at all of the formed corners of the multicorner elements.

The data of figure 1 represent the first set of table 1 and cover one material, 2024-T3 aluminum alloy, with a wide variation in the $t_w/t_s$ parameter. The second set of data covers nine different materials with a wide variation in E and $\sigma_{cy}$ for $t_w/t_s = 1$. This second set of data is presented in figure 2.

In figure 2(a), the data are presented in terms of $\left(A/t^2\right)\left(\sigma_{cy}/E\right)^{1/2}$ and include test values up to $\bar{\sigma}_f/\sigma_{cy} = 1$. On the right side, the heavy line corresponds to equation (1) with $c = 3$ and $\beta_c = 1.26$. It can be observed that a considerable portion of the data falls below the line corresponding to equation (1).

Careful scrutiny of these data suggested that for some panels wrinkling probably occurred (see section entitled "Strength of Short Riveted Panels") and therefore these panels could not be considered as monolithic from the standpoint of crippling strength. It was decided to use the test data for those panels identified as 25-50-20 and 37.5-75-20 only since, according to the criteria of the section "Strength of Short Riveted Panels," these panels appeared to be unaffected by wrinkling. The data for this group of panels for the nine materials listed in table 1 are shown in figure 2(b). It can be observed that, for these panels, the crippling strength can be predicted adequately by equation (1), utilizing $c = 3$ and $\beta_c = 1.26$.

The final set of data listed in table 1 consists of potential-strength estimates of 2024-T3 and 7075-T6 aluminum-alloy Z-stiffened panels. The potential or maximum attainable strength was defined as the highest average stress at maximum load that can be obtained for a given panel by varying rivet diameter and pitch to find the optimum. The potential strength corresponds closely to the crippling strength of a monolithic panel of the same construction.

These data are shown in figure 3 in conjunction with equation (1) for $c = 3$ and $\beta_c = 1.26$. Again, it can be observed that the potential-strength data correlate well according to the methods proposed herein.

To summarize the available data on the monolithic crippling strength of formed Z-stiffened panels, the data from the three sources listed in table 1 are presented in figure 4 grouped according to the $t_w/t_s$ values. Satisfactory correlation is obtained with equation (1) in all cases, using $c = 3$ and $\beta_c = 1.26$. This correlation holds up to a value of $\bar{\sigma}_f/\sigma_{cy} = 1$.

## Hat-Stiffened Panels

The crippling-strength analysis of formed hat-stiffened panels is essentially the same as that used for the Z-stiffened panels. The test data of reference 5 cover a range of $b_h/b_w$ values ($b_h$ is width of top web; $b_w$ is height of side webs) between 0.6 and 1.2 and a range of $t_w/t_s$ values of 1.25, 1.00, 0.63, and 0.39. For a typical hat-stiffened-panel area element, the factor $c = 6$ in equation (1), consisting of 4 corners for the hat plus 2 rivet lines.

The test data for each value of $t_w/t_s$ are shown in figure 5 and are based on the nominal values of the geometric parameters and the compressive yield strength of 44 ksi. All data correlate well with equation (1) although there is a small systematic variation of the $\beta_c$ value with the parameter $t_w/t_s$, as shown in table 2, that may be due to the raised yield effect in the corners. The absence of a $\beta_c$ variation for the Z-section suggests, however, that possibly the closed form of the hat section has some influence.

For the particular riveting used for the hat-stiffened panels there is some evidence of wrinkling at $\bar{\sigma}_f/\sigma_{cy}$ values greater than 0.8 as shown in figure 5. Furthermore, an analysis of the panels with $t_w/t_s = 0.39$ in reference 6 indicates definite possibilities of wrinkling. This may account for the somewhat anomalous behavior of the data shown in figure 5(d) in which the $\beta_c$ value for the group with $b_s/t_s = 75$ is somewhat higher than for the groups of $b_s/t_s = 25$, 35, and 50. Because of the suspicion of wrinkling, it is recommended that a cutoff of $\bar{\sigma}_f/\sigma_{cy} = 0.8$ be placed on equation (1) for hat-stiffened panels and that caution be exercised in using this equation for panels with $t_w/t_s = 0.39$.

## CRIPPLING STRENGTH OF PANELS WITH EXTRUDED STIFFENERS

In attempting to extend the generalized crippling-strength analysis to panels with extruded stiffeners, in the manner demonstrated in the section "Crippling Strength of Panels With Formed Stiffeners," an essential difficulty is encountered. This difficulty centers around the selection of the number of corners for an extruded section in which several flanges or webs may meet at a common juncture.

Also, as shown in reference 1, the behavior of the junction of adjacent web or flange elements has a significant influence on the crippling strength. For example, the junction of the flange elements of an angle is subject to distortion after buckling. On the other hand, the flange elements of a cruciform section are horizontally opposed so that the junction of the flange elements remains essentially straight. For this reason, it was found that the crippling strength per flange of the cruciform which is essentially composed of two angles is greater than the crippling strength per flange of the angle alone.

In order to characterize this difference in behavior the following nomenclature has been adopted: "Angle-type" is used to refer to two adjacent elements which meet at a junction, whereas "T-type" refers to

three or more adjacent elements meeting at a common juncture. With these definitions it can be observed that all formed sections are composed of angle-type elements, whereas extruded sections may be composed of angle- and/or T-type elements.

Thus, for extruded sections composed of only angle-type elements, the generalized-crippling-analysis procedure of the preceding section may be used. In such cases, there is no major difference between comparable extruded and formed sections. The minor differences include fillet radius effects for the extrusion and raised yield corner effects for the formed section. Any differences in yield strength are accounted for directly in the crippling-strength formula.

For extruded sections composed wholly or partially of T-type elements, the corner concept in equation (1) is now replaced by a new concept which involves cutting the section into a series of flanges. In order to justify this method of analysis, test data on V-groove plates, extruded angles, square tubes, T-, H-, and cruciform sections are reviewed. The analysis is then extended to stiffened panels with extruded Y stiffeners. Finally, in the interest of a single method of analysis for all types of multicorner sections and stiffened panels, the data of the preceding section on Z- and hat-stiffened panels are reviewed in terms of the analysis of this section.

## Angle and T-Type Elements

In reference 1, equation (1) was used to correlate test data on square and rectangular tubes. It was found that a value of $\beta_c = 1.42$ for $c = 4$ gave excellent correlation with the available test data on four different aluminum alloys.

By cutting the tube into a series of four angles as shown in figure 6 and correlating the test data according to the parameter $g$ which is the total number of cuts plus flanges, the following relation for angle-type elements is obtained:

$$\frac{\bar{\sigma}_f}{\sigma_{cy}} = \beta_g \left[ \frac{gt^2}{A} \left( \frac{E}{\sigma_{cy}} \right)^{1/2} \right]^{0.85} \tag{2}$$

By use of equation (1), it is evident that

$$\beta_g = \beta_c (c/g)^{0.85} \tag{3}$$

Thus, for the extruded tubes

$$\beta_g = 1.42(4/12)^{0.85} = 0.558 \tag{4}$$

The correlation according to equations (2) and (4) for the extruded-tube test data of reference 1 is shown in figure 7(a) by the line designated angle type. Also shown with this line are some test data from reference 1 on extruded angles for which $g = 2$ and on V-groove plates for which $g = 3$. Good correlation is obtained with these data although the extruded-angle data are too few in number to permit definite conclusions to be drawn.

The analysis for T-type extrusions is based on the following relation established in reference 1 from test data on cruciform extrusions:

$$\frac{\bar{\sigma}_f}{\sigma_{cy}} = \beta_g \left[ \frac{gt^2}{A} \left( \frac{E}{\sigma_{cy}} \right)^{1/2} \right]^{0.40} \tag{5}$$

For the cruciform $\beta_g = 0.670$ and $g = 4$ as shown in figure 6. This relationship also correlates well with some limited test data on T-extrusions as shown in figure 7(a).

Rather extensive test data on H-extrusions of four aluminum alloys and one magnesium alloy are available to test further the g-correlation scheme. In reference 1, the H-extrusion was treated as a special type of two-corner element and the generalized crippling analysis was not applied to this section.

As shown in figure 6, $g = 7$ for an H-extrusion. The test data correlated according to the parameter $A/gt^2$ are illustrated in figure 7(b). It can be observed that satisfactory correlation with equation (5) is obtained by utilizing the $\beta_g$ value for the cruciform for $\bar{\sigma}_f/\sigma_{cy} \leqq 3/4$. As discussed in reference 1, beyond this cutoff

$$\bar{\sigma}_f = \sigma_{cr} \qquad / \tag{6}$$

for $\bar{\sigma}_f/\sigma_{cy} > 3/4$.

From the results presented in figure 7, it appears that the g-correlation scheme for angle- and T-type extrusions permits an integrated approach to the crippling-strength analysis of extruded elements.

## Y-Stiffened Panels

In analyzing the crippling strength of monolithic stiffened panels utilizing extruded Y-stringers, certain additional considerations are encountered which have not arisen previously. These include:

(1) The method of determining $g$ for a stiffened panel.

(2) The thicknesses of the various flanges of the extrusion may not be constant.

(3) The compressive yield strength of the extruded stiffener may be significantly different from that of the sheet.

The method of determining $g$ for a Y-stiffened panel is illustrated in figure 8. Since the test data are for panels tested with six stiffeners, it is desirable to determine an average value of $g$ for a typical area element equal to the stiffener spacing. It can be noted from figure 8 that the cuts midway between stiffeners are credited to the element to the left of the cut. Thus the last element on the right has a value of $g$ of one unit less than the other elements. Thus, the average value of $g = 18.83$ for the Y-stiffened panel accounts for this fact.

For the particular Y-extrusion used in reference 7, the thickness of the horizontally opposed flanges at the top of the section is greater than that of the other elements in the cross section, as shown in figure 8. Consequently, in determining the effective thickness of the stiffener $\bar{t}_w$ for use in the generalized crippling relation, the following method of weighting was used:

$$\bar{t}_w = \frac{\Sigma\, b_i t_i}{\Sigma\, b_i} \tag{7}$$

In equation (7), $b_i$ and $t_i$ refer to the length and thickness, respectively, of the cross-sectional elements.

Similarly, for the 7075-T6 aluminum-alloy panels, the compressive yield strength of the stiffener $\left(\sigma_{cy_w} = 78 \text{ ksi}\right)$ was significantly higher than that of the sheet $\left(\sigma_{cy_s} = 67 \text{ ksi}\right)$. The following weighting procedure was used:

$$\bar{\sigma}_{cy} = \frac{\sigma_{cy_s} + \sigma_{cy_w}\left[\left(\bar{t}/t_s\right) - 1\right]}{\bar{t}/t_s} \tag{8}$$

where $\bar{t}$ is the effective thickness of the stiffened panel.

As a consequence of these weighting procedures, the generalized crippling relation for the Y-stiffened panel has the form

$$\frac{\bar{\sigma}_f}{\bar{\sigma}_{cy}} = \beta_g\left[\frac{g\bar{t}_w t_s}{A}\left(\frac{E}{\bar{\sigma}_{cy}}\right)^{1/2}\right]^m \tag{9}$$

The test data of reference 7 for 2024-T3 and 7075-T6 aluminum-alloy panels were correlated according to the parameters of equation (9) for three different $\bar{t}_w/t_s$ ratios. In all cases nominal dimensions were used. Since the Y-extrusion is composed of both angle- and T-type elements, the value of $m$ in equation (9) is not evident a priori. As shown in figure 9, satisfactory correlation is obtained by considering the Y-extrusion to be an angle-type element so that $m = 0.85$. The $\beta_g$ values vary somewhat with the parameter $\bar{t}_w/t_s$ as given in table 3. This variation was previously observed for the hat-stiffened panels.

## Panels With Formed Stiffeners

In view of the desirability of having one method of analysis for both formed and extruded sections, if possible, the results of the section "Crippling Strength of Panels With Formed Stiffeners" on panels with formed Z and hat stiffeners are reviewed. These panels were analyzed according to equation (1) for multicorner elements as demonstrated in reference 1.

By use of equation (3), the c-correlation method can be converted to the g-correlation method. The results are listed in table 4. Similarly, by use of figure 8, the values of $g$ can be obtained for the stiffened panels and the $\beta_c$ values converted to $\beta_g$ values by use of equation (3). Such results are given in table 4.

All $\beta_g$ values are summarized as a function of $\bar{t}_w/t_s$ in figure 10. It can be observed that at $\bar{t}_w/t_s = 1$ all $\beta_g$ values are in good agreement. Furthermore, the variation of $\beta_g$ with $\bar{t}_w/t_s$ for the hat- and Y-stiffened panels is substantially the same.

## STRENGTH OF SHORT RIVETED PANELS

In the preceding sections, the crippling strength of monolithic panels was considered. Such panels include integral forms of construction such as machined, extruded, forged or rolled, and generally bonded or seamwelded panels. In riveted or spotwelded panels, the discrete locations of the attachments can permit the occurrence of additional buckling and failure modes which reduce the crippling or column strength of the panel below that of the corresponding monolithic panel.

Spotwelds generally can be placed sufficiently close together so that the monolithic strength can be readily achieved in spotwelded panels. For panels with riveted attachments, however, careful design is often required to achieve monolithic strength levels, particularly in short panels of heavy-sheet and light-stringer construction. In such cases, closely spaced large-diameter rivets are often required.

The additional buckling or failure modes that can destroy the monolithic behavior of riveted panels are interrivet buckling, wrinkling or forced crippling, and rivet failure. In the present section, the behavior of stiffened panels subjected to these additional buckling and failure modes is reviewed and available theories are presented. Design criteria are given that present a rational approach to the achievement of monolithic strength levels for riveted panels.

### Additional Failure Modes

The interrivet mode involves buckling of the skin of the stiffened panel as a wide column upon essentially undistorted stringers so that separation occurs between the skin and stringers. The width of the wide column is generally equal to that of the panel and the length corresponds to the rivet spacing. Different rivet types such as flat-head or countersunk rivets provide differing end restraints, thereby reducing the effective length of the column. Since failure and buckling of a wide column are essentially coincident, interrivet buckling terminates the ability of the skin to carry additional loads beyond buckling.

Failure in the wrinkling mode has the same general appearance as the initial instability and occurs at a somewhat higher stress level. It has been termed "wrinkling" because of certain similarities with wrinkling of the faces in sandwich construction. At failure, the buckles have grown so that the skin acts as a wide column on an elastic foundation. However, in contrast with the interrivet mode, the stringer distorts appreciably as the attachment flange follows the buckled skin contour. Since the rivets are active in causing the flange to conform to the skin, rivet-strength considerations are of importance here. The

distorted attachment flange causes distortion of other elements in the stringer section and hence the term "forced crippling" is also used for this phenomenon. The buckle wave length is greater than the rivet spacing and depends upon the effective foundation characteristics of the stringer.

In figure 11, the various failure modes of a short, riveted, stiffened panel are shown schematically. It is assumed here that only the rivet spacing is varied. For small rivet spacings, the monolithic strength level of the panel is attained and can be predicted by the methods of the sections "Crippling Strength of Panels With Formed Stiffeners" and "Crippling Strength of Panels With Extruded Stiffeners." For moderate rivet spacings, wrinkling occurs at a wave length greater than the rivet spacing. At large spacings, interrivet buckling occurs at an overall wave length equal to the rivet pitch.

## Interrivet Buckling

Historically, interrivet buckling was observed shortly after the introduction of all-metal construction in the airframe. Howland (ref. 8) analyzed this problem for panels with flathead rivets by assuming that the skin acts as a wide column which is clamped at the ends where the rivets are located. Thus, the interrivet buckling stress is given by

$$\sigma_i = \frac{e\pi^2 \eta \bar{\eta} E}{12(1 - \nu^2)} \left(\frac{t_s}{p}\right)^2 \tag{10}$$

In equation (10), $\eta$ and $\bar{\eta}$ are the plasticity-reduction factor and cladding reduction factor, respectively, for plate columns as discussed in Part I of this Handbook (ref. 9).

A survey of some limited test data on interrivet buckling indicates that the value of end-fixity coefficient $e$ in equation (10) is generally close to that for clamping except for machine countersunk rivets. From these data, the values of end-fixity coefficient given in table 5 from references 8, 10, and 11 are tentatively suggested for use with equation (10). Although no published data are available on rivets in dimpled joints, it may be tentatively assumed that the value of $e = 1$ for countersunk rivets may be used in this case in the absence of substantiating data.

After interrivet buckling occurs, it is reasonable to expect that under continued deformation the skin will continue to carry the load at buckling but no additional load since the behavior of the skin is that of a wide column. Thus, the failing stress of the riveted panel in this case is

$$\bar{\sigma}_{f_r} = \frac{\sigma_i 2b_{ei}t_s + \bar{\sigma}_{f_{st}}A_{st}}{2b_{ei}t_s + A_{st}} \tag{11}$$

where $2b_{ei}$ is the total effective width of skin corresponding to the interrivet buckling stress $\sigma_i$ given by equation (10). The crippling stress of the stringer alone $\bar{\sigma}_{f_{st}}$ can be determined by the methods of Part IV of this Handbook (ref. 1).

## Rivet Geometry and Strength

With the use of heavier skin gages which approach or exceed the stringer thickness, interrivet buckling is rarely a factor in decreasing the strength of short panels. However, it has been observed that the rivet diameter and pitch and rivet strength are factors of considerable importance in achieving monolithic-panel strength levels.

The NACA has conducted an extensive experimental program to establish the effects of the rivet variables upon the strength of short panels that fail in the local instability and wrinkling modes. The results of a program for short 2024-T3 and 7075-T6 aluminum-alloy Z-stiffened panels with 2117-T4 flathead rivets in which the rivet diameter and pitch were varied (ref. 4) are summarized in figure 12(a). The ordinate of figure 12(a) represents the ratio of the strength of the riveted panel $\bar{\sigma}_{f_r}$ to that of a corresponding monolithic panel. The latter can be obtained by the methods of the section "Crippling Strength of Panels With Formed Stiffeners" as discussed therein for Z-stiffened panels.

Test data of reference 12 indicate that the strength of panels of moderate slenderness ratio ($L'/\rho = 35$) is affected considerably less than that of short panels by rivet pitch and diameter variations. The strength of long panels ($L'/\rho = 60$) was negligibly affected by rivet configuration in the range tested.

Another experimental investigation of reference 13 was concerned with the influence of rivet tensile strength upon the strength of short 7075-T6 aluminum-alloy Z-stiffened panels. The results for eight rivet types are summarized in figure 12(b) in terms of substantially the same quantities used in figure 12(a). The sole difference is the use of an effective rivet diameter $d_e$ defined in terms of a standard rivet taken as an 2117-T4 aluminum-alloy rivet with the following tensile properties:

$$\left.\begin{aligned} s &= 57 \text{ ksi} && d_e/t_{av} \leqq 1.67 \\ s &= \frac{190}{d_e/t_{av}} - \frac{160}{(d_e/t_{av})^2} && d_e/t_{av} > 1.67 \end{aligned}\right\} \quad (12)$$

where $t_{av}$ is the average of skin and stringer thickness in inches.

The effective diameter of a rivet of another material is

$$d_e/d = (s_r/s)^{1/2} \quad (13)$$

where $s_r$ is the tensile strength of the rivet defined as maximum tensile load divided by shank area in ksi units.

## Failure in Wrinkling Mode

The data presented in figure 12 relate the strength of short riveted panels to the crippling strength of the corresponding monolithic panel. However, these data are of little value from the design standpoint of providing criteria to achieve monolithic strength levels. Furthermore, recent analyses of the wrinkling phenomenon have provided a more detailed understanding of the influence of the rivet variables upon the compressive strength of panels.

Argyris and Dunne (ref. 14) appear to have been the first to consider the occurrence of the wrinkling phenomenon in riveted panels in the published literature. They discussed it qualitatively in terms of the rivet offset distance from the plane of the stiffener web.

Bijlaard and Johnston (ref. 15) have presented an extensive analysis of the forced-crippling phenomenon. Buckling coefficients for this case are presented for a limited range of riveted-panel-configuration variables, and effective-width data are given from which the failure load of the panel in the wrinkling mode can be estimated. The results of the analysis are in reasonable agreement with test data on several stiffened panels used to check the theory.

A more recent analysis of wrinkling by Semonian and Peterson (ref. 6) utilizes a structural parameter which combines the rivet pitch, diameter, and offset distance from the web plane of the stiffener into a single parameter, the effective rivet offset. The latter is evaluated by use of a relatively rigorous instability analysis in conjunction with experimental data on riveted panels. A semiempirical failing-strength analysis of the

wrinkling mode based on this parameter is presented therein. Comparisons of the results of the analysis with a large group of test data on 2024-T3 and 7075-T6 aluminum-alloy Z- and hat-stiffened panels indicate good agreement although it was found that the analysis requires some modification for panels of other materials.

## Effective Rivet Offset

The governing parameter in this analysis of the effective rivet offset was evaluated by relating the experimentally observed buckling stress in the wrinkling mode to the theoretical value. The theoretical values are presented in figure 13(a) and the experimental, in figure 13(b) in terms of the effective rivet offset distance f, and therefore f can be determined from each panel tested. The best fit to these data was determined from successive cross plotting and the results are shown in figure 14. Since this chart is based on experimental data, certain limitations as given below are implied in its use.

The data of figure 14 were obtained primarily from 2024-T3 and 7075-T6 aluminum-alloy-panel tests utilizing 2117-T4 aluminum-alloy NACA countersunk rivets. Apparently the influence of other aluminum-alloy rivet types such as universal-head or flathead rivets on the wrinkling stress is small and therefore figure 14 may be used. However, figure 14 was established from tests on panels with rivets having a diameter greater than 90 percent of the skin thickness. Therefore, figure 14 should not be used for $d/t_s < 0.9$ without confirmation.

Since the rivet stiffness is a contributing factor in the effective-rivet-offset parameter, changes in rivet material from the aluminum alloys can result in f-values different from those given in figure 14. Test data indicate, however, that rivet materials with a higher elastic modulus and strength than 2117-T4 aluminum alloy do not significantly increase the strength of the panel. On the other hand, aluminum-alloy panels with FS-1 magnesium rivets or Cherry Blind rivets failed at loads less than those of corresponding panels with 2117-T4 rivets. Therefore, figure 14 should be used with caution for aluminum-alloy panels utilizing rivet materials of lower strengths and stiffnesses than 2117-T4 rivets.

The data used to construct figure 14 are based on panel tests using formed stiffeners. The use of extruded stringers with sharp exterior corners usually eliminates the wrinkling mode because the rivet offset distance can be reduced and the stiffness of the filleted attachment flange is greater than for the formed stiffener. The available tests on panels with extruded stiffeners indicate that figure 14 provides a conservative estimate of f although the data are too few to permit the construction of a chart such as figure 14 for this case.

## Wrinkling Instability of Panel

In the analysis of a short riveted panel with a prescribed configuration, three buckling modes are possible: Local buckling which is treated in Part II of this Handbook (ref. 16), interrivet buckling which was considered previously in the present section, and buckling in the wrinkling mode. The latter can be determined by use of figure 13(a) in conjunction with the usual relation:

$$\sigma_{cr} = \frac{k\pi^2 \eta \bar{\eta} E}{12(1 - \nu)^2}\left(\frac{t_s}{b_s}\right)^2 \tag{14}$$

In equation (14), the appropriate values of the plasticity-reduction factor $\eta$ and cladding reduction factor $\bar{\eta}$ are for long simply supported compressed plates as given in reference 9.

## Wrinkling Failure of Skin

The failure strength of a monolithic stiffened panel is given by the crippling analysis of the sections "Crippling Strength of Panels With Formed Stiffeners" and "Crippling Strength of Panels With Extruded Stiffeners." For riveted panels, failure can occur in the wrinkling mode and less frequently as a result of rivet failure or the growth of interrivet buckling. In such cases, the compressive strength is lower than the monolithic crippling strength and can be determined by the methods given below.

In the wrinkling mode, the average stress at failure exceeds the buckling stress given by equation (14) by a relatively small amount. At failure, the lateral forces on the stringers generally become large and force crippling of the stringers, thereby destroying their capacity to carry additional loads.

By use of a semiempirical analysis, Semonian and Peterson (ref. 6) have determined the wrinkling-failure coefficients presented in figure 13(b) which are to be used in conjunction with

$$\bar{\sigma}_w = \frac{k_w \pi^2 \eta \bar{\eta} E}{12(1 - \nu)^2}\left(\frac{t_s}{b_s}\right)^2 \tag{15}$$

to determine failure of the skin in the wrinkling mode. For hat-stiffened panels or those with unequal stiffener springs, an average value of $b_s/t_s$ may be used in equation (15).

Tests have indicated that the redistribution of stress after buckling in the wrinkling mode is relatively moderate. In fact, the average stress end-shortening relation for panels that wrinkle nearly coincides with the stress-strain curve of the material until just prior to failure. Therefore, it has been recommended that the values of $\eta$ and $\overline{\eta}$ corresponding to a long simply supported plate at $\overline{\sigma}_w$ be used in equation (15). Tests appear to be in reasonably good agreement with this assumption.

## Wrinkling Failure of Aluminum-Alloy Panels

Equation (15) can be used to determine the wrinkling strength of the skin. In estimating the wrinkling strength of a short panel, however, it is necessary to determine the crippling strength of the stringer alone to ascertain if it is stable or unstable at wrinkling failure of the skin. In such an analysis, the following quantities are of importance:

$\overline{\sigma}_{f_{st}}$ crippling strength of stringer alone which can be determined by methods of Part IV of this Handbook (ref. 1)

$\overline{\sigma}_w$ wrinkling strength of skin which can be estimated from equation (15)

$\overline{\sigma}_f$ monolithic crippling strength of panel which can be determined by methods of the sections "Crippling Strength of Panels With Formed Stiffeners" and "Crippling Strength of Panels With Extruded Stiffeners"

$\overline{\sigma}_{f_r}$ strength of riveted panel which can be determined as given below

After $\overline{\sigma}_{f_{st}}$ and $\overline{\sigma}_w$ have been determined, it will be known if the stringer is stable or not in the following way:

(1) If $\overline{\sigma}_{f_{st}} \geqq \overline{\sigma}_w$, the stringer is stable. Therefore, the panel fails completely in the wrinkling mode and

$$\overline{\sigma}_{f_r} = \overline{\sigma}_w \tag{16}$$

(2) If $\overline{\sigma}_{f_{st}} < \overline{\sigma}_w$, the stringer is unstable. An approximation suggested in reference 6 which yields predictions which are slightly high when the stringers are unstable but gives satisfactory results over the entire practical range of panel proportions is that the stringers carry the same stress as the skin up to $\overline{\sigma}_{f_{st}}$. Beyond this the stringers carry no additional load. Thus, the failing stress of the short panel is

$$\overline{\sigma}_{f_r} = \frac{\overline{\sigma}_w b_s t_s + \overline{\sigma}_{f_{st}} A_{st}}{b_s t_s + A_{st}} \tag{17}$$

(3) In either case, the failing strength of the riveted panel cannot exceed the crippling strength of the corresponding monolithic panel. Therefore, the lower of the two values $\overline{\sigma}_{f_r}$ or $\overline{\sigma}_f$ is to be taken as the failing strength of the short panel.

## Rivet Criteria

The maximum-strength analysis of compression panels given in the preceding section requires certain limitations on the pitch and strength of rivets in order that the panel will carry the predicted load. The rivets must be spaced closely enough and have adequate strength to make the stringer flange follow the plate contour. If the spacing is too large, the panel may fail by interrivet buckling. If the strength is insufficient, the panel may fail prematurely because of rivet failure.

A criterion for the rivet pitch found from test data which results in failure in the wrinkling mode rather than as a result of interrivet buckling is

$$p/b_s < 1.27/k_w^{1/2} \tag{18}$$

where $k_w$ is given in figure 13(b).

The lateral force required to make the stringer attachment flange conform to the wrinkled-skin contour loads the rivet in tension. An approximate criterion for rivet strength derived from that given in reference 6 is

$$s_r > \frac{0.7}{E_{st}} \frac{b_s}{d} \frac{p}{d} \left(\frac{\overline{\sigma}_w}{\eta}\right)^2 \tag{19}$$

The tensile strength of the rivet $s_r$ is defined in terms of the shank area. It may be associated with either shank failure or pulling of the countersunk head of the rivet through the skin. Values of $s_r$ for 2117-T4 aluminum-alloy rivets are given by equations (12).

## Wrinkling Failure of Panels of Other Materials

The wrinkling-failure coefficient $k_w$ in equation (15) was evaluated by Semonian and Peterson (ref. 6) from test data on the failure strength of short 2024-T3 and 7075-T6 aluminum-alloy panels. When this method of analysis was used to check the test data of reference 3 on short panels of other aluminum alloys, magnesium alloy, steel, copper, and titanium, it was found that the theory was optimistic by as much as 230 percent when compared with the test data in some cases. Further, it was determined that the failure strength in the wrinkling mode is apparently related to the $\sigma_{cy}/E$ ratio of the material. Therefore, in this section an attempt is made based on the available test data to extend the analysis of reference 6 to include the effects of the physical properties of the materials.

An alternate form of equation (15) given by Semonian and Peterson for the wrinkling failure of short aluminum-alloy panels is

$$\bar{\sigma}_w = \frac{\eta\bar{\eta}E}{1 - \nu^2}\left[\frac{1}{3}\frac{t_s}{b_s}\left(\frac{t_w}{f}\right)^3\frac{(3f/b_w) + 1}{(3f/b_w) + 4}\right]^{1/2} \tag{20}$$

This equation can be very well approximated by the following, for $\nu = 0.3$:

$$\bar{\sigma}_w = 0.48\eta\bar{\eta}E\left(\frac{t_w}{f}\right)^{4/3}\left(\frac{t_w}{b_w}\right)^{1/6}\left(\frac{t_s}{b_s}\right)^{1/2} \tag{21}$$

Equation (21) is equivalent to equation (20) and equation (15) and is in a convenient form for correlation purposes since it does not require use of figure 13(b) to determine $k_w$.

Test data on short aluminum-alloy hat- and Z-stiffened panels are shown in figure 15 in terms of the parameters of equation (21). It can be observed that the data correlate reasonably well within ±10-percent limits. It is to be noted that the agreement of the test data of figure 15 with equations (20) or (15) is relatively the same as that

obtained for equation (21). Therefore, it appears that equation (21) is in reasonable agreement with wrinkling test data on short hat- and Z-stiffened panels of 2024-T3 and 7075-T6 aluminum alloys.

Equation (21) was used to correlate test data of reference 3 on wrinkling failure of panels of other materials that first buckled in the wrinkling mode in the elastic range. For these data a systematic variation with the $E/\sigma_{cy}$ ratio is observed as shown in figure 16. The test data shown here are for panels of the same geometry, with identical rivet offset, relatively the same rivet strengths, and relatively similar compressive yield properties in the corners of the formed Z stiffener. Therefore, only the physical properties of the panel materials were varied in this series of tests.

From figure 16, it was found that for specific values of $(b_s/t_s)(b_w/t_w)^{1/3}(f/t_w)^{8/3}$

$$\bar{\sigma}_{f_r}/E \propto (\sigma_{cy}/E)^{3/4} \tag{22}$$

Consequently, equation (21) can be modified to include the effects of physical-property variations in the following form by noting that the theory apparently applies for a value of $E/\sigma_{cy}$ equal to 125:

$$\frac{\bar{\sigma}_{f_r}}{\sigma_{cy}} = 17.9\left(\frac{t_w}{f}\right)^{4/3}\left(\frac{t_w}{b_w}\right)^{1/6}\left[\frac{t_s}{b_s}\left(\frac{\bar{\eta}E}{\sigma_{cy}}\right)\right]^{1/2} \tag{23}$$

It can be noted that equation (23) is in a form similar to that obtained in the generalized crippling study presented in the section "Crippling Strength of Panels With Formed Stiffeners" and "Crippling Strength of Panels With Extruded Stiffeners." In fact both wrinkling and crippling test data can be correlated on one chart by noting that

$$\alpha = \frac{A/t_w t_s}{b_s/t_s} \tag{24}$$

Thus, the generalized crippling formula for formed Z-stiffened panels becomes, from equation (1),

$$\frac{\overline{\sigma}_f}{\sigma_{cy}} = 1.26\left[\frac{3}{\alpha}\frac{t_s}{b_s}\left(\frac{\overline{\eta}E}{\sigma_{cy}}\right)^{1/2}\right]^{0.85} \tag{25}$$

All of the test data of reference 3 have been plotted in figure 17. On the right side, monolithic crippling behavior according to equation (25) is indicated for $\alpha = 1.3$ and 1.8, which covers the range of panels tested. On the left and upper portions, the open symbols are for the aluminum and magnesium alloys which do not experience significant raised yield effects in the formed corners of the Z as indicated by the $\overline{\sigma}_{cy}/\sigma_{cy}$ ratios given in figure 17. These data are in good agreement with equation (23).

The solid symbols are for the materials which have values of $\overline{\sigma}_{cy}/\sigma_{cy}$ greater than 1.4. Titanium is included in this group, since it was severely anisotropic and moreover had considerable scatter in yield strength. These data are reasonably well correlated according to equation (23) using a coefficient of 20.5 in place of 17.9 in this formula.

On the basis of available test data, equation (23) with a suitable coefficient that depends upon $\overline{\sigma}_{cy}/\sigma_{cy}$ may be used to determine the strength of short riveted panels which fail by wrinkling. In conjunction with equation (23), $f/t_w$ values are to be determined from figure 14, and equation (17) is to be used if the stringer is unstable. Because of the empirical nature of Semonian and Peterson's analysis (ref. 6) and that contained in this section, the above conclusions must be regarded as tentative, subject to further substantiation by panel tests.

## COLUMN STRENGTH OF STIFFENED PANELS

In the preceding sections, the compressive strength of short monolithic and riveted stiffened panels has been considered. Since the column strength of the panel decreases as the length increases, the strength of short panels is essentially the maximum strength which can be achieved for the particular cross-sectional configuration and sheet-stiffener fastening arrangement. Having established methods for estimating the crippling strength, it is now pertinent to consider the column strength of panels of various lengths.

Prior to about 1945, it was customary to present charts of the column strength of stiffened panels in terms of the effective slenderness ratio of the panel. Methods of constructing such charts are well known

in the aircraft industry and are summarized in the books of Sechler and Dunn (ref. 17) and others on aircraft structures.

Since 1945, there has been a growing tendency to use direct-reading design charts for stiffened panels in which the column strength is presented as a function of the structural index $N/L'$. The index contains the loading per inch $N$ and the effective column length $L'$ and is in a convenient form for minimum-weight studies of stiffened panels.

In figure 18, the two types of stiffened-panel column charts are presented. Figure 18(a) represents the Euler- and tangent-modulus behavior of a stiffened panel with sturdy stiffeners and not subject to buckling of the skin. In figures 18(b) and 18(c) crippling of the stiffener occurs generally preceded by local buckling of the skin or stiffener elements. This is the usual type of behavior of stiffened panels and is discussed in some detail as follows.

## Column-Strength Ranges

(1) Below the local buckling stress of the panel, the column strength is usually in the long-column range and can generally be represented by the Euler relation

$$\sigma_e = \pi^2 E_t \Big/ (L'/\rho)^2 \tag{26}$$

for $\sigma_e \leqq \sigma_{cr}$. This equation is generally valid with the exception of panels with stiffeners of very poor torsional rigidity.

For direct-reading design charts, such as figure 18(c), the Euler relation is

$$\sigma_e = \left[\pi^2 E_t (\rho/\bar{t})^2 (N/L')^2\right]^{1/3} \tag{27}$$

for $\sigma_e \leqq \sigma_{cr}$. Here, $\rho/\bar{t}$ is a dimensionless shape parameter of the panel and $N/L'$ is the structural index.

(2) The local buckling strength of the panel which represents the limit of application of equations (26) and (27) can be obtained from Part II of this Handbook (ref. 16). Figures 13 and 14 therein present compressive-local-buckling coefficients for various types of integral panels. Figures 3, 5, and 6 of reference 16 give coefficients for individual stiffeners or stiffener elements and figure 19(a) of the same reference can be used to estimate the buckling stress of the skin.

(3) The crippling strength of monolithic panels and wrinkling strength of riveted panels which pertain to the short-panel range may be obtained by the methods presented in the section "Crippling Strength of Panels With Formed Stiffeners" to the section "Strength of Short Riveted Panels" herein.

Thus, theory is available for determining the column strength in the Euler range as well as for the cutoff at the local-buckling-strength level. Semiempirical methods are available for the short-panel strength. The remaining column-strength range is the transition from the Euler range to the short-panel range. In this transition range, there is a considerable reliance on the use of panel tests. In fact, the major portion of the extensive NACA program on direct-reading design charts was concerned with test data in this transition region.

## Transition Range

To return to the type of column chart shown in figure 18(b) for the moment, a very useful approximation in this transition range which has been used quite extensively is the parabolic column curve. For stiffened panels subject to local buckling and crippling, the parabolic approximation has the following form:

$$\frac{\overline{\sigma}_{co}}{\overline{\sigma}_f} = 1 - \left(1 - \frac{\sigma_{cr}}{\overline{\sigma}_f}\right)\frac{\sigma_{cr}}{\sigma_e} \tag{28}$$

for $\overline{\sigma}_{co} > \sigma_{cr}$ where

$$\sigma_e = \pi^2 E/(L'/\rho)^2 \tag{29}$$

In equation (28), $\sigma_{cr}$ and $\overline{\sigma}_f$ are known for the panel cross-sectional configuration, and $\sigma_e$ is the Euler stress for the particular panel length. This relation is essentially an interaction-type equation for the transition range. From equation (28), $\overline{\sigma}_{co}/\overline{\sigma}_f = 1$ for $L'/\rho = 0$ and $\overline{\sigma}_{co} = \sigma_{cr}$ for $\sigma_e = \sigma_{cr}$.

For the direct-reading design charts, it is also possible to employ equation (28) in the transition region. In this case, however, equation (28) is to be used in conjunction with

$$\sigma_e = \left[\pi^2 E(\rho/\overline{t})^2(N/L')^2\right]^{1/3} \tag{30}$$

As indicated previously, $\bar{\sigma}_{co} = \bar{\sigma}_f$ for $L'/\rho = 0$. However, in most crippling tests, the value of $\bar{\sigma}_f$ is obtained at $L'/\rho = 20$. In fact, the crippling method of the sections "Crippling Strength of Panels With Formed Stiffeners" and "Crippling Strength of Panels With Extruded Stiffeners" is based on such tests. Consequently, it is desirable that equation (28) be modified so that $\bar{\sigma}_{co} = \bar{\sigma}_f$ at $L'/\rho = 20$. This is readily accomplished by the addition of a correction term to equation (28):

$$\frac{\bar{\sigma}_{co}}{\bar{\sigma}_f} = 1 - \left(1 - \frac{\sigma_{cr}}{\bar{\sigma}_f}\right)\frac{\sigma_{cr}}{\sigma_e}\left(\frac{\sigma_{20}^{1/2} - \sigma_e^{1/2}}{\sigma_{20}^{1/2} - \sigma_{cr}^{1/2}}\right)^2 \tag{31}$$

In equation (31), $\sigma_{20}$ represents the stress obtained from equation (29) for $L'/\rho = 20$. As previously, equation (31) applies for $\bar{\sigma}_{co} > \sigma_{cr}$. In cases where $\sigma_{cr} > \sigma_{pl}$ ($\sigma_{pl}$ is the proportional limit stress) $\sigma_{pl}$ replaces $\sigma_{cr}$ in equations (28) and (31).

To demonstrate briefly the use of the parabolic approximation for direct-reading design charts, figure 19 has been prepared based on Z-stiffened-panel test data of Schuette (ref. 18). In this figure, $\sigma_e$ was obtained from equation (30), $\bar{\sigma}_f$ from equation (1) using $c = 3$ and $\beta_c = 1.26$, and $\sigma_{cr}$ by use of figure 14 of Part II of this Handbook (ref. 16). The transition region is represented by equation (31). It can be observed that the method is in satisfactory overall agreement with test data in this case.

## Direct-Reading Column Charts

The NACA has engaged in an extensive experimental program for the purpose of constructing direct-reading column charts of several different types for hat-, Y-, and Z-stiffened panels (refs. 7 and 18 to 25). The use of these charts in design depends upon whether axial compressive considerations govern or the minimum skin thickness is an overriding condition. Because of the extensive number of these charts, the pertinent reference is listed in table 6 and no attempt is made to reproduce the series of charts herein.

The panels tested in this program utilized strongly riveted connections between the skin and the stiffener. In spite of this precaution, however, wrinkling or forced crippling probably occurred in many of the panels. Consequently, these results will be conservative when applied to corresponding panels of monolithic construction.

It is to be noted that minimum-weight panel designs obtained by use of these charts generally result in high buckling stresses of the skin as a result of very closely spaced stiffeners. For larger stiffener spacings, without a resulting significant decrease in structural efficiency, the use of magnesium-alloy skins in conjunction with aluminum-alloy stringers offers an interesting possibility in design (ref. 19).

## OPTIMUM STIFFENED PANELS

Although it is not practical to reproduce herein the entire series of direct-reading column curves obtained by the NACA, it is convenient to summarize the results of this investigation in the form of optimum-column curves. These curves can be of considerable value in preliminary design studies and represent the envelope of all minimum-weight stiffened-panel designs for specified structural-loading parameters.

In this section, optimum-column curves for hat-, Y-, and Z-stiffened panels are presented in two forms: Plots of $\bar{\sigma}_{co}$ against $N/L'$ and plots of $\bar{\sigma}_{co}$ against $N/t_s$ for specified values of $N/L'$. The latter form of presentation is useful when design conditions require the use of a minimum skin thickness.

In order to extend the results of the optimum-stiffened-panel study to materials with physical properties other than those investigated, methods of generalizing the optimum results are considered. These methods are based on available theories for the design and analysis of stiffened panels of minimum weight.

### Optimum-Panel Theories and Results

Theory and test data in the available literature on optimum stiffened panels have been reviewed and considered in detail by Gerard (ref. 26). The theory of the design of monolithic stiffened panels of minimum weight has been considered by Zahorski (ref. 27) and Farrar (ref. 28), and the results of these analyses can be summarized in the following formula:

$$\bar{\sigma}_{co} = \alpha_p (N\bar{\tau}E/L')^{1/2} \tag{32}$$

From the theory, the panel efficiency coefficient $\alpha_p$ and the plasticity-reduction factor for the optimum panel $\bar{\tau}$ are

$$\alpha_p = \left[\frac{\pi^4 k}{12(1 - \nu^2)}\right]^{1/4} \left(\frac{\rho}{b_s} \frac{t_s}{\bar{t}}\right)^{1/2} \tag{33}$$

$$\bar{\tau} = \left(E_s/E\right)\left(E_t/E_s\right)^{1/2} \tag{34}$$

From equation (33), it can be observed that increases in structural efficiency are obtained when the radius of gyration $\rho$ is large, the stiffener spacing $b_s$ is small, and $t_s/\bar{t}$ approaches unity, which implies relatively thick skins. Farrar (ref. 28) has actually carried the analysis up to the point where $\alpha_p$ has been evaluated for monolithic hat-, Y-, and Z-stiffened panels. His results, in fact, are within 8 percent of the values obtained from the NACA experimental program on minimum-weight riveted panels.

The results of the NACA investigation are shown in figure 20, for optimum Z-, hat-, and Y-stiffened panels. The data used to construct these charts were obtained from the references listed in table 7.

In figure 20, the straight-line portions of the data were extrapolated to represent a hypothetical elastic material. It is significant that the slope of this line on the logarithmic plot in all cases is almost exactly one-half of that predicted by the theory of equation (32). This is remarkable in view of the fact that this line represents the envelope of a large set of empirical curves obtained by varying the stiffened-panel geometry.

By appropriately accounting for the modulus of elasticity of the panel materials, the experimental values of the riveted-panel efficiency coefficients given in table 8 were determined. Also shown are the theoretical values of Farrar (ref. 28) for monolithic panels.

Recently, Catchpole (ref. 29) investigated the optimum design of stiffened panels having unflanged integral stiffeners. The theoretical panel efficiency coefficient for this case was found to be $\alpha_p = 0.81$. The cross-sectional proportions of the optimum configuration are $b_w/b_s = 0.65$ and $t_w/t_s = 2.25$. There is no published experimental substantiation of these results.

### Specified Skin Thickness

In certain design cases, it is necessary that the stiffened panel satisfy a skin-thickness requirement in addition to carrying a compressive

load. This situation commonly arises when torsional-stiffness requirements govern. In such cases, the minimum-weight charts presented in figure 21 for Z-, hat-, and Y-stiffened panels are useful. These charts were taken from the references listed in table 7.

Toward the right-hand sides of these charts the value of $\bar{\sigma}_{co}$ corresponding to specified values of $N/L'$ approaches the optimum indicated in figure 20. As the value of $N/t_s$ decreases, however, the stress level decreases and some weight penalty is incurred.

It is interesting to note in figure 21 that since the ordinate represents $\bar{\sigma}_{co} = N/\bar{t}$ and the abscissa is $N/t_s$, secants drawn from the origin represent lines of constant values of $t_s/\bar{t}$. Micks (ref. 30) has considered this problem in somewhat greater detail by cross-plotting charts such as figure 21 in the form of figure 20 for specified values of $t_s/\bar{t}$. From this, he is able to estimate the weight penalty associated with designs based on specified values of $t_s/\bar{t}$.

## Geometric Proportions

For panels of optimum design, it is assumed that local buckling of all the cross-sectional elements occurs simultaneously with failure of the panel in the Euler mode. Consequently, it is possible to estimate various geometric parameters of the panel.

The effective thickness of the panel can be obtained directly from equation (32):

$$\bar{t}_o = \frac{1}{\alpha_p}\left(NL'/\bar{\tau}E\right)^{1/2} \tag{35}$$

The $b/t_s$ ratio of the skin follows from the familiar plate-buckling equation for $k = 4$ and $\nu = 0.3$

$$\left(b_s/t_s\right)_o = 3.62\bar{\tau}E/\bar{\sigma}_{co} \tag{36}$$

From equation (34), for $k = 4$ and $\nu = 0.3$,

$$\left(\rho/\bar{t}\right)_o = 0.167\alpha_p{}^2 b_s/t_s \tag{37}$$

By substituting equation (36) into equation (37),

$$(\rho/\bar{t})_o = 0.605\alpha_p^{2}\bar{\tau}E\,\bar{\sigma}_{co} \tag{38}$$

Micks has presented formulas for determining the cross-sectional properties of panels required to satisfy specified values of $(\rho/\bar{t})_o$ (ref. 30).

## Inelastic Buckling

A comparison of the values of $\bar{\tau}$ obtained from tests on 2024-T3 aluminum-alloy hat-, Y-, and Z-stiffened panels with the theoretical values of $\bar{\tau} = (E_s/E)(E_t/E_s)^{1/2}$ as given in equation (34) is shown in figure 22, which is taken from reference 26. A typical stress-strain curve for 2024-T3 aluminum alloy having a compressive yield strength of 44 ksi was used to find the values of $E_t/E$, $E_s/E$, and the theoretical value of $\bar{\tau}$. Since the proportional-limit stress of the typical stress-strain curve appeared to be somewhat higher than the stress at which the curves of $\bar{\sigma}_{co}$ against $N/L'$ departed from a linear relationship in figure 20, a nondimensional representation was used in figure 22. The abscissa represents values of $\bar{\sigma}/\bar{\sigma}_{pl}$ where $\bar{\sigma}_{pl}$ is the stress at which the curves depart from a straight-line relationship on the plot of $\bar{\sigma}_{co}$ against $N/L'$.

Within the limitations imposed by the lack of precise stress-strain data for the stiffened panels, it appears that satisfactory correlation is obtained between test data and the theoretical value of $\bar{\tau}$. However, it is of interest to consider possible reasons for the apparent low value of $\bar{\sigma}_{pl}$ of the riveted panels.

One cause may be associated with the stress concentrations at the rivet holes in a built-up structure resulting in an apparent lowering of the proportional limit. This phenomenon has been observed in other built-up structures such as stiffened cylinders. A second cause may be attributed to wrinkling or forced-crippling failures of the panels. The Z-stiffened panels are particularly suspect in this regard and there is some additional evidence to be presented in the following discussion which supports this contention.

It is to be noted that both of these reasons are associated with riveted structures. Therefore, it may be expected that the value of $\bar{\tau}$ given by equation (34) would apply directly to a monolithic structure without any uncertainties concerning the effective proportional limit.

## Generalizations for Other Materials

Since most of the available data are for riveted stiffened panels, however, it is pertinent to consider methods of generalizing the results on optimum panels of one material to panels of other materials. Such methods have been considered by Younger (ref. 31), Micks (ref. 30), and Schnitt, Brull, and Wolko (ref. 32). The following procedure is based on the results of optimum-panel theory as given by equation (32).

According to the principles of buckling similitude discussed by Steinbacher and Gerard (ref. 33), the buckling-stress equation can be written so that the physical-property parameters can be equated to the geometric and loading parameters of the problem. Thus, from equation (32) for the optimum stiffened panel:

$$\bar{\sigma}_{co} \Big/ (\bar{\tau}E)^{1/2} = \alpha_p (N/L')^{1/2} \tag{39}$$

To compare panels of the same type of construction, the panel efficiency coefficient is constant and therefore

$$\frac{\left[\bar{\sigma}_{co} \Big/ (\bar{\tau}E)^{1/2}\right]_1}{\left[\sigma_{co} \Big/ (\bar{\tau}E)^{1/2}\right]_2} = \frac{(N/L')_1}{(N/L')_2} \tag{40}$$

Further, since it is desired to compare optimum stiffened panels at the same value of $N/L'$, set $(N/L')_1 = (N/L')_2$ in equation (40) with the result

$$\left[\bar{\sigma}_{co} \Big/ (\bar{\tau}E)^{1/2}\right]_1 = \left[\bar{\sigma}_{co} \Big/ (\bar{\tau}E)^{1/2}\right]_2 \tag{41}$$

It is convenient to solve this problem on plots such as those of figure 23 where $(\bar{\tau}E)^{1/2}$ is plotted as a function of $\bar{\sigma}_{co}$. Here, secants drawn from the origin represent constant values of $(\tau E)^{1/2} \Big/ \bar{\sigma}_{co}$ and hence $\left[\alpha_p (N/L')^{1/2}\right]^{-1}$, according to equation (39).

In figure 23(a), theoretical and test results on optimum Z-stiffened panels of 2024-T3 and 7075-T6 aluminum alloys are compared. The lines marked theory are from $\bar{\tau}$ values computed from typical stress-strain curves according to equation (34). The points represent data as

computed from figure 20(a). The curve for the 7075-T6 panels derived from the test data on 2024-T3 panels was obtained by ratioing stress levels along a secant as follows:

$$\bar{\sigma}_{exp_{75}} = \bar{\sigma}_{exp_{24}}\left(\bar{\sigma}_{th_{75}}/\sigma_{th_{24}}\right) \tag{42}$$

The subscripts exp and th refer to experiment and theory, respectively, and the subscripts 75 and 24 are derived from the alloy designations.

It can be observed that the agreement between the derived curve for 7075-T6 aluminum alloy and the corresponding test data is not good. However, when this method was applied to the optimum Y-stiffened panels shown in figure 23(b), relatively good agreement was obtained. This difference in the degree of correlation between the Z- and Y-stiffened panels is attributed to wrinkling or forced crippling of the Z-stiffened panels. This failure mode was not accounted for in deriving equation (32) and consequently the discrepancy may be attributed to this factor.

It is to be noted that in deriving the theoretical value of $\bar{\tau}$ for the 7075-T6 aluminum-alloy Y-stiffened panels, it was necessary to account for a fairly large difference in properties of the Alclad sheet and extruded stiffeners. This was accomplished by using the root mean square of the $\bar{\tau}$ values computed individually for the sheet and stiffener.

## STIFFENED-PANEL BOX CONSTRUCTION

The material presented in the preceding sections has been concerned with the compressive strength of isolated stiffened panels. In aircraft construction, of course, such panels are an integral portion of wing and tail structures and are formed by the use of spars and ribs to subdivide the compression cover. Consequently, it is of importance to investigate the influence of the boundary restraints provided by the spar and rib supporting structure as well as lateral pressure loads on the strength of stiffened panels as used in box structures. These factors are considered in this section.

The column-strength relationships for stiffened panels presented in the sections "Column Strength of Stiffened Panels" and "Optimum Stiffened Panels" indicate that the strength is inversely related to the effective column length. Thus, the use of a lateral supporting structure consisting of ribs or formers provides an effective means of obtaining higher panel strength with an accompanying increase in structural efficiency.

From the standpoint that the ribs act solely to stabilize the compression cover, it is possible to derive rib-stiffness criteria based on certain simplifying assumptions. However, in an aircraft wing the rib structure plays an additional role in transmitting the airloads to the spars. Thus, since the airloading and compressive loading on the cover are related, it is generally necessary to include strength considerations in the rib design in addition to the stiffness requirements for general stability.

In tests of aircraft wing structures, effective column lengths different from the rib spacing have been observed. Some of the most likely causes for this behavior are the following:

(1) General instability of the compression surface

(2) Torsional restraint provided by the rib structure

(3) Continuity of the stiffener over the rib structure

(4) Lateral airload effects on the panel

(5) Presence of spars at the unloaded panel edges resulting in orthotropic plate behavior

(6) Membrane effects caused by interspar curvature of the panel

The above factors are considered in the present section.

## Stabilization of Compression Cover

The rib structure of a wing or tail provides the primary means of stabilizing the compression surface. In order to avoid general instability of this surface, certain flexural-stiffness requirements must be satisfied by the rib structure. If these requirements are met, the effective length of the stiffened panel corresponds to the rib spacing. Continuity of the panel over the rib structure as well as the torsional rigidity of the ribs can provide restraints which further decrease the effective panel length.

Thus the design of the rib structure to achieve a desired value of end-fixity coefficient at the loaded edges of a stiffened panel entails certain flexural- and torsional-stiffness requirements. These requirements have been considered in certain idealized cases: Budiansky, Seide, and Weinberger (ref. 34) treated the buckling of a single column supported by 1, 2, 3, and an infinite number of equally spaced deflectional and rotational springs; Zahorski (ref. 35) analyzed the buckling of a grid of columns supported by 1, 2, 3, and an infinite number of

equally spaced flexural-type lateral stiffeners of various torsional rigidities. For plates, Budiansky and Seide (ref. 36) considered buckling of a simply supported plate resting on an infinite number of equally spaced flexural-type lateral stiffeners of various torsional rigidities.

An analysis of these references indicated that the results for a single column, grid of columns, or simply supported plate of aspect ratio less than 0.20 can be reduced to a unique functional relationship for the case of an infinite number of lateral stiffeners (practically, three or more) of zero torsional rigidity (ref. 26). This relationship is shown in figure 24(a) which shows the end-fixity coefficient e in terms of the stiffness parameter $KL^3/B$.

The definition of the terms in the stiffness parameter for various cases is as follows: The grid of columns (ref. 35):

$$B = (\tau EI)_{st}/b_{st} \tag{43}$$

The plate (ref. 36):

$$B = \eta Et^3/12(1 - \nu^2) \tag{44}$$

The flexural-type lateral stiffener with hinged ends (refs. 35 and 37):

$$K = \pi^4(EI)_r/w^4 \tag{45}$$

The flexural-type lateral stiffener with clamped ends (ref. 37):

$$K = 500(EI)_r/w^4 \tag{46}$$

The shear-type lateral stiffener (ref. 37):

$$K = \pi^2 C_r/w \tag{47}$$

The effective spring constants K of the various types of rib structures have been considered by Langhaar in reference 37. The values given by equations (45) to (47) are from this paper.

The application of these results to stiffened-panel—rib construction requires consideration of the behavior of the panel. Grid action is approached as a limiting case for panels composed of heavy stiffeners and very thin skins; in the other limit of thick skins with light stiffeners, plate behavior is approached. Since the results for these two cases coincide when given in terms of the parameters of figure 24(a), it is assumed that figure 24(a) can be used also for stiffened panels. The value of B for a stiffened panel can be obtained from the following column relationship:

$$N = \pi^2 \bar{EI} / (L')^2 b_{st} \tag{48}$$

By letting

$$B = \bar{EI} / b_{st} \tag{49}$$

Then combining equations (48) and (49)

$$B = N(L')^2 / \pi^2 \tag{50}$$

The results given in figure 24(a) assume that a large number of lateral stiffeners of zero torsional rigidity are used. In applying these results to develop a rib-stiffness criterion, it is assumed that the tension surface of the wing does not contribute to the effective spring constant of the rib. For formers (partial-depth ribs) this assumption is valid, although for ribs attached to the tension surface this assumption will be conservative.

## General Instability

For the purpose of avoiding general instability, a suitable design criterion for the rib given in reference 26 is based on the requirement that the ribs of zero torsional rigidity possess sufficient flexural rigidity to achieve an end-fixity coefficient of unity. From figure 24(a) it can be observed that effectively rigid ribs are obtained when

$$KL^3/B = 4\pi^2 \tag{51}$$

In fact, any increase in the value of $KL^3/B$ beyond that given by equation (51) does not result in any increase in end-fixity coefficient for ribs of zero torsional rigidity.

By combining equations (51), (50), (45), and (46), the following minimum rib-flexural-rigidity criteria are obtained for an end-fixity coefficient of $e = 1$: Ribs with hinged ends:

$$(EI)_r = 4\left(\frac{w}{\pi}\right)^4 \frac{N}{L} \tag{52}$$

Ribs with clamped ends:

$$(EI)_r = \frac{w^4}{125} \frac{N}{L} \tag{53}$$

Flexural-type ribs with elastic restraint at the ends will have stiffness requirements intermediate to the value given by equations (52) and (53). For shear-type rib structures, by combining equations (51), (50), and (47), the minimum shear rigidity is obtained:

$$C_r = 4\left(\frac{w}{\pi}\right)^2 \frac{N}{L} \tag{54}$$

## Rotational-Stiffness Considerations

The analysis of the previous section indicates the rib minimum-flexural-rigidity requirements necessary to avoid general instability of a compression cover-supporting structure composed of many ribs of zero torsional rigidity. It is evident from figure 24(a) that once the ribs have sufficient flexural rigidity to achieve an end-fixity coefficient of unity, no further increase in fixity can be obtained by increasing the flexural rigidity. Further increases can only be obtained by the rotational restraints provided by the rib structure for the stiffened panel continuous over this rib structure. The restraint is generally characterized by a rotational spring constant $\theta$.

Many investigations have considered the influence of rotational restraints provided by intermediate lateral supports on the instability of continuous columns, grids of columns, and simply supported plates (see, e.g., refs. 34-39). The details of the individual analyses are summarized in table 9 and reference to these papers is suggested where such details may be of importance.

In general, however, it is possible to represent the significant aspects of these analyses by considering a panel with many intermediate

supports (practically, three or more) of overall aspect ratio $L/w < 0.20$. In this case, the results apply to columns, grids of columns, and plates and can be assumed to apply to stiffened panels by using the stiffness value defined by equations (49) and (50).

In figure 24(b), the end-fixity coefficient e is presented as a function of the deflectional spring stiffness parameter $KL^3/B$ and the rotational spring stiffness parameter $\theta L/B$. It can be observed that once the minimum value of $KL^3/B$ needed to avoid general instability is achieved, no further increase in e is obtained with increases in $KL^3/B$. This region is denoted as an effectively rigid deflectional spring system.

In figure 25, the characteristics of the effectively rigid deflectional spring system are presented in terms of the rotational-restraint parameter $\theta L/B$. For a given value of $\theta L/B$, the end-fixity coefficient and the minimum value of $KL^3/B$ for an effectively rigid system may be determined. Also shown are the values of $KL^3/B$ needed to achieve an end-fixity coefficient of $e = 1$ in the presence of rotational restraints.

## Lateral-Pressure Effects

Stiffened panels under combined compressive and pressure loads with free unloaded edges were investigated experimentally by McPherson, Levy, and Zibritosky (ref. 40) at a pressure up to 16 psi. This work indicated that a simple correction to account for the reduction in strength of the panel due to pressure effects could be evaluated from the following semi-empirical equation:

$$\bar{\sigma}_p = \bar{\sigma}_{co}\left(1 - 0.39qL^3/B\right) \tag{55}$$

In equation (55), B is the bending stiffness of the panel per chordwise inch including the actual area of sheet (not effective area) and $\bar{\sigma}_{co}$ is the panel strength under compression only as determined from the section "Column Strength of Stiffened Panels."

Unfortunately, there are no other published data on the effects of lateral pressure on the strength of stiffened panels. While equation (55) does provide some information, it is of little use for panel applications where the rib and spar structures can help to develop significant membrane effects in the panel under lateral-pressure loads.

In addition to the reduction of panel strength, the airloads impose certain strength requirements on the rib structure. These requirements are in addition to the deflectional and rotational stiffness considerations

discussed previously. For a brief presentation of rib-strength requirements, refer to references 26 and 41.

## Influence of Spars

In stiffened-panel tests, the unloaded edges are generally unsupported and therefore the panel acts as a wide orthotropic column. In a wing or tail structure, spars are generally located at the unloaded edges. Consequently, the influence of the edge support provided by the spars upon the panel strength may be of importance in certain cases.

If the overall aspect ratio of the panel in a box structure formed by the rib and spar structure is somewhat less than unity, then the panel usually acts as a wide column. In such cases, the results of panel tests can be applied directly to the wing structure.

When the panel aspect ratio approaches or exceeds unity, particularly for thick-skin panels, the stiffened panel behaves as an orthotropic plate in the box structure. In such cases, the results of panel tests may be conservative and it is necessary to use orthotropic plate theory to determine the increased compressive strength of the panel with unloaded-edge support.

Sandorff (ref. 38) has treated this problem briefly. More complete results can be obtained by utilizing figure 10 of Part II of this Handbook (ref. 16). These charts indicate the compressive-buckling coefficients of simply supported flat plates with a large number of stiffeners. In estimating the flexural stiffness of the stiffened panel required for use of these charts, equations (48) to (50) may be used.

In addition to the unloaded-edge support provided by the spars, further increases in panel strength in a box structure may result from interspar curvature of the panel. Such strength increases are associated with the membrane effects contributed by the spar structure and are not from the curvature of the panel itself. The curvatures considered here generally do not result in any significant increase in strength of the panel when tested with free unloaded edges.

Langhaar (ref. 42) has considered this problem by treating the compression surface of a cambered wing between ribs as an orthotropic curved plate with rotational restraints at the loaded edges. The ribs were assumed to be an effectively rigid deflectional system.

The theory developed was checked against several idealized beam tests with good agreement. It is significant that end-fixity coefficients up to 3 were realized for cambered beams whereas $e = 1$ was obtained for corresponding beams with flat covers.

## Optimum Construction

Optimum forms of stiffened-panel construction are considered in some detail in reference 26. Information on optimum rib spacing and the efficiency of stiffened-panel construction relative to other forms of construction is presented.

Research Division, College of Engineering,
New York University,
New York, N. Y., April 17, 1956.

# APPENDIX A

## APPLICATION SECTION

The results of this part of the Handbook of Structural Stability that may be of importance from the standpoint of analysis and design are summarized in this section

### Crippling Strength

The generalized crippling analysis of reference 1 has been extended to monolithic stiffened panels in the sections entitled "Crippling Strength of Panels With Formed Stiffeners" and "Crippling Strength of Panels With Extruded Stiffeners." In doing so, the results obtained in reference 1 on individual elements have been combined with the stiffened-panel analysis.

Angle-type elements.- The crippling strength of sections composed of a series of two adjacent elements which meet at a junction is given by

$$\frac{\overline{\sigma}_f}{\sigma_{cy}} = \beta_g \left[ \frac{gt^2}{A} \left( \frac{\overline{\eta} E}{\sigma_{cy}} \right)^{1/2} \right]^{0.85} \tag{A1}$$

where $g$ is the number of cuts plus flanges as discussed in the section "Crippling Strength of Panels With Extruded Stiffeners" and illustrated in figures 6 and 8. The appropriate values of $\beta_g$ are given in table 4 and figure 10.

For stiffened panels, the quantity $A/t^2$ in equation (A1) is to be replaced by $A/t_w t_s$. For complex stiffener shapes such as Y-sections, a weighted value of $\overline{t}_w$ should be used as defined by equation (7). In cases where the sheet properties are different from those of the stiffener, a weighted value of $\overline{\sigma}_{cy}$ defined by equation (8) should be used.

T-type elements.- Extruded sections composed of a series of three or more elements which meet at a common juncture (e.g., T- or H-sections) are referred to as T-type elements. The crippling strength of such sections is given by

$$\frac{\overline{\sigma}_f}{\sigma_{cy}} = 0.67 \left[ \frac{gt^2}{A} \left( \frac{E}{\sigma_{cy}} \right)^{1/2} \right]^{0.40} \tag{A2}$$

Equation (A2) is valid for $\bar{\sigma}_f/\sigma_{cy} \leqq 3/4$. Beyond this value equation (6) holds true:

$$\bar{\sigma}_f = \sigma_{cr} \tag{6}$$

Short riveted panels.- Short riveted panels can have strengths lower than the monolithic crippling strengths as a result of interrivet buckling and wrinkling or forced crippling. The strength of panels with interrivet buckling may be determined from equations (10) and (11) and table 5.

The strength of panels with forced crippling is given by equations (16) to (19) and (23).

## Column Strength of Panels

The column strength of stiffened panels is treated in the section by that name. For columns in the Euler range, equations (26) and (27) apply. In the length range intermediate to the Euler and crippling ranges, equations (28) or (31) may be satisfactory.

The pertinent NACA reports containing direct-reading column charts for hat, Y-, and Z-stiffened panels are listed in table 6.

Panels of optimum design for minimum weight are considered in the section "Optimum Stiffened Panels." The efficiency of various stiffener shapes is given in table 8 and figure 20. Panels with a specified skin thickness are presented in figure 21. Methods of generalizing test results to panels of other materials are shown in figure 23.

## Box Construction

Rib-stiffness criteria necessary to avoid general instability of transversely stiffened panels are given by equations (52) to (54). The end fixity contributed by the continuity of the panel over ribs possessing rotational restraints is presented in figures 24 and 25. Lateral-pressure effects and the side support contributed by the spar structure are also considered in the section "Stiffened Panel Box Construction."

## REFERENCES

1. Gerard, George: Handbook of Structural Stability. Part IV - Failure of Plates and Composite Elements. · NACA TN 3784, 1957.

2. Gallaher, George L., and Boughan, Rolla B.: A Method of Calculating the Compressive Strength of Z-Stiffened Panels That Develop Local Instability. NACA TN 1482, 1947.

3. Dow, Norris F., Hickman, William A., and Rosen, B. Walter: Data on the Compressive Strength of Skin-Stringer Panels of Various Materials. NACA TN 3064, 1954.

4. Dow, Norris F., and Hickman, William A.: Effect of Variation in Rivet Diameter and Pitch on the Average Stress at Maximum Load for 24S-T3 and 75S-T6 Aluminum-Alloy, Flat, Z-Stiffened Panels That Fail by Local Instability. NACA TN 2139, 1950.

5. Hickman, William A., and Dow, Norris F.: Compressive Strength of 24S-T Aluminum-Alloy Flat Panels With Longitudinal Formed Hat-Section Stiffeners Having Four Ratios of Stiffener Thickness to Skin Thickness. NACA TN 1553, 1948.

6. Semonian, Joseph W., and Peterson, James P.: An Analysis of the Stability and Ultimate Compressive Strength of Short Sheet-Stringer Panels With Special Reference to the Influence of Riveted Connection Between Sheet and Stringer. NACA TN 3431, 1955.

7. Dow, Norris F., and Hickman, William A.: Design Charts for Flat Compression Panels Having Longitudinal Extruded Y-Section Stiffeners and Comparison With Panels Having Formed Z-Section Stiffeners. NACA TN 1389, 1947.

8. Howland, W. Lavern: Effect of Rivet Spacing on Stiffened Thin Sheet in Compression. Jour. Aero. Sci., vol. 3, no. 12, Oct. 1936, pp. 434-439.

9. Gerard, George, and Becker, Herbert: Handbook of Structural Stability. Part I - Buckling of Flat Plates. NACA TN 3781, 1957.

10. Levy, Samuel, McPherson, Albert E., and Ramberg, Walter: Effect of Rivet and Spot-Weld Spacing on the Strength of Axially Loaded Sheet-Stringer Panels of 24S-T Aluminum Alloy. NACA TN 856, 1942.

11. Brook, E. A.: Behavior in Compression of Aluminum Alloy Panels Having a Flat Skin With Corrugated Reinforcement. R. & M. No. 2598, British A.R.C., 1945.

12. Dow, Norris F., and Hickman, William A.: Effect of Variation in Diameter and Pitch of Rivets on Compressive Strength of Panels With Z-Section Stiffeners - Panels of Various Lengths With Close Stiffener Spacing. NACA TN 1421, 1947.

13. Dow, Norris F., Hickman, William A., and Rosen, B. Walter: Effect of Variation in Rivet Strength on the Average Stress at Maximum Load for Aluminum-Alloy, Flat, Z-Stiffened Compression Panels That Fail by Local Buckling. NACA TN 2963, 1953.

14. Argyris, J. H., and Dunne, P. C.: Structural Principles and Data, Part 2, Structural Analysis. Handbook of Aero., no. 1, fourth ed; Sir Isaac Pitman & Sons, Ltd. (London), 1952, pp. 179-185.

15. Bijlaard, P. P., and Johnston, G. S.: Compressive Buckling of Plates Due to Forced Crippling of Stiffeners. Preprint No. 408, S.M.F. Fund Paper, Inst. Aero. Sci., Jan. 1953.

16. Becker, Herbert: Handbook of Structural Stability. Part II - Buckling of Composite Elements. NACA TN 3782, 1957.

17. Sechler, Ernest E., and Dunn, Louis G.: Airplane Structural Analysis and Design. John Wiley & Sons, Inc., 1942.

18. Schuette, Evan H.: Charts for the Minimum-Weight Design of 24S-T Aluminum-Alloy Flat Compression Panels With Longitudinal Z-Section Stiffeners. NACA Rep. 827, 1945.

19. Dow, Norris F., Hickman, William A., and McCracken, Howard L.: Compressive-Strength Comparisons of Panels Having Aluminum-Alloy Sheet and Stiffeners With Panels Having Magnesium-Alloy Sheet and Aluminum-Alloy Stiffeners. NACA TN 1274, 1947.

20. Dow, Norris F., and Keevil, Albert S., Jr.: Direct-Reading Design Charts for 24S-T Aluminum-Alloy Flat Compression Panels Having Longitudinal Formed Z-Section Stiffeners. NACA TN 1778, 1949.

21. Hickman, William A., and Dow, Norris F.: Direct-Reading Design Charts for 75S-T6 Aluminum-Alloy Flat Compression Panels Having Longitudinal Extruded Z-Section Stiffeners. NACA TN 2435, 1952.

22. Hickman, William A., and Dow, Norris F.: Direct-Reading Design Charts for 24S-T3 Aluminum-Alloy Flat Compression Panels Having Longitudinal Formed Hat-Section Stiffeners and Comparisons With Panels Having Z-Section Stiffeners. NACA TN 2792, 1953.

23. Dow, Norris F., Hubka, Ralph E., and Roberts, William M.: Direct-Reading Design Charts for 24S-T Aluminum-Alloy Flat Compression Panels Having Longitudinal Straight-Web Y-Section Stiffeners. NACA TN 1777, 1949.

24. Dow, Norris F., and Hickman, William A.: Direct-Reading Design Charts for 75S-T Aluminum-Alloy Flat Compression Panels Having Longitudinal Straight-Web Y-Section Stiffeners. NACA TN 1640, 1948.

25. Dow, Norris F., and Hickman, William A.: Comparison of the Structural Efficiency of Panels Having Straight-Web and Curved-Web Y-Section Stiffeners. NACA TN 1787, 1949.

26. Gerard, George: Minimum Weight Analysis of Compression Structures. New York Univ. Press (New York), 1956.

27. Zahorski, Adam: Effects of Material Distribution on Strength of Panels. Jour. Aero. Sci., vol. 11, no. 3, July 1944, pp. 247-253.

28. Farrar, D. J.: The Design of Compression Structures for Minimum Weight. Jour. R.A.S., vol. 53, Nov. 1949, pp. 1041-1052.

29. Catchpole, E. J.: The Optimum Design of Compression Surfaces Having Unflanged Integral Stiffeners. Jour. R.A.S., vol. 58, no. 527, Nov. 1954, pp. 765-768.

30. Micks, W. R.: A Method of Estimating the Compressive Strength of Optimum Sheet-Stiffener Panels for Arbitrary Material Properties, Skin Thickness, and Stiffener Shapes. Jour. Aero. Sci., vol. 20, no. 10, Oct. 1953, pp. 705-715.

31. Younger, Dewey G.: The Development of Optimum Design Envelope Curves for Sheet-Stiffener Compression Panels Having Hat, Z, or Y-Section Stiffeners for Various Materials and Temperature Environments. Proc. First Midwestern Conf. on Solid Mech., College of Eng., Univ. of Ill., Apr. 1953, pp. 5-10.

32. Schnitt, Arthur, Brull, Maurice A., and Wolko, Howard S.: Optimum Stresses of Structural Elements at Elevated Temperatures. Paper 56-AV-11, Symposium on Structures for Thermal Flight (Mar. 14-16, 1956, Los Angeles), Aviation Div. Conf., A.S.M.E., 1956.

33. Steinbacher, Franz R., and Gerard, George: Aircraft Structural Mechanics. Pitman Pub. Corp. (New York), 1952, pp. 302-304.

34. Budiansky, Bernard, Seide, Paul, and Weinberger, Robert A.: The Buckling of a Column on Equally Spaced Deflectional and Rotational Springs. NACA TN 1519, 1948.

35. Zahorski, Adam: Efficiency of Lateral Stiffeners in Panels. Jour. Aero. Sci., vol. 11, no. 4, Oct. 1944, pp. 299-306.

36. Budiansky, Bernard, and Seide, Paul: Compressive Buckling of Simply Supported Plates With Transverse Stiffeners. NACA TN 1557, 1948.

37. Langhaar, H. L.: Parallel Columns With Common Lateral Supports. Jour. Appl. Mech., vol. 12, no. 4, Dec. 1945, pp. A-253 - A-256.

38. Sandorff, Paul E.: Notes on Columns. Jour. Aero. Sci., vol. 11, no. 1, Jan. 1944, pp. 1-12.

39. Tu, Shou-Ngo: Column With Equal-Spaced Elastic Supports. Jour. Aero. Sci., vol. 11, no. 1, Jan. 1944, pp. 67-72, 75.

40. McPherson, A. E., Levy, Samuel, and Zibritosky, George: Effect of Normal Pressure on Strength of Axially Loaded Sheet-Stringer Panels. TN 1041, 1946.

41. Shanley, Francis Reynolds: Weight-Strength Analysis of Aircraft Structures. First ed., McGraw-Hill Book Co., Inc., 1952, pp. 159-173.

42. Langhaar, Henry L.: Stability of Semimonocoque Wing Structures. Jour. Aero. Sci., vol. 13, no. 3, Mar. 1946, pp. 119-125.

43. Dow, Norris F., and Hickman, William A.: Effect of Variation in Diameter and Pitch of Rivets on Compressive Strength of Panels with Z-Section Stiffeners. Panels of Various Stiffener Spacings That Fail by Local Buckling. NACA TN 1467, 1947.

44. Dow, Norris F., and Hickman, William A.: Effect of Variation in Diameter and Pitch of Rivets on Compressive Strength of Panels with Z-Section Stiffeners. Panels that Fail by Local Buckling and Have Various Values of Width-to-Thickness Ratio for the Webs of the Stiffeners. NACA TN 1737, 1948.

TABLE 1

NACA CRIPPLING-STRENGTH TEST DATA ON Z-STIFFENED PANELS

| Reference | Material | $t_w/t_s$ variation | Figure | Remarks |
|---|---|---|---|---|
| TN 1482 (ref. 2) | 2024-T3 | 1.00, 0.79, 0.63, 0.51 | 1 | Strongly riveted panels |
| TN 3064 (ref. 3) | 7075-T6<br>6061-T6<br>5052-1/4H<br>7075-0<br>SAE 1010<br>Copper<br>FS-1h<br>18-8-3/4H<br>Ti-1/4H | 1.00 | 2 | Data for panels identified as 25-50-20 and 37.5-75-20 used since other panels indicated evidence of wrinkling |
| TN 2139 (ref. 4) | 2024-T3<br>7075-T6 | 1.00, 0.63 | 3 | Potential-strength estimates |

TABLE 2

$\beta_c$ VALUES FOR HAT-STIFFENED PANELS

| $t_w/t_s$ | $\beta_c$ |
|---|---|
| 1.25 | 1.42 |
| 1.00 | 1.35 |
| .63 | 1.20 |
| .39 | [a]1.16 |

[a]For $b_s/t_s \leq 50$.

TABLE 3

$\beta_g$ VALUES FOR Y-STIFFENED PANELS;

$g = 18.83$

| $t_w/t_s$ | $\bar{t}_w/t_s$ | $\beta_g$ |
|---|---|---|
| 1.00 | 1.16 | 0.562 |
| .63 | .732 | .505 |
| .40 | .464 | .478 |

TABLE 4

SUMMARY OF EXPERIMENTAL VALUES OF $\beta$ FOR ANGLE- AND T-TYPE ELEMENTS AND STIFFENED PANELS

| Element | c | $t_w/t_s$ | $\beta_c$ | g | $t_w/t_s$ | $\beta_g$ |
|---|---|---|---|---|---|---|
| Angle-type element; m = 0.85 | | | | | | |
| V-groove plates | ------ | ----- | ------- | 3 | ------ | [a] 0.558 |
| Extruded angles | ------ | ----- | ------- | 2 | ------ | [a] .558 |
| Extruded tubes | 4 | ----- | [a] 1.42 | 12 | ------ | [a] .558 |
| Formed multicorner sections | 3 to 8 | ----- | [a] 1.30 | [b] 3c-1 | ------ | [a,c] .55 |
| Formed Z-stiffened panels | 3 | ----- | 1.26 | 7.83 | ------ | .558 |
| Formed hat panels | 6 | 1.25 | [d] 1.42 | 16.83 | 1.25 | [d] .591 |
| | | 1.00 | [d] 1.36 | | 1.00 | [d] .561 |
| | | .63 | [d] 1.20 | | .63 | [d] .499 |
| | | .39 | [d,e] 1.16 | | .39 | [d,e] .483 |
| Extruded Y-stiffened panels | ------ | ----- | ------- | 18.83 | [f] 1.16 | .562 |
| | | | | | [f] .732 | .505 |
| | | | | | [f] .464 | .478 |
| T-type element; m = 0.40 | | | | | | |
| Extruded T-section | ------ | ----- | ------- | 3 | ------ | [a] .670 |
| Extruded cruciform | ------ | ----- | ------- | 4 | ------ | [a] .670 |
| Extruded H-section | ------ | ----- | ------- | 7 | ------ | [a] .670 |

[a] For $\bar{\sigma}_f/\sigma_{cy} \leqq 3/4$.

[b] c is number of corners.

[c] Average value.

[d] For $\bar{\sigma}_f/\sigma_{cy} \leqq 0.8$.

[e] For $b_s/t_s \leqq 50$.

[f] $\bar{t}_w/t_s$ value.

TABLE 5

END-FIXITY COEFFICIENTS FOR INTERRIVET BUCKLING

| Fastener type | e | Reference |
|---|---|---|
| Flathead rivet | 4 | 8 |
| Spotwelds | 3.5 | 10 |
| Brazier-head rivet | 3 | 10 |
| Countersunk rivet | 1 | 11 |

TABLE 6

NACA DIRECT-READING COLUMN CHARTS FOR ALUMINUM-ALLOY STIFFENED PANELS

| Stiffener | Material | Type of column chart (a) | Reference |
|---|---|---|---|
| Z-formed | 2024-T3 | A | Report 827 (ref. 18) |
| | | B, C | TN 1778 (ref. 20) |
| Z-extruded | 7075-T6 | B, C | TN 2435 (ref. 21) |
| Hat-formed | 2024-T3 | B, C | TN 2792 (ref. 22) |
| Y-extruded | 2024-T3 | A | TN 1389 (ref. 7) |
| | | B, C | TN 1777 (ref. 23) |
| Y-extruded | 7075-T6 | A | TN 1389 (ref. 7) |
| | | B, C | TN 1640 (ref. 24) |
| Curved Y-extruded | 7075-T6 | A, B, C | TN 1787 (ref. 25) |

[a] A, presentation of $\sigma_{co}$ against $N/L'$; B, presentation of $N/t_s$ against $N/L'$; C, presentation of $\bar{\sigma}_{co}$ against $N/t_s$.

TABLE 7

NACA OPTIMUM-STIFFENED-PANEL DATA

| Stiffener | Aluminum-alloy material | Reference |
|---|---|---|
| Z-formed | 2024-T3 | TN 1389 (ref. 7) |
| Z-extruded | 7075-T6 | TN 2435 (ref. 21) |
| Hat-formed | 2024-T3 | TN 2792 (ref. 22) |
| Y-extruded | 2024-T3 | TN 1389 (ref. 7) |
| Y-extruded | 7075-T6 | TN 1389 (ref. 7) |
| Curved Y-extruded | 7075-T6 | TN 1787 (ref. 25) |

TABLE 8

EXPERIMENTAL VALUES OF PANEL EFFICIENCY COEFFICIENT

| Stiffener | Panel efficiency coefficient, $\alpha_p$ | Farrar's theoretical $\alpha_p$ (ref. 28) |
|---|---|---|
| Z-extruded | 1.02 | 0.95 |
| Hat-formed | .99 | .96 |
| Y-extruded | 1.15 | 1.25 |
| Curved Y-extruded | 1.22 | ---- |

TABLE 9

INVESTIGATIONS OF CONTINUOUS COLUMNS AND PLATES SUPPORTED BY DEFLECTIONAL AND ROTATIONAL SPRINGS

| Reference | Structure | Support and Boundary Conditions[a] |
|---|---|---|
| 38 | Column on rotational spring supports | 2, 3, 4, $\infty$ number of supports of $K = \infty$, $0 \leqq \theta \leqq \infty$; $\theta$ of neighboring supports can be unequal |
| 39 | Column on deflectional spring supports | 1, 2, 3, $\infty$ number of intermediate supports of $0 \leqq K \leqq \infty$, $\theta = 0$; supports at ends of column of $K = \infty$, $\theta = 0$ or $\theta = \infty$ |
| 35 | Grid of columns on simply supported lateral flexural stiffener | 1, 2, $\infty$ number of columns on 1 or 2 lateral stiffeners of $0 \leqq K \leqq \infty$, $0 \leqq \theta \leqq \infty$; supports at ends of columns of $K = \infty$, $0 \leqq \theta \leqq \infty$ |
| | | $\infty$ number of columns on $\infty$ lateral stiffeners of $0 \leqq K \leqq \infty$, $\theta = 0$ |
| 34 | Column on deflectional and rotational spring supports | 1, 2, 3, $\infty$ number of intermediate supports of $0 \leqq K \leqq \infty$, $0 \leqq \theta \leqq \infty$; supports at ends of column of $K = \infty$, $0 \leqq \theta \leqq \infty$ |
| 36 | Plate on simply supported lateral flexural stiffener | Plates of $L/w = 0.50, 0.35, 0.20, <0.20$ on infinitely many supports of $0 \leqq K \leqq \infty$, $0 \leqq \theta \leqq \infty$ |
| 37 | Effective deflectional spring stiffness of various types of ribs | Flexural types of ribs with supports at ends of ribs of $K = \infty$, $0 \leqq \theta \leqq \infty$ |
| | | Shear type of rib |

[a] $K$, deflectional spring stiffness of supports; $\theta$, rotational spring stiffness of supports.

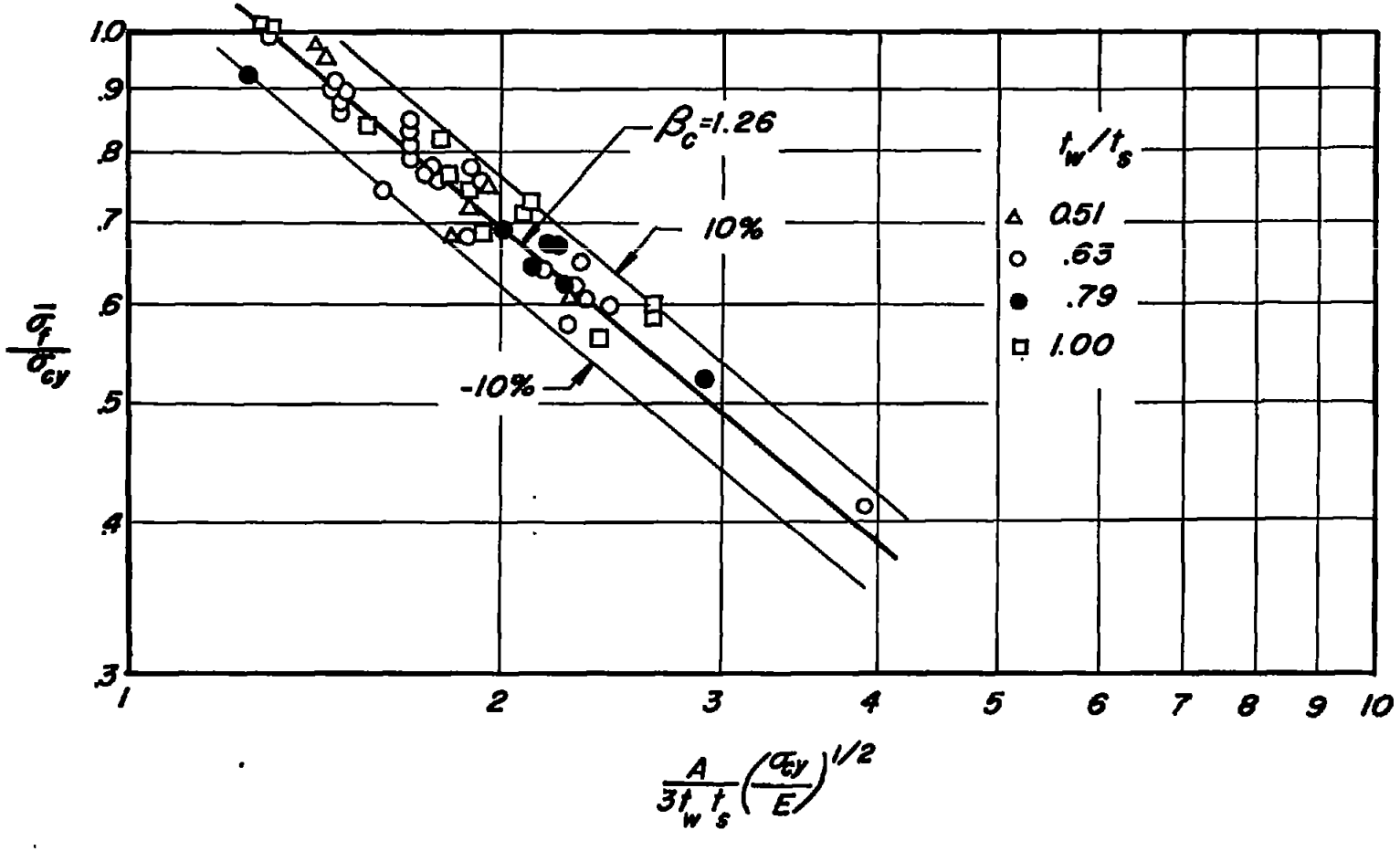


Figure 1.- Crippling data for 2024-T3 aluminum-alloy Z-stiffened panels of reference 2.

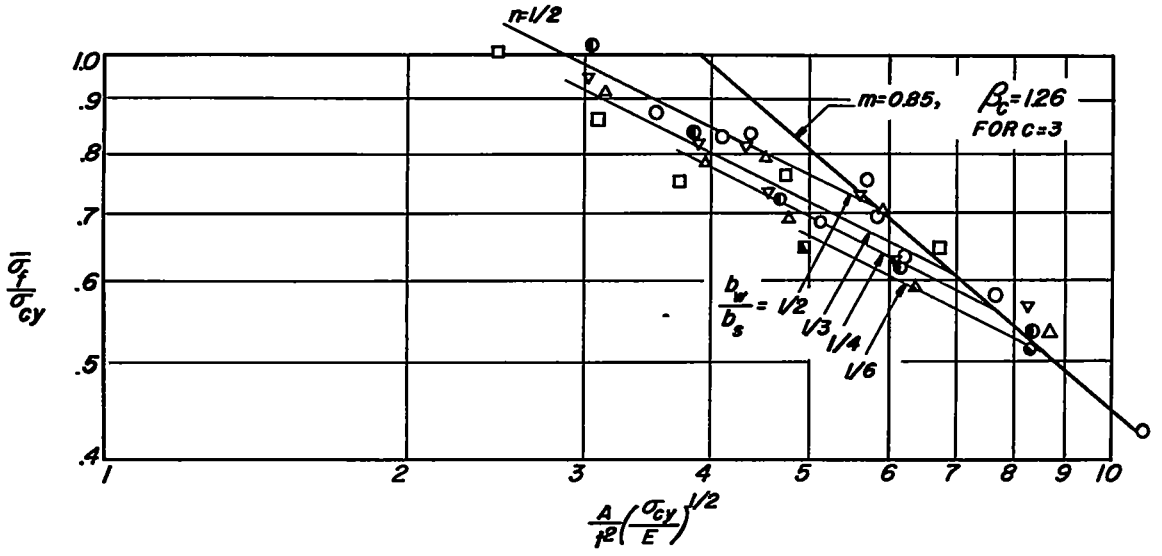


(a) Test data for all panels.

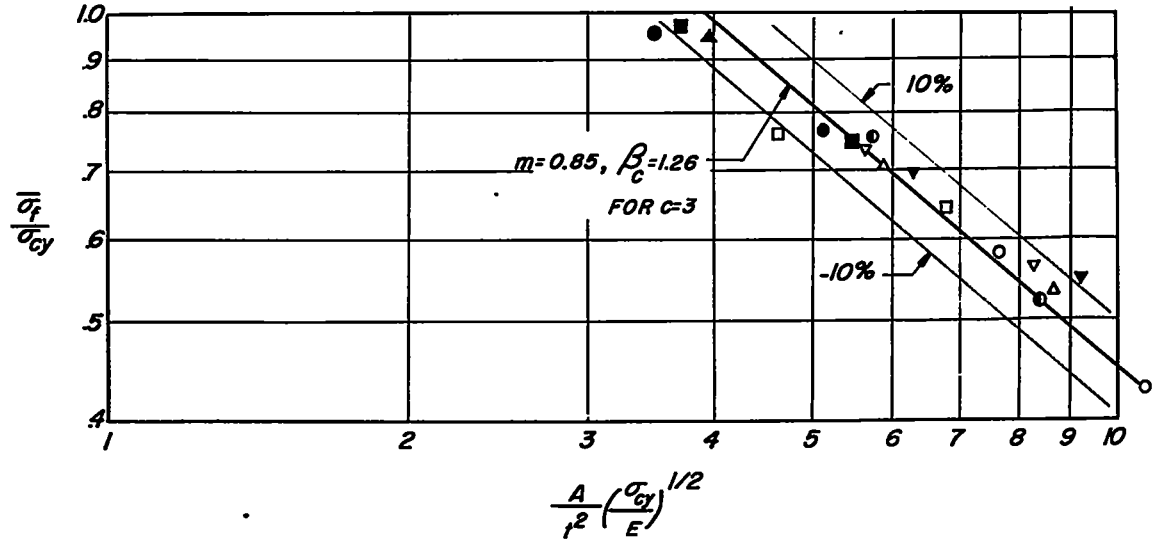


(b) Data for 25-50-20 and 37.5-75-20 panels only (see ref. 3).

Figure 2.- Crippling data for Z-stiffened panels of various materials of reference 3. $t_w/t_s = 1$.

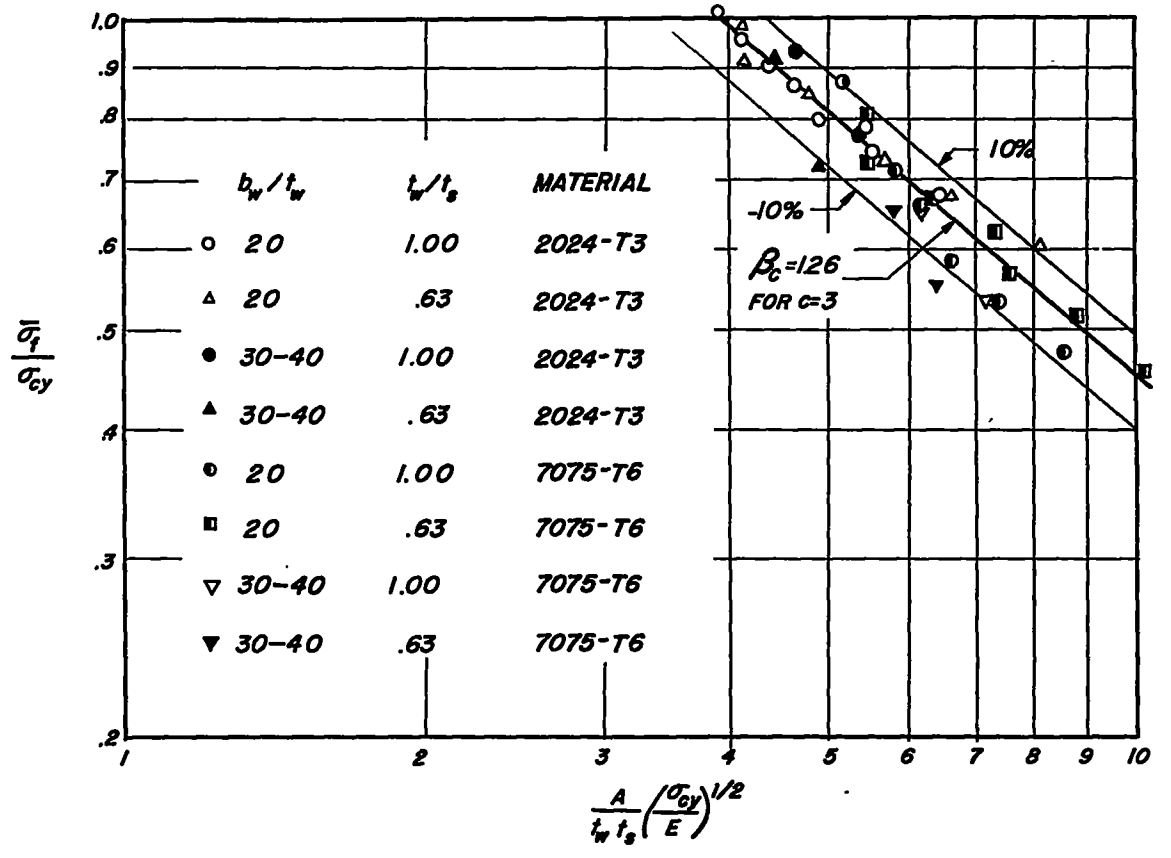


Figure 3.- Potential-strength data for aluminum-alloy Z-stiffened panels of references 4, 43, and 44.

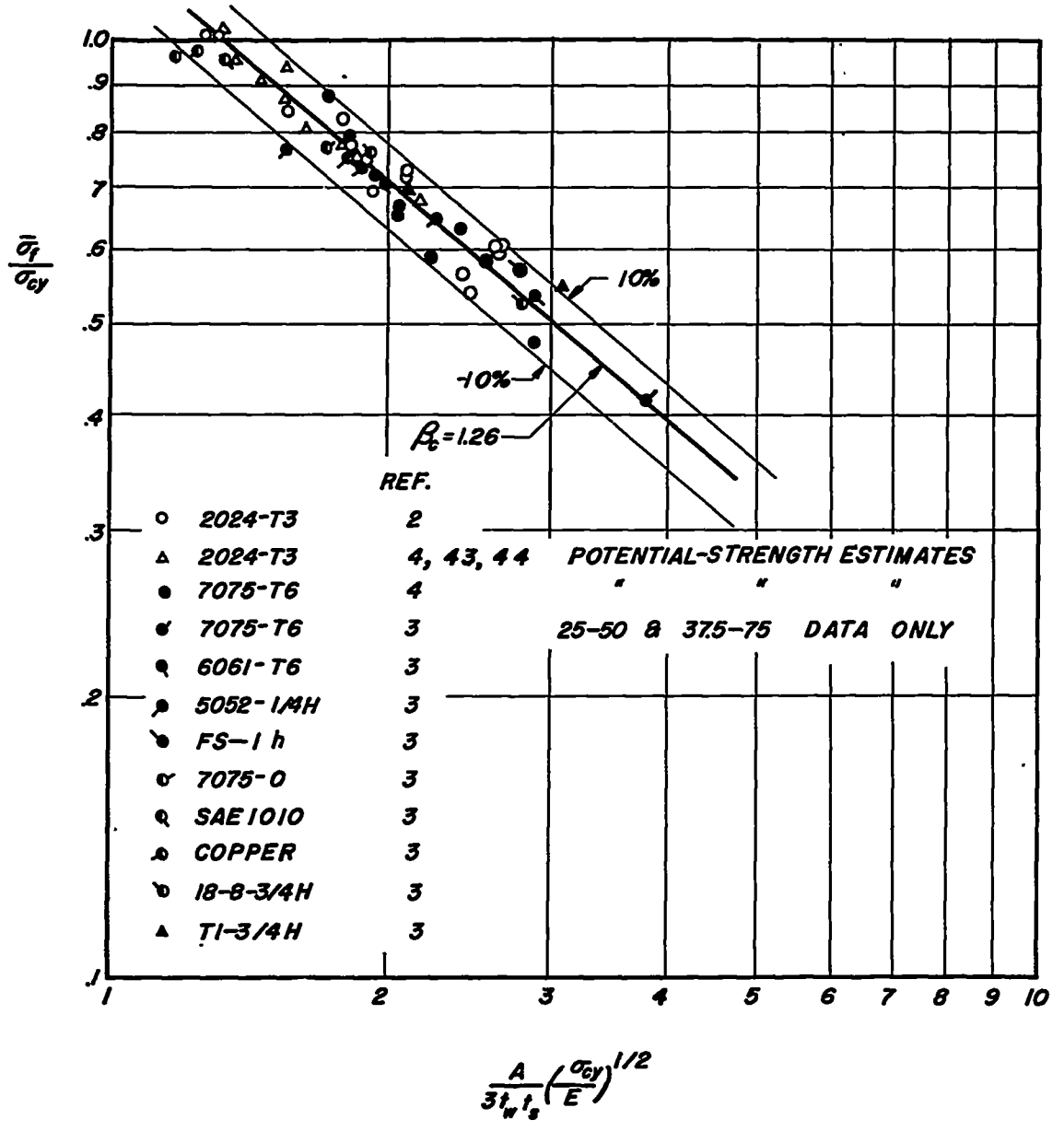


(a) $t_w/t_s = 1.00$.

Figure 4.- Crippling data for Z-stiffened panels.

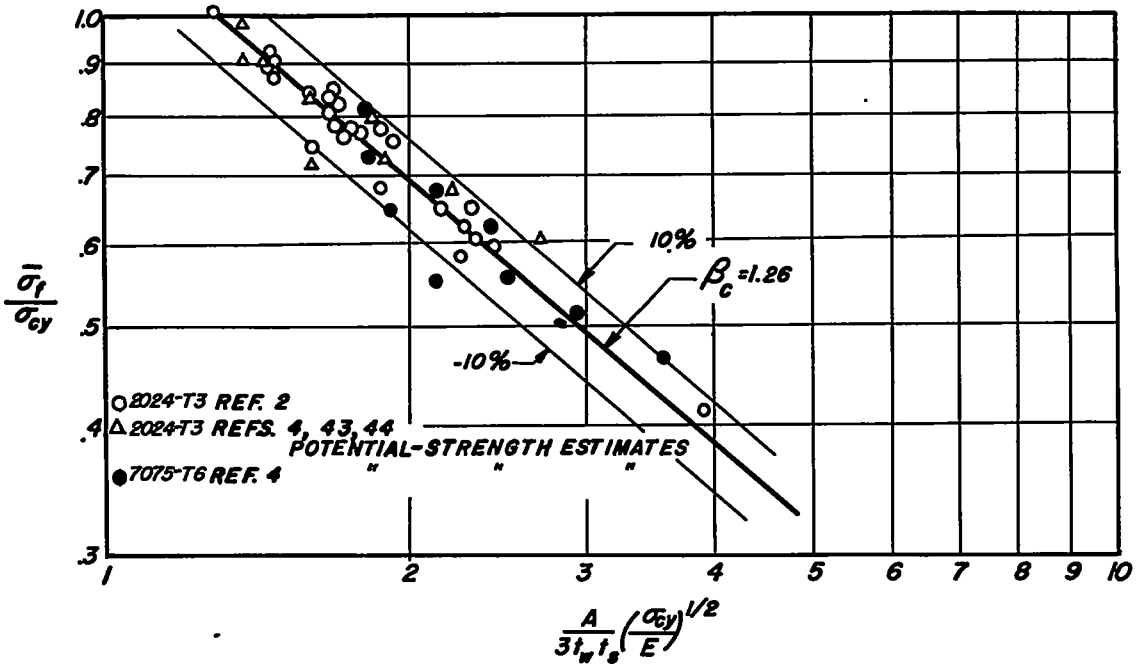


(b) $t_w/t_s = 0.63$.

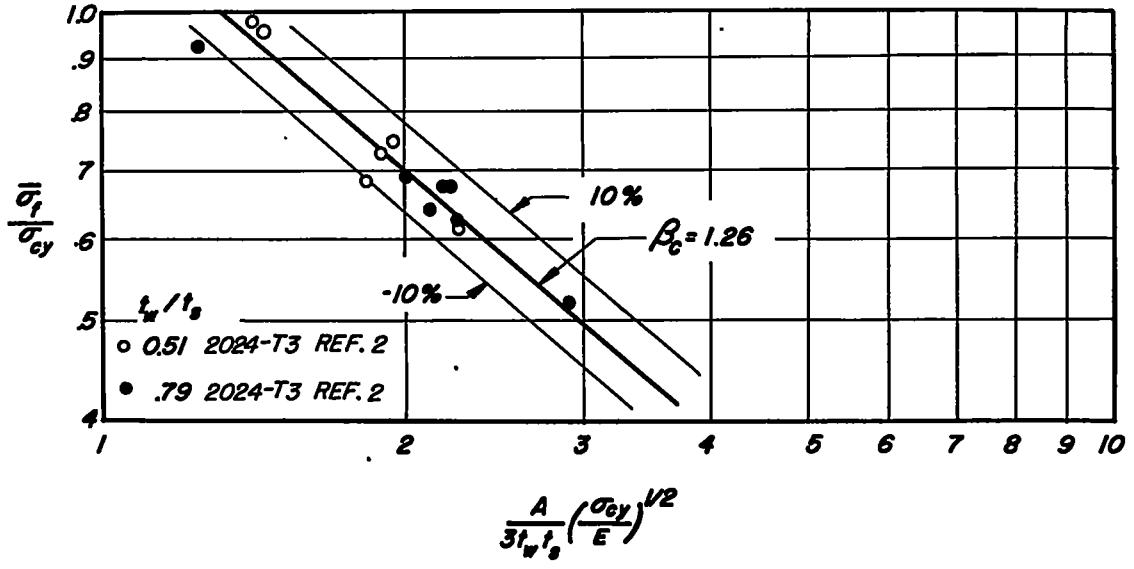


(c) $t_w/t_s = 0.51$ and 0.79.

Figure 4.- Concluded.

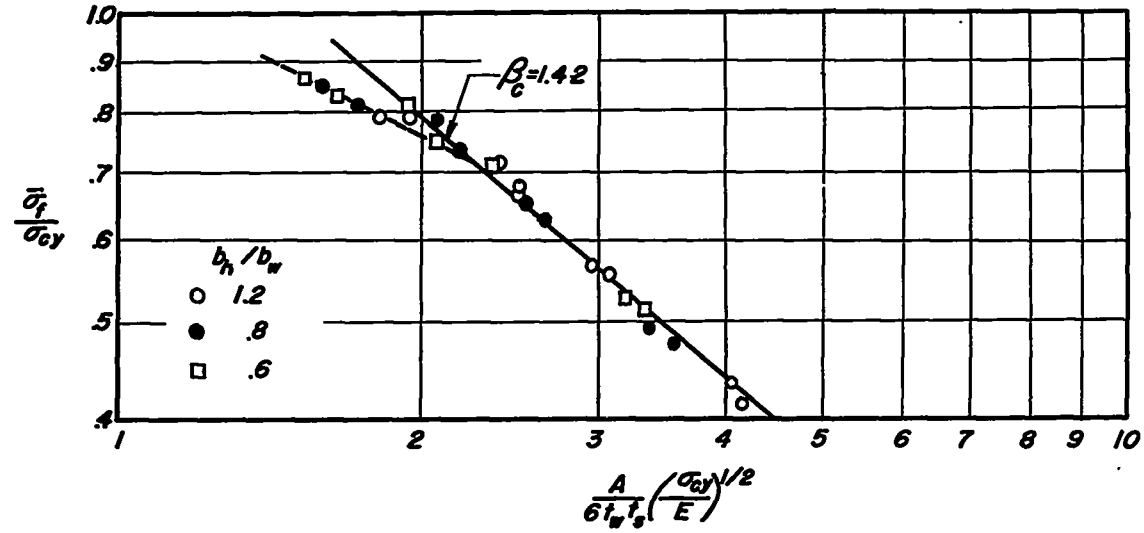


(a) $t_w/t_s = 1.25$.

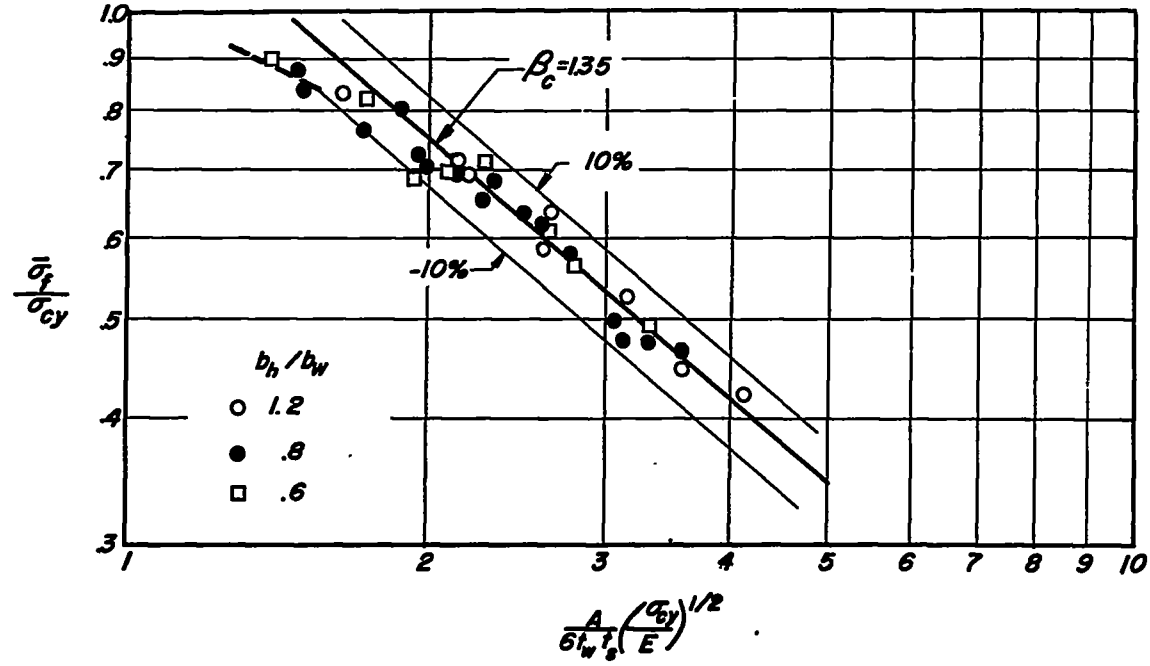


(b) $t_w/t_s = 1.00$.

Figure 5.- Crippling data for hat-stiffened panels of reference 5. Compressive yield strength, 44 ksi.

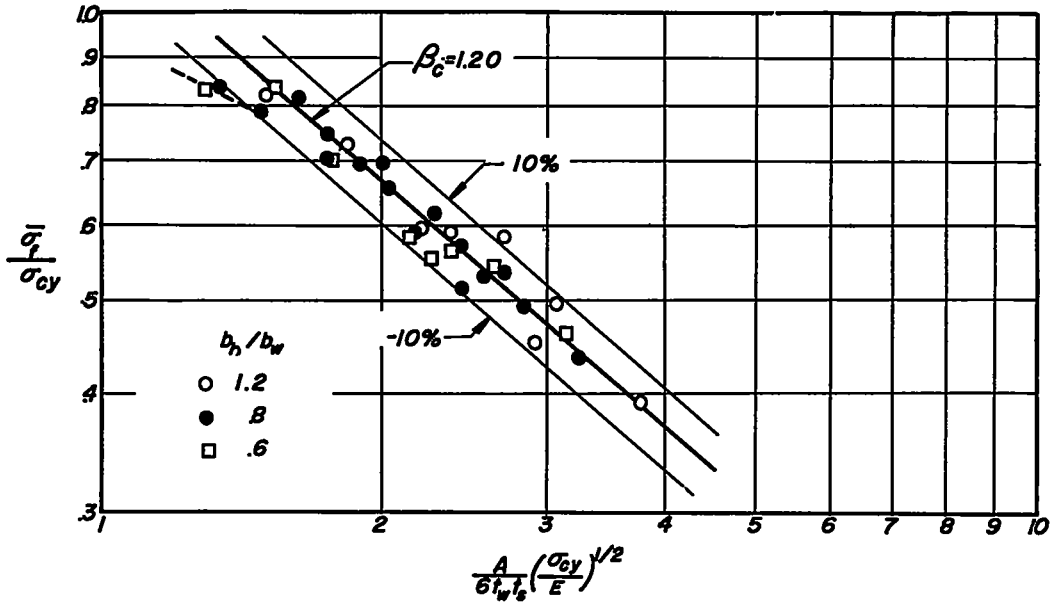


(c) $t_w/t_s = 0.63$.

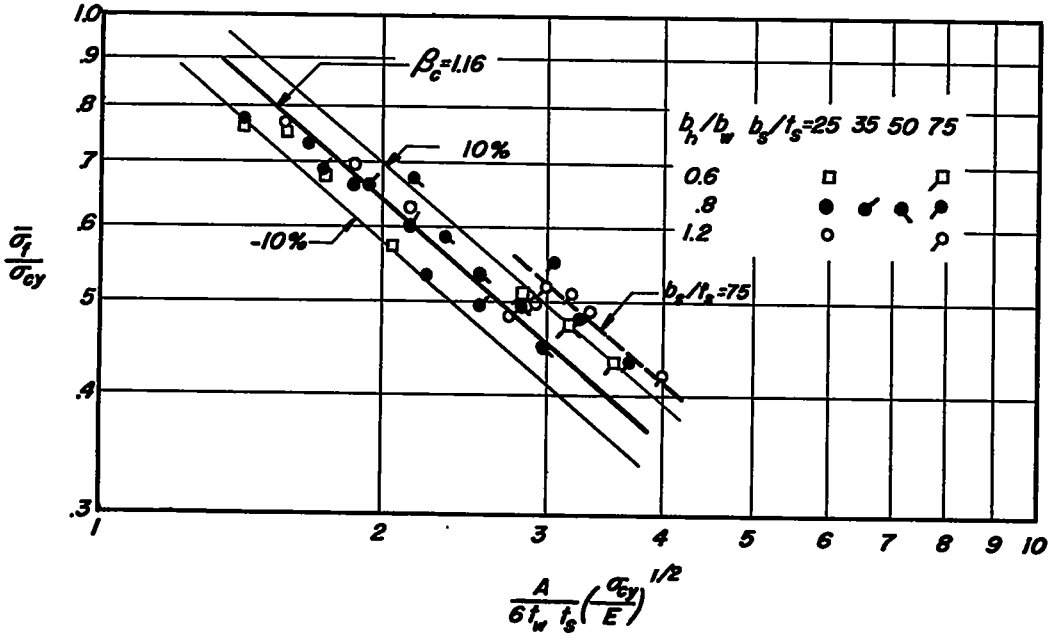


(d) $t_w/t_s = 0.39$.

Figure 5.- Concluded.

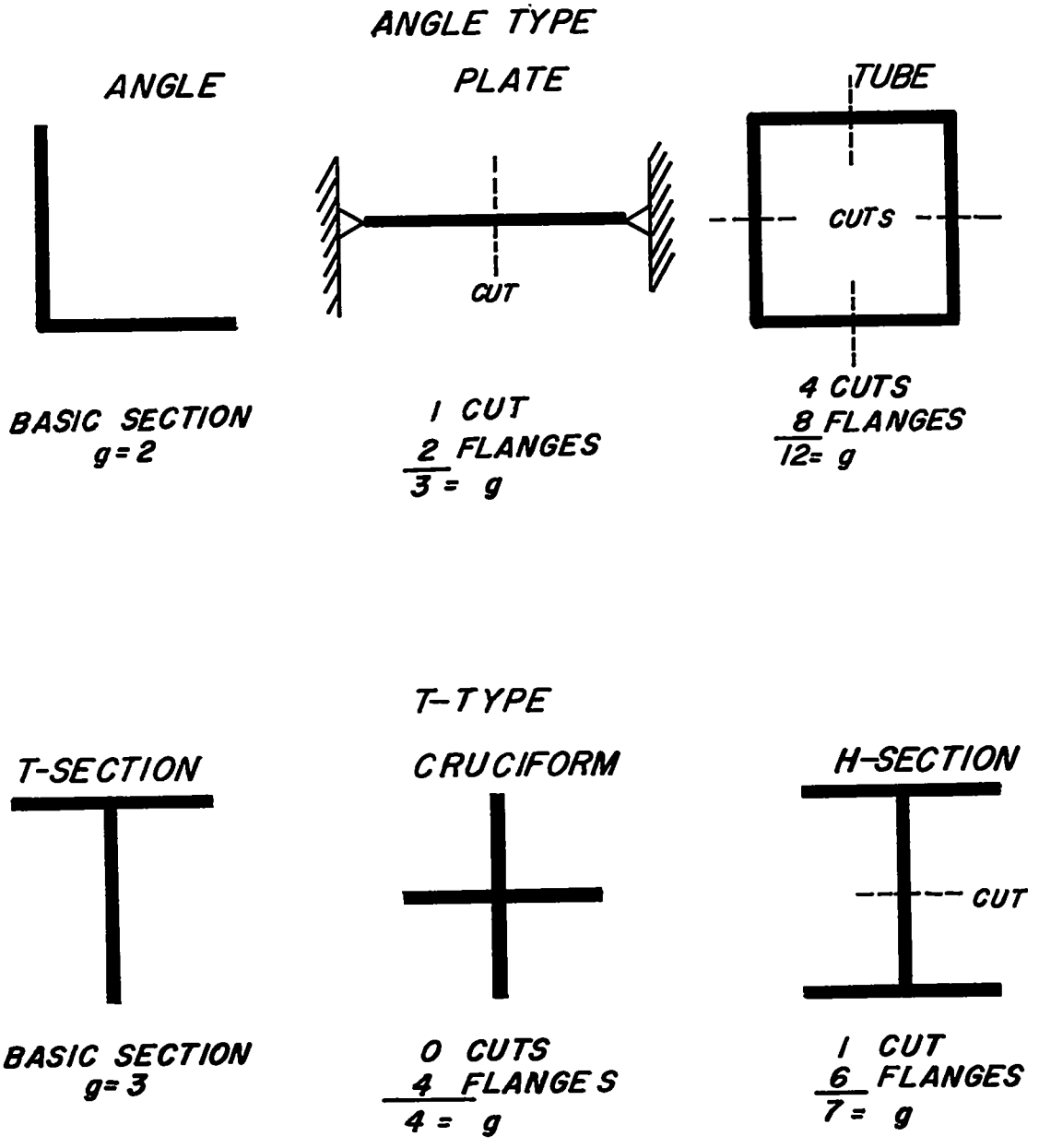


Figure 6.- Method of cutting simple elements to determine g (g is number of cuts plus flanges).

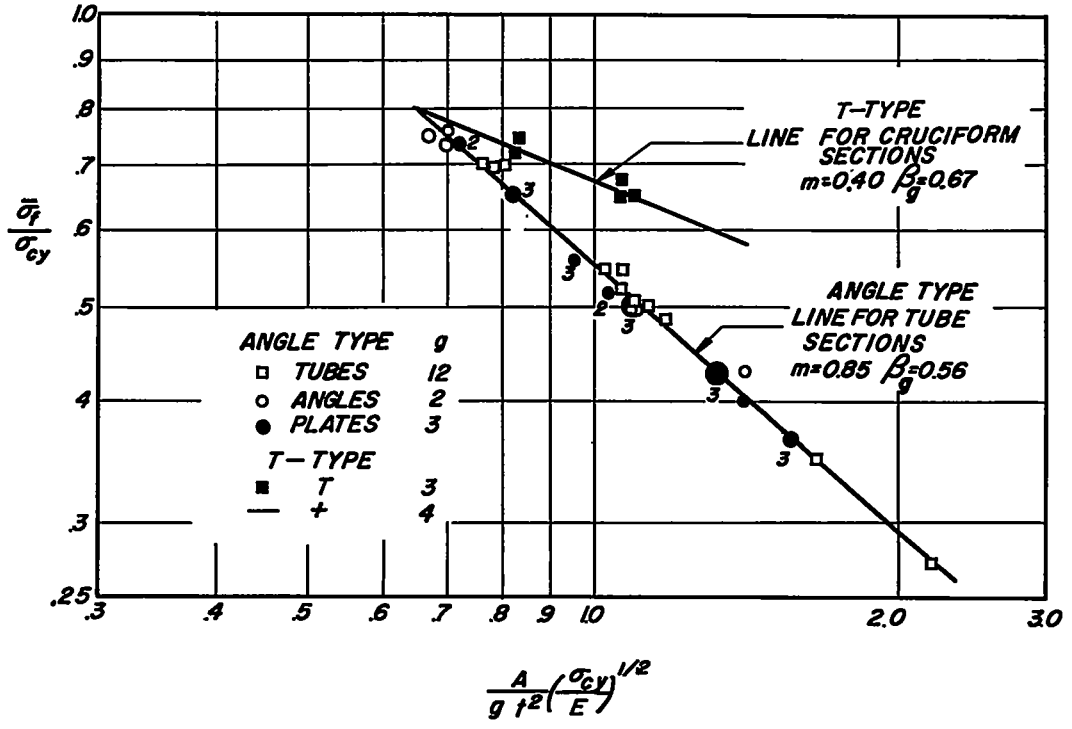


(a) Correlation according to equations (2) and (4).

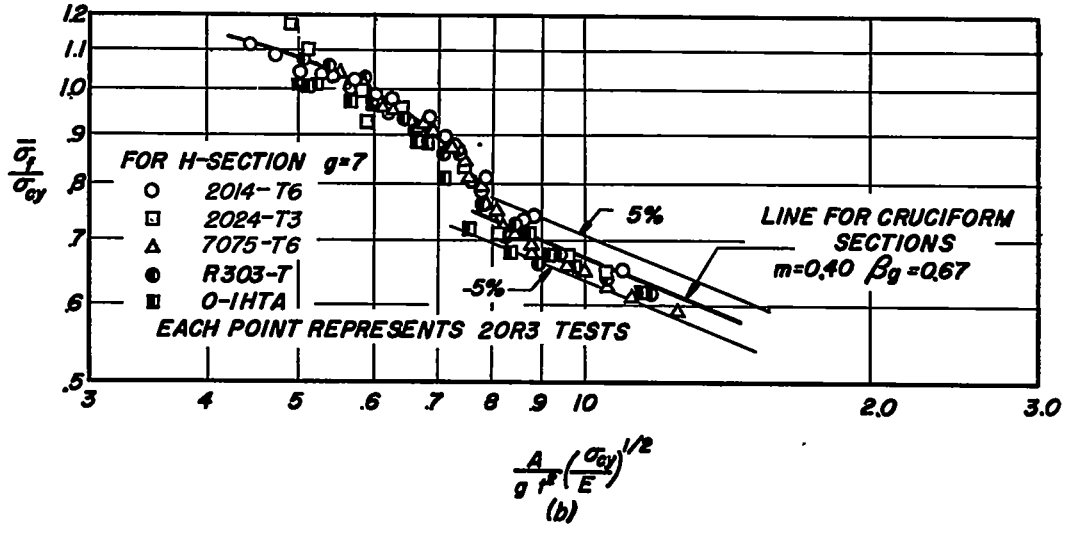


(b) Correlation according to equation (5). Each point represents two or three tests.

Figure 7.- Crippling data for angle and T-type elements of reference 1.

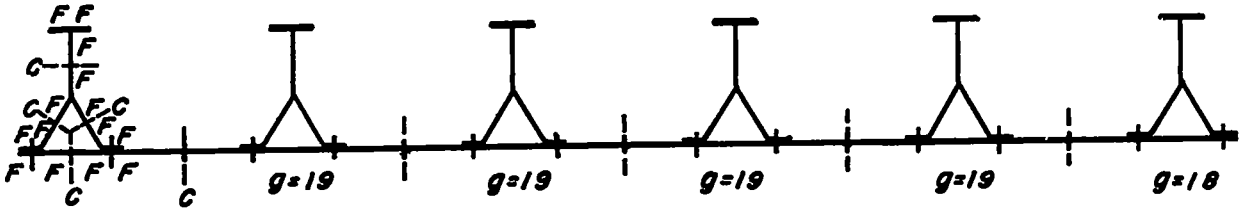


AVERAGE g = 18.83

5 CUTS
14 FLANGES
19 = g

(a) Y-stiffened panel.

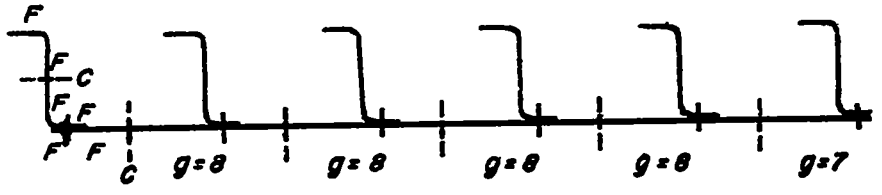


AVERAGE g = 7.83

2 CUTS
6 FLANGES
8 = g

(b) Z-stiffened panel.

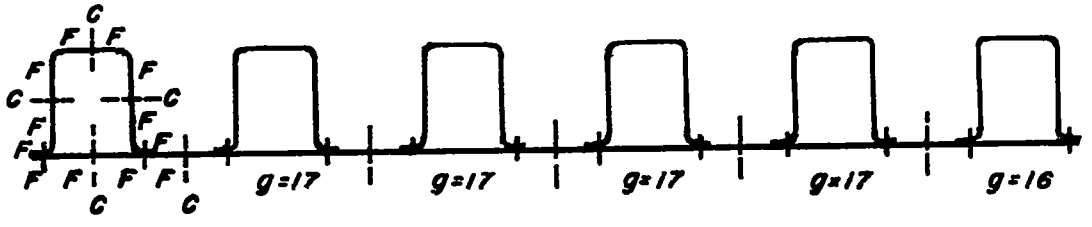


AVERAGE g = 16.83

5 CUTS
12 FLANGES
17 = g

(c) Hat-stiffened panel.

Figure 8.- Method of cutting stiffened panels to determine g.

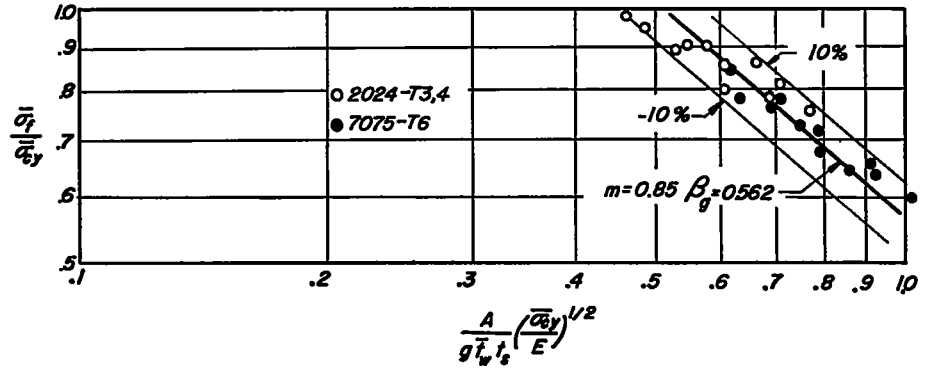


(a) $t_w/t_s = 1.00$; $\bar{t}_w/t_s = 1.16$.

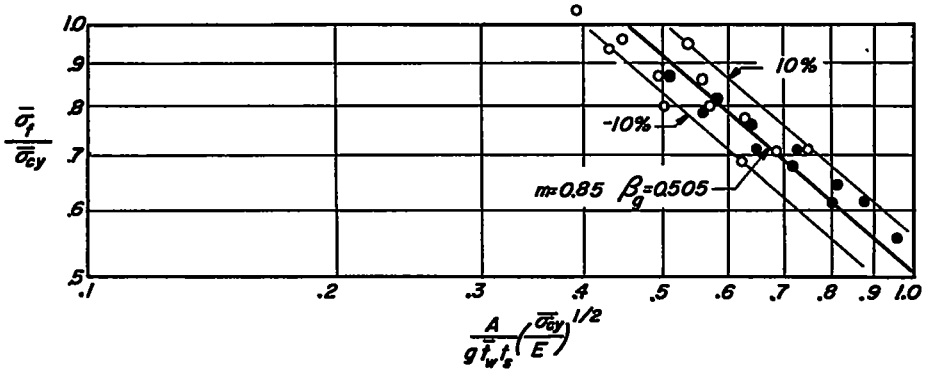


(b) $t_w/t_s = 0.63$; $\bar{t}_w/t_s = 0.73$.

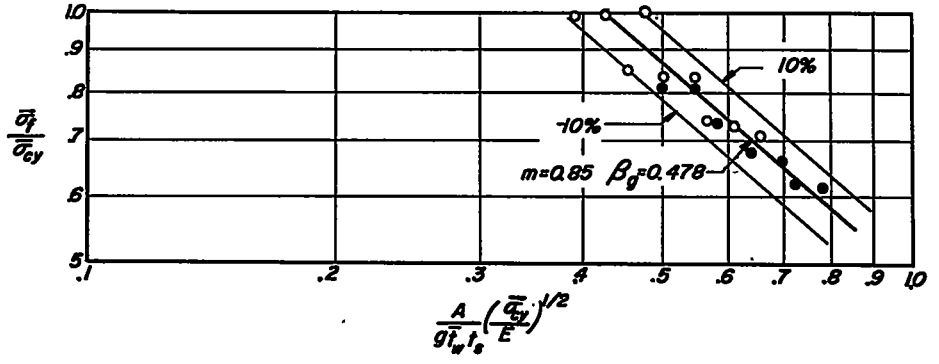


(c) $t_w/t_s = 0.40$; $\bar{t}_w/t_s = 0.46$.

Figure 9.- Crippling data for Y-stiffened panels of reference 7.

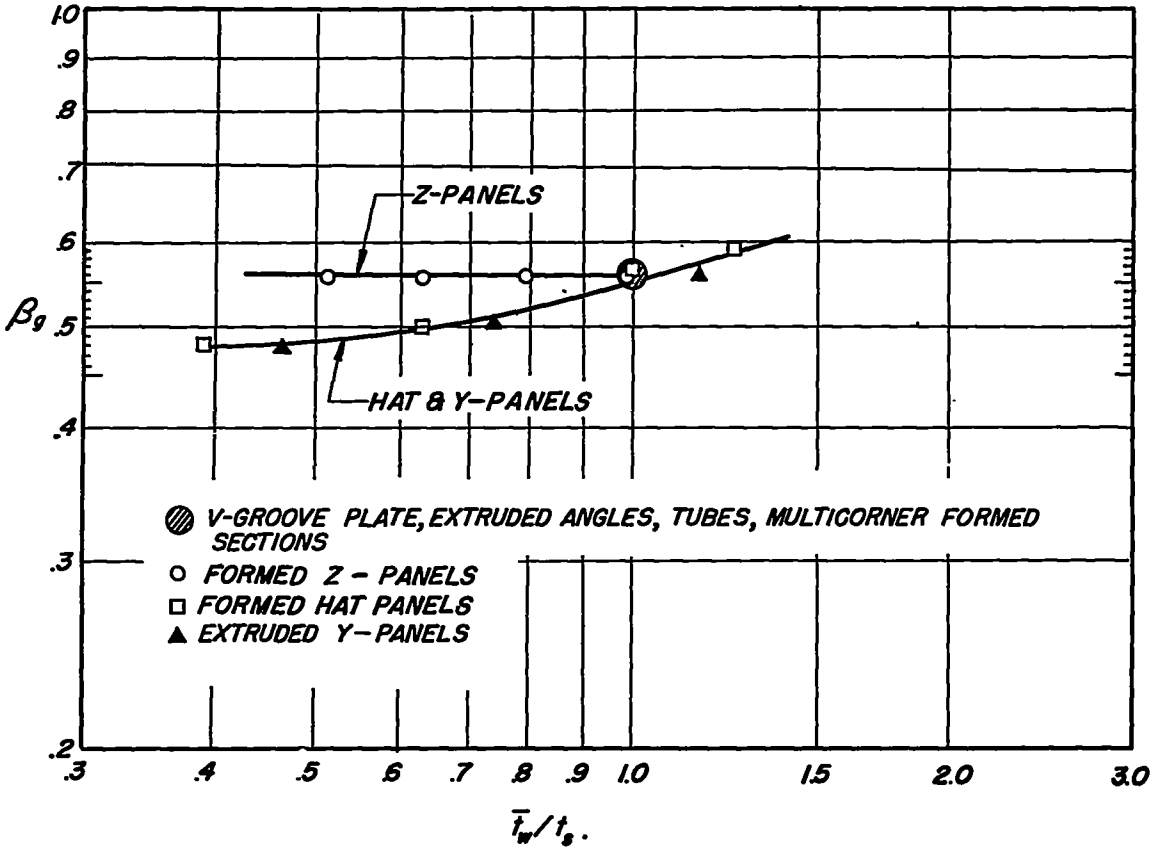


Figure 10.- Crippling coefficients for angle-type elements.

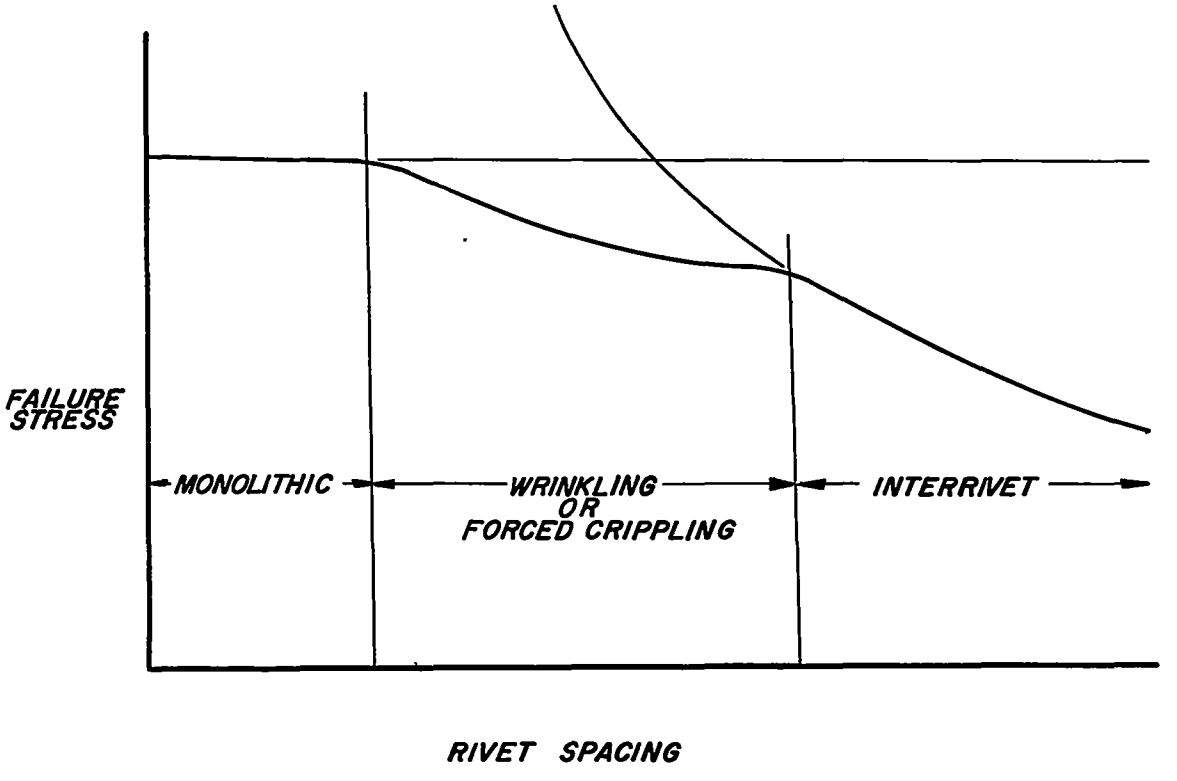


Figure 11.- Various failure modes of short riveted panels.

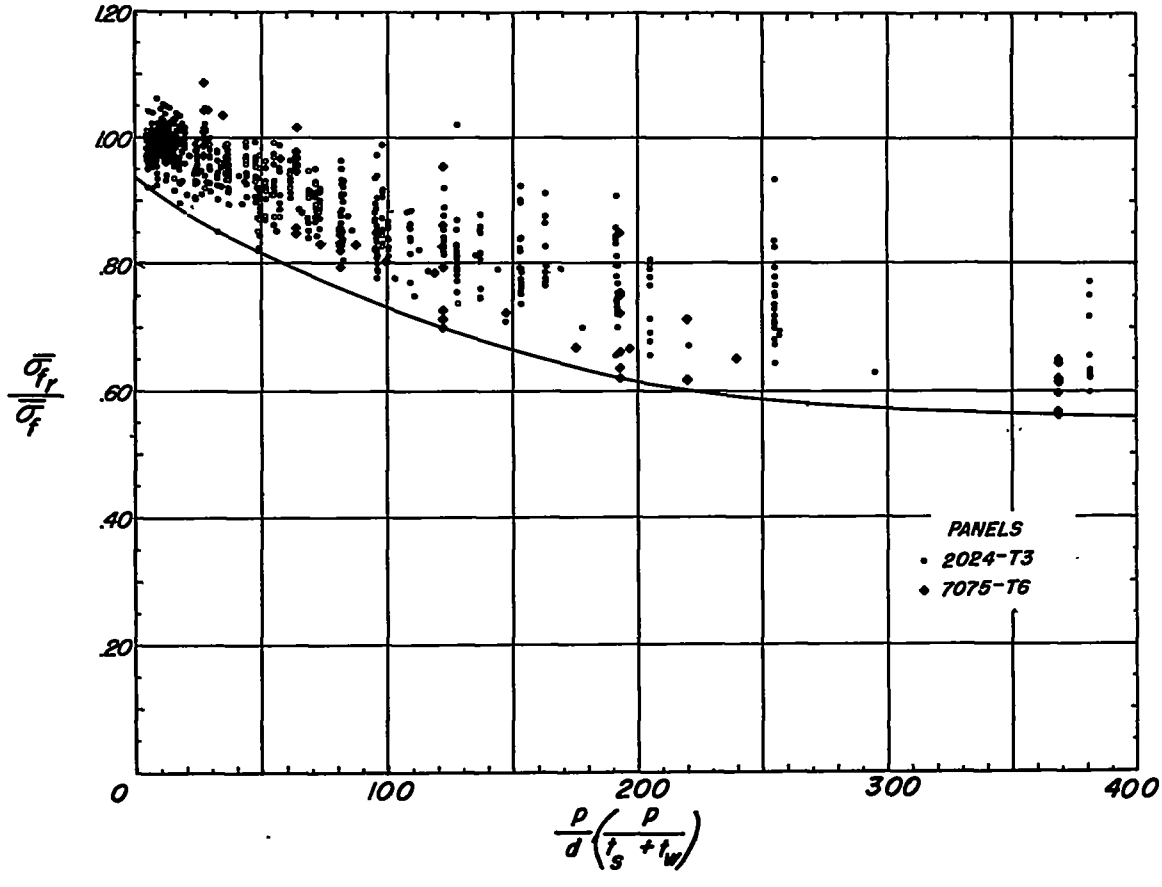


(a) 2117-T4 rivets. Data from reference 4.

Figure 12.- Effect of rivet tensile strength, pitch, and diameter upon compressive strength of short, riveted, aluminum-alloy Z-panels.

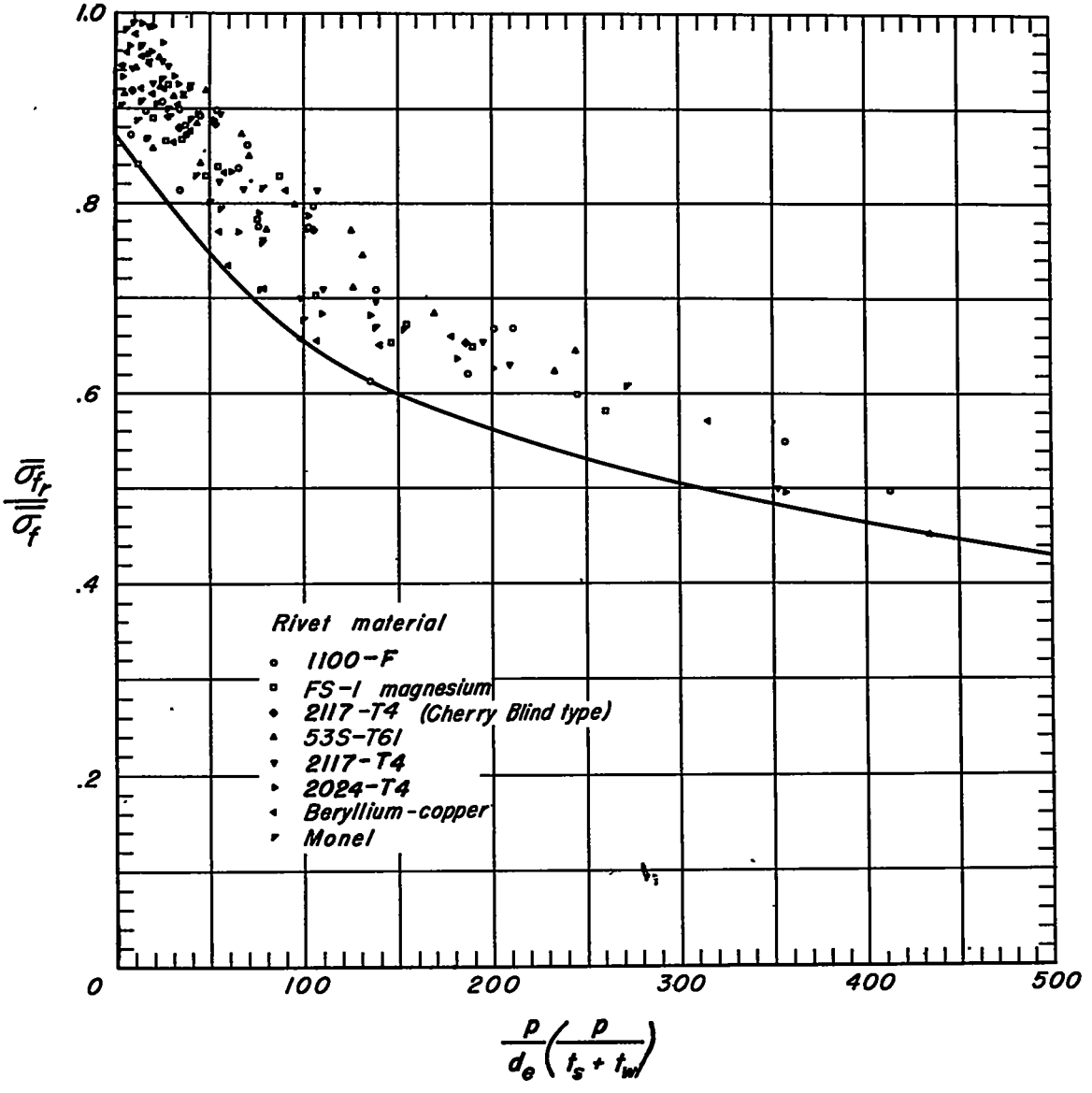


(b) Various rivet materials. Data from reference 13.

Figure 12.- Concluded.

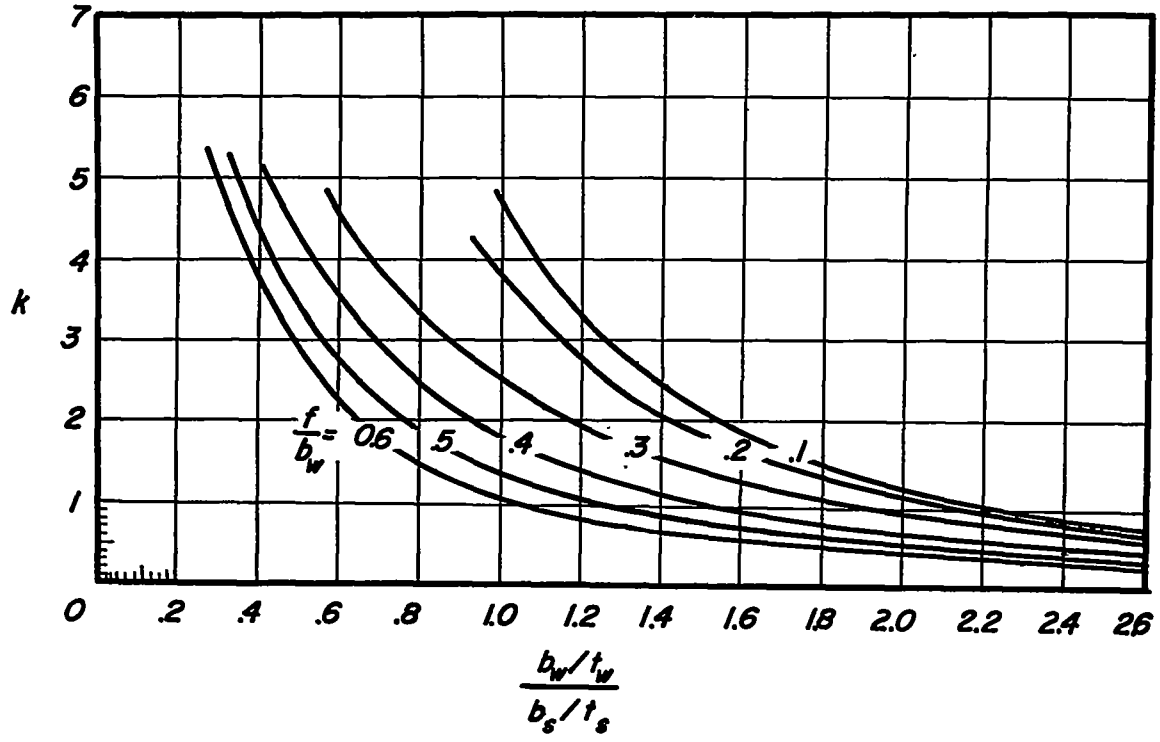


(a) Theoretical coefficients for buckling.

Figure 13.- Theoretical and experimentally determined coefficients for buckling and wrinkling failure of short riveted panels (data from reference 6).

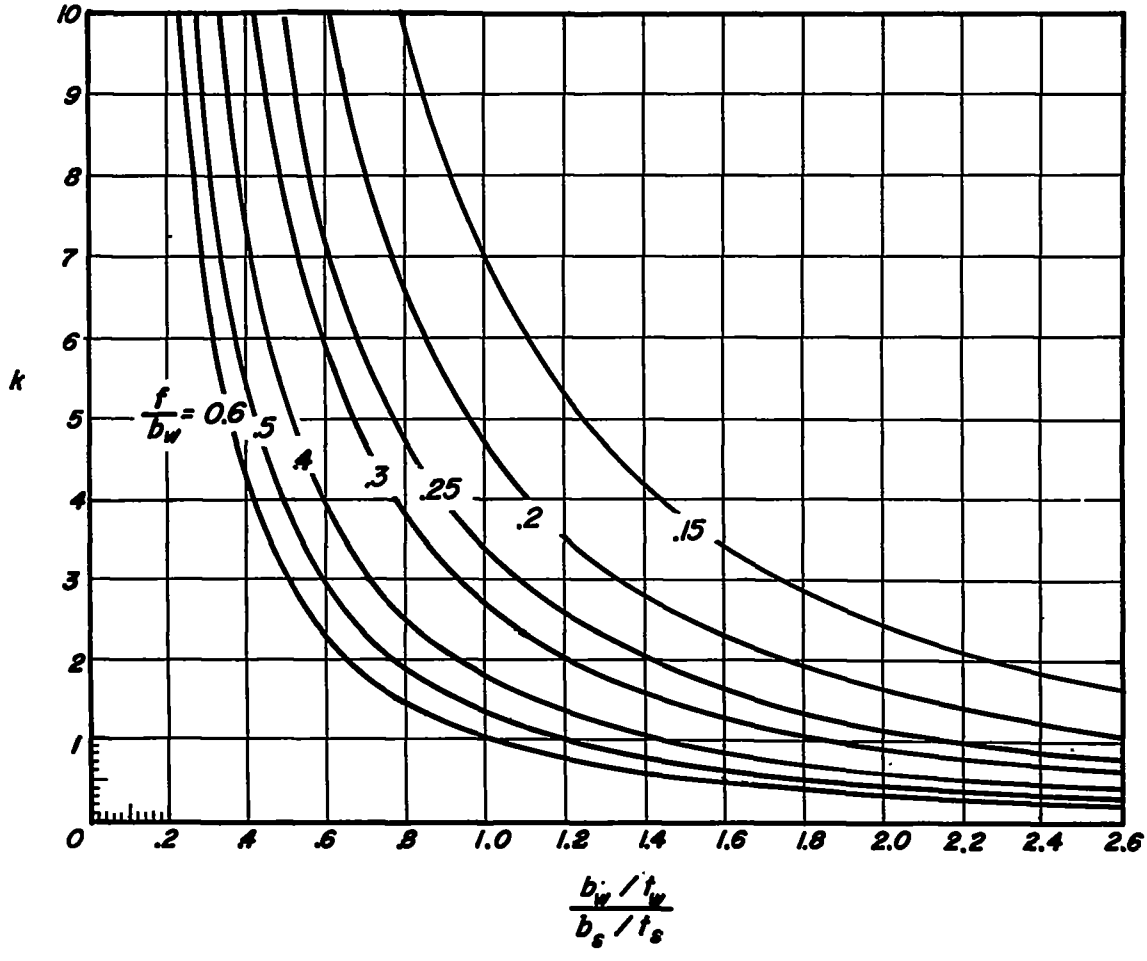


(b) Experimentally determined coefficients for failure in wrinkling mode.

Figure 13.- Concluded.

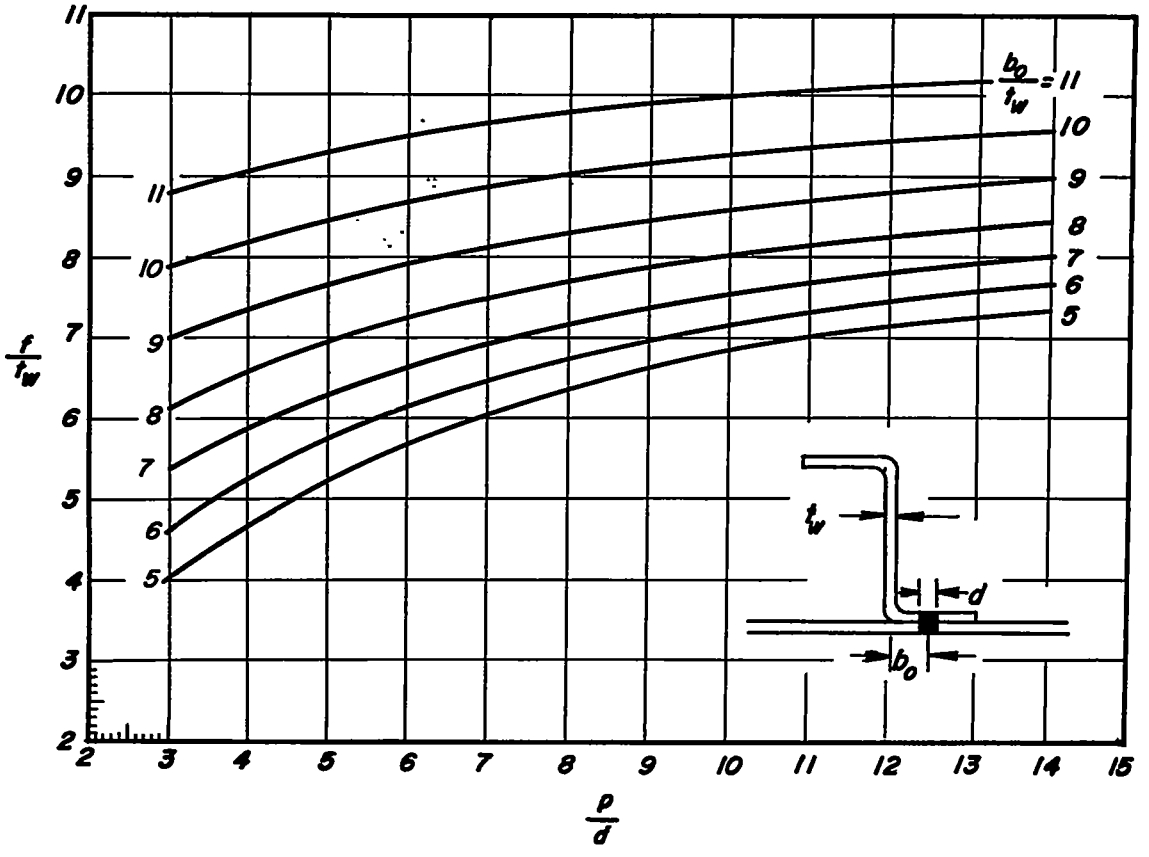


Figure 14.- Experimentally determined values of effective rivet offset (data from ref. 6).

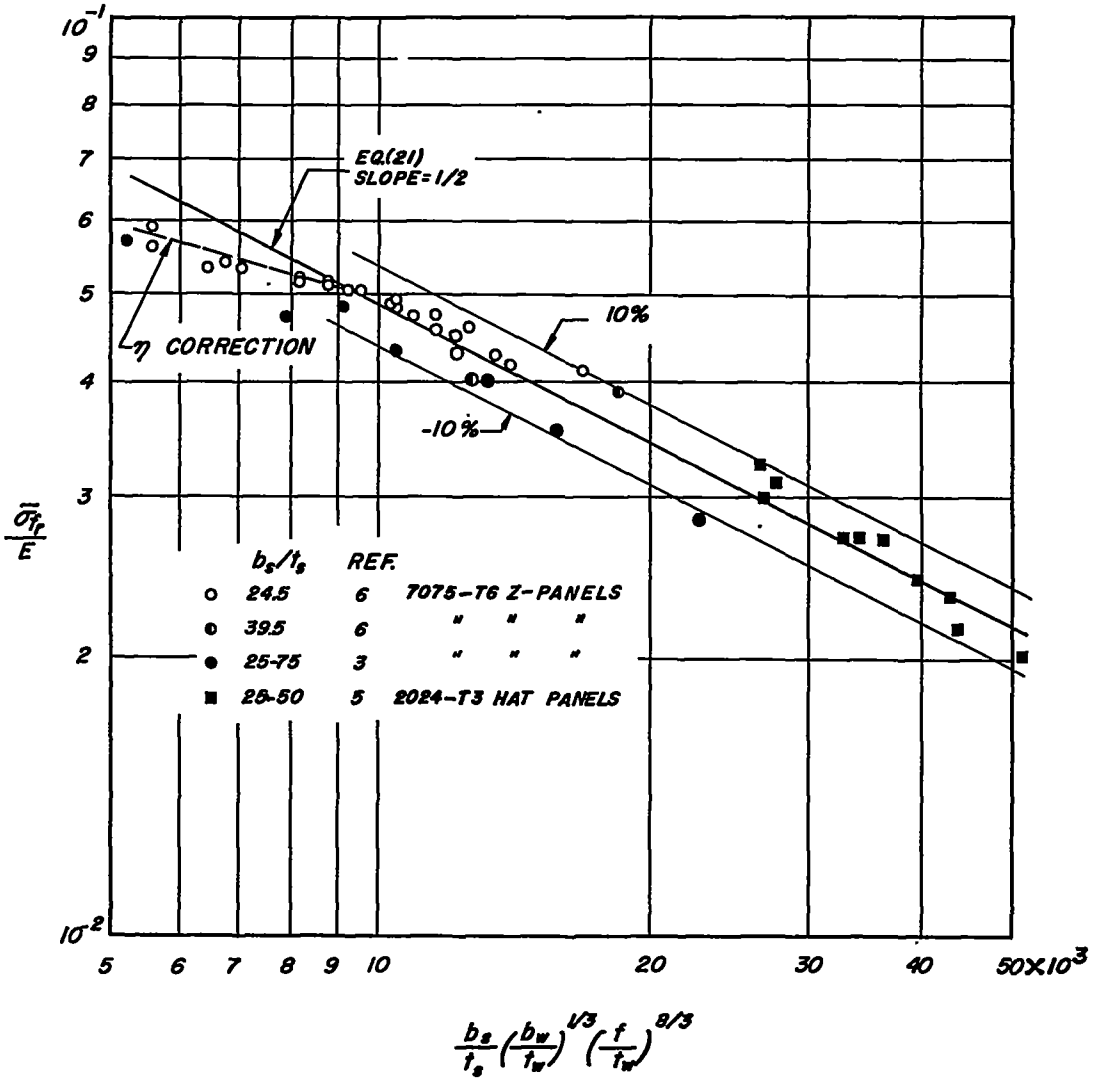


Figure 15.- Wrinkling data on short riveted panels.

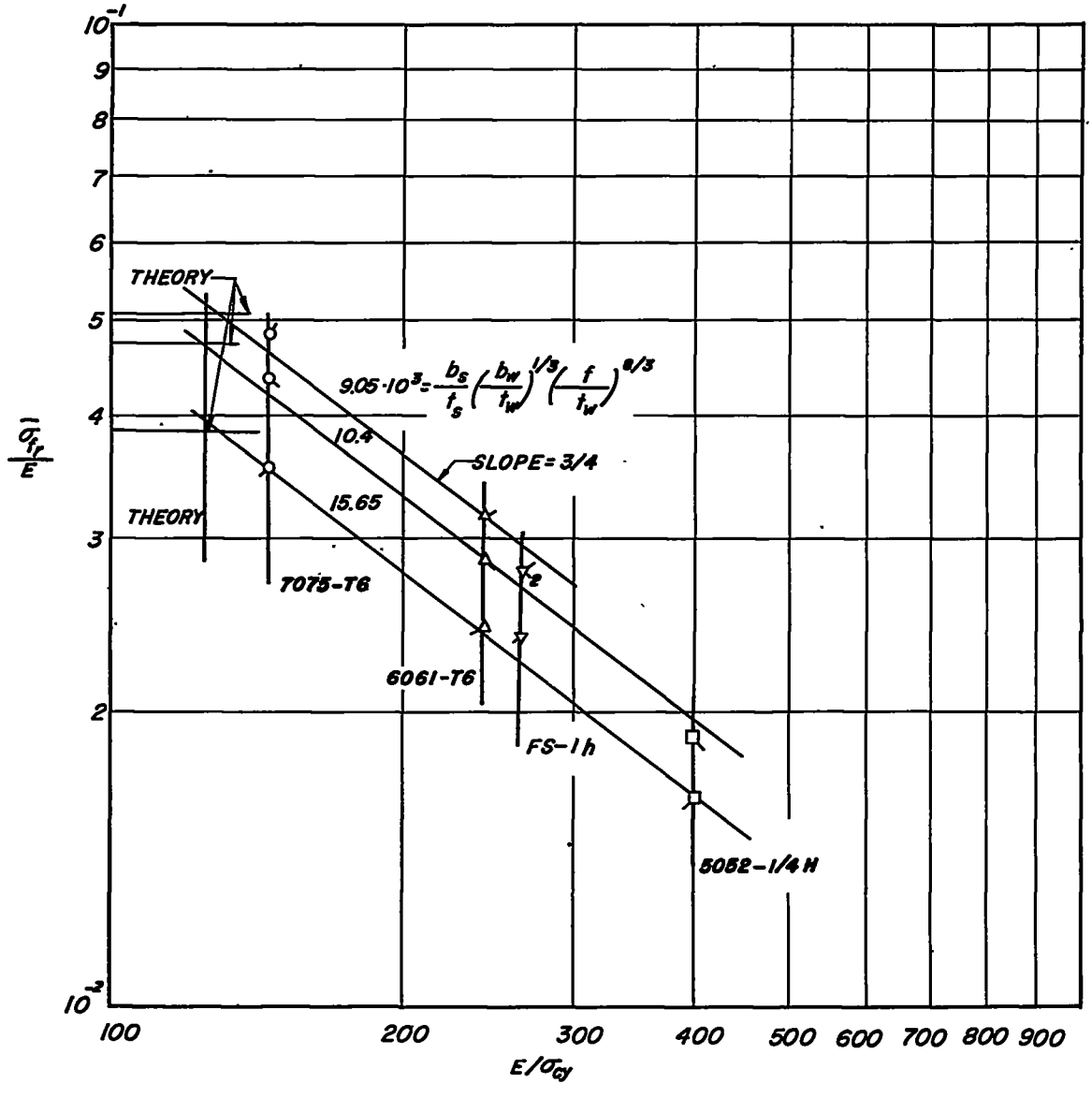


Figure 16.- Influence of $E/\sigma_{cy}$ upon wrinkling strength of short riveted panels. Elastic-buckling data only of reference 3.

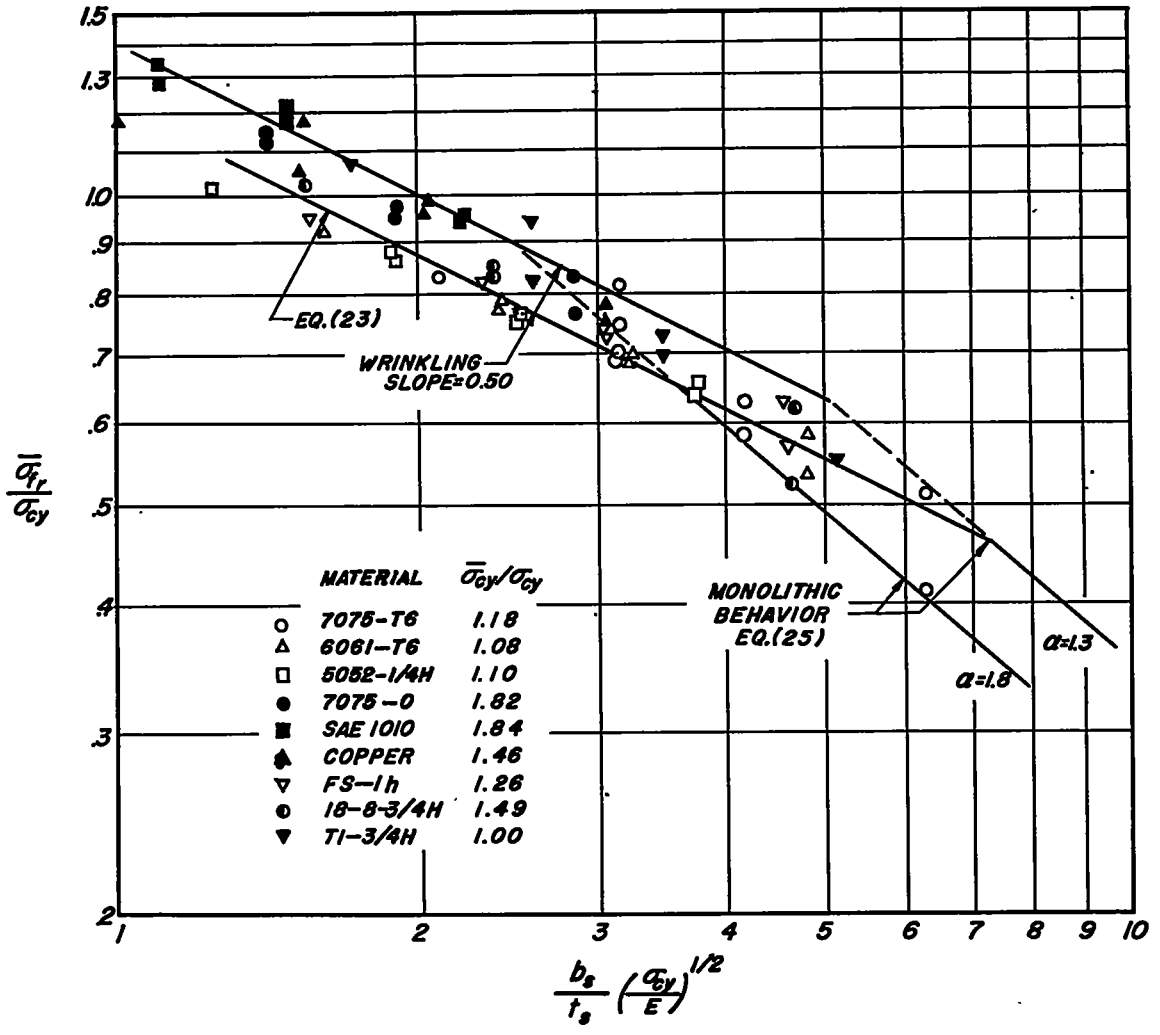


Figure 17.- Crippling and wrinkling data on Z-stiffened riveted panels of reference 3. $\frac{f}{t_w} = 5.4$; $\frac{b_w}{t_w} = 12.5$.

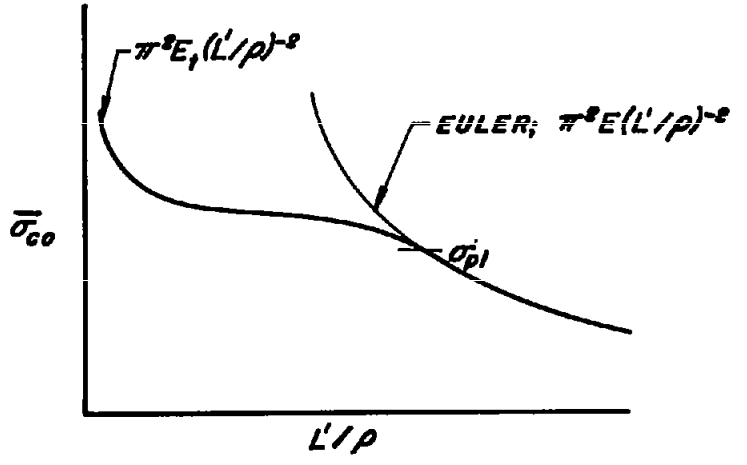


(a) No crippling of stiffener; no buckling of skin. Conventional chart.

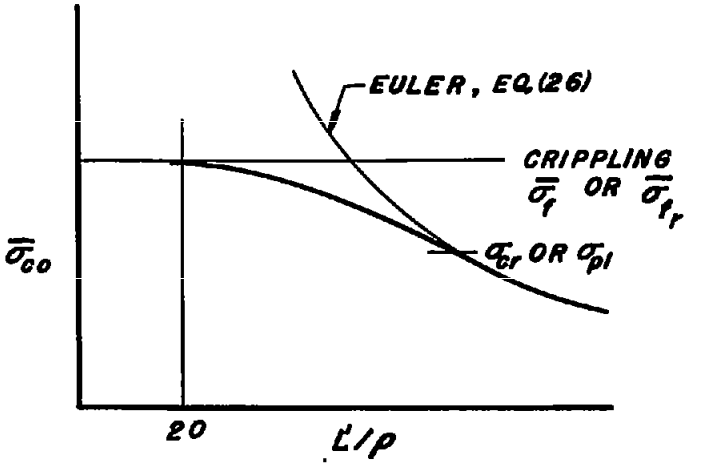


(b) Crippling of stiffener; buckling of skin or stiffener. Conventional chart.

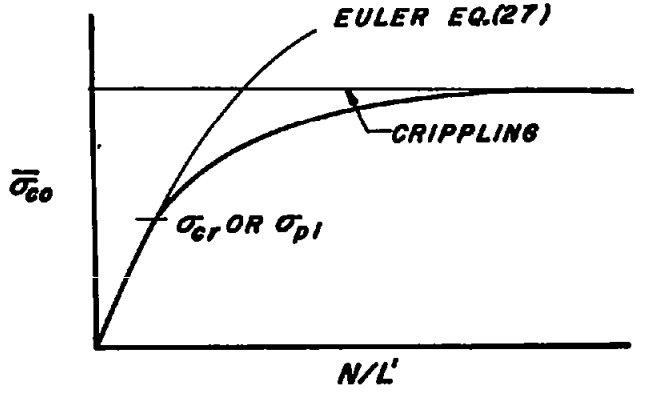


(c) Crippling of stiffener; buckling of skin or stringer. Direct-reading chart.

Figure 18.- Stiffened-panel column charts.

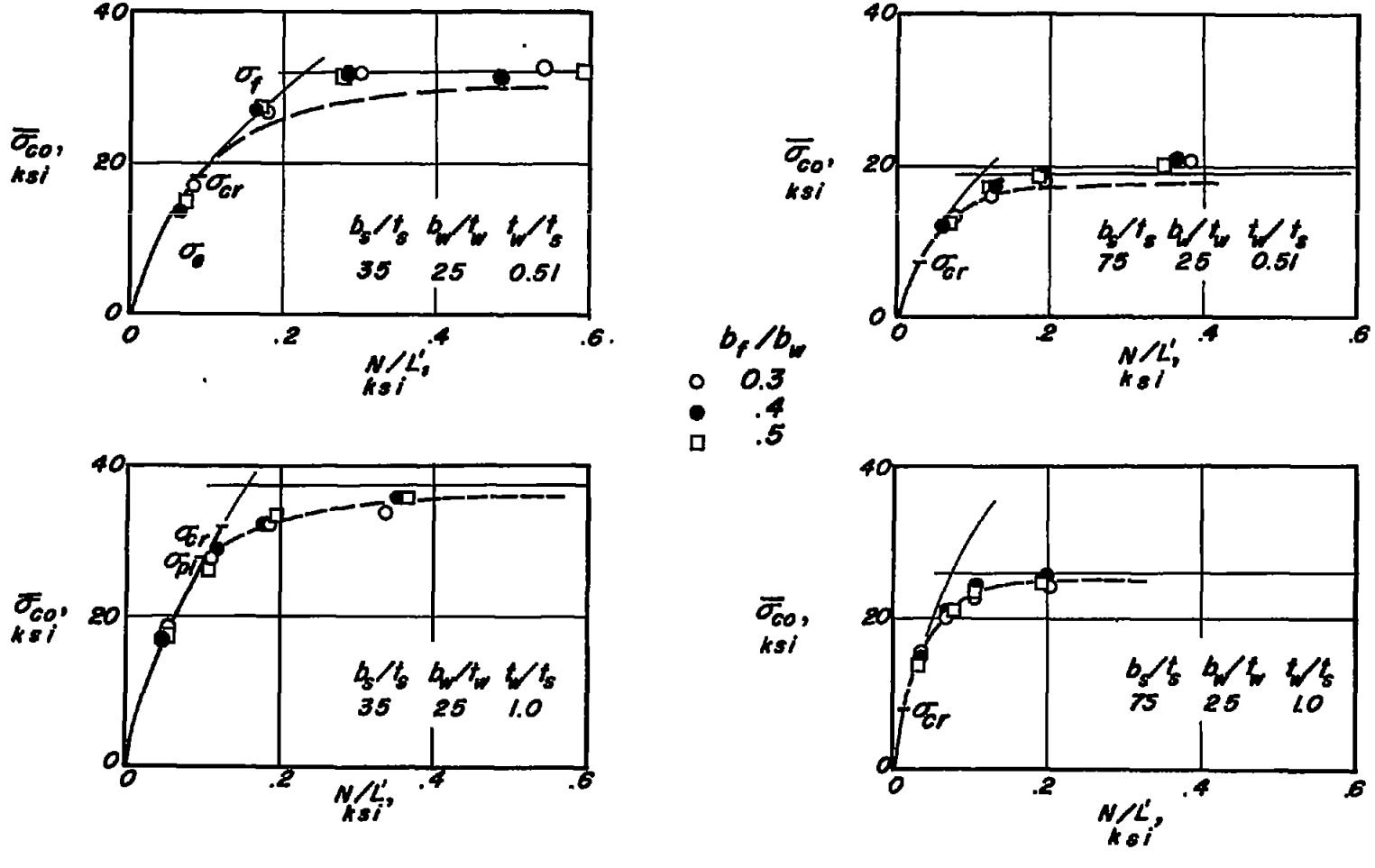


Figure 19.- Comparison of derived column curves and test data of reference 18.

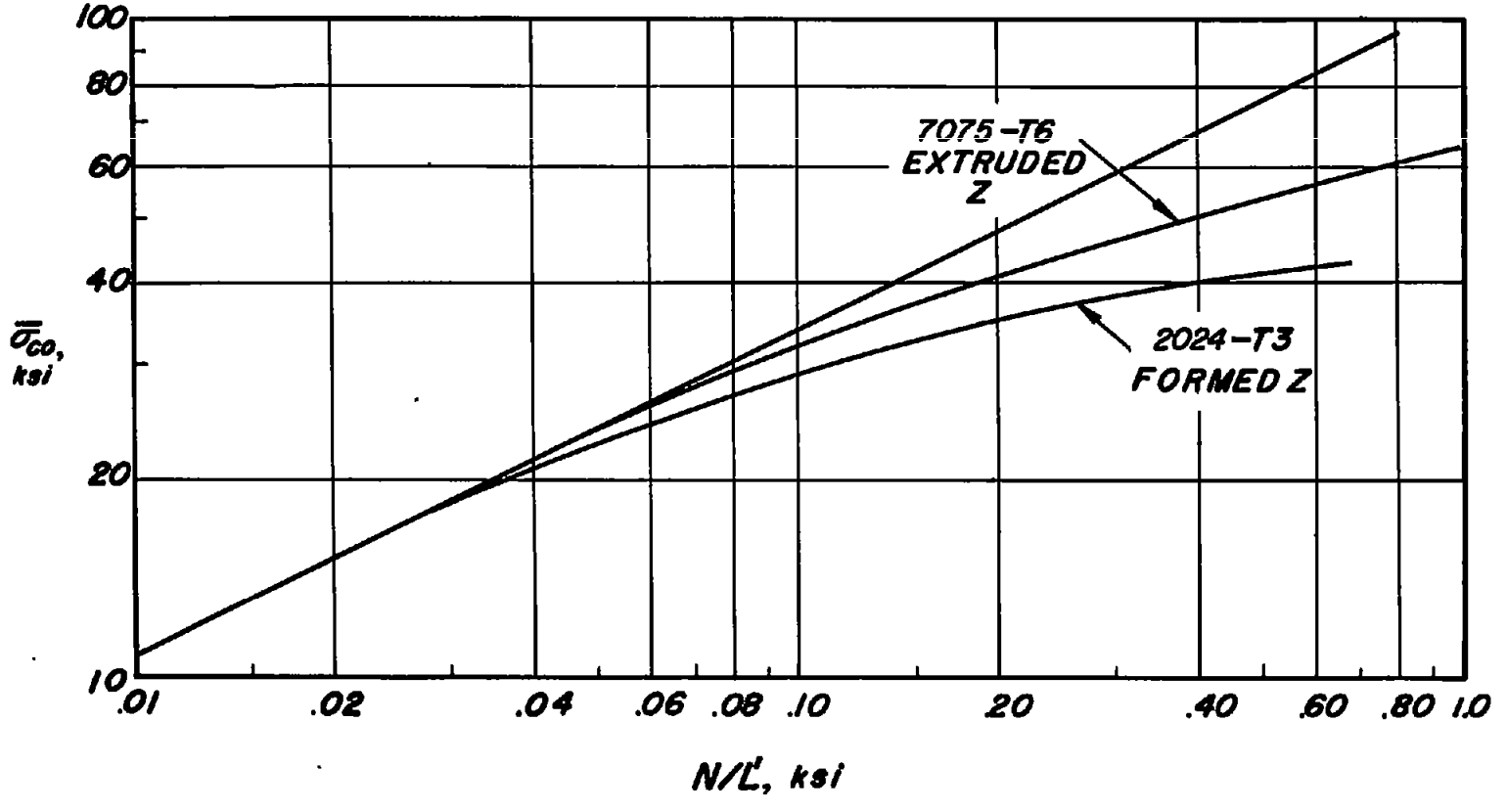


(a) Z-stiffened panels. $E = 10.5 \times 10^6$ psi.

Figure 20.- Optimum-column charts for stiffened panels.

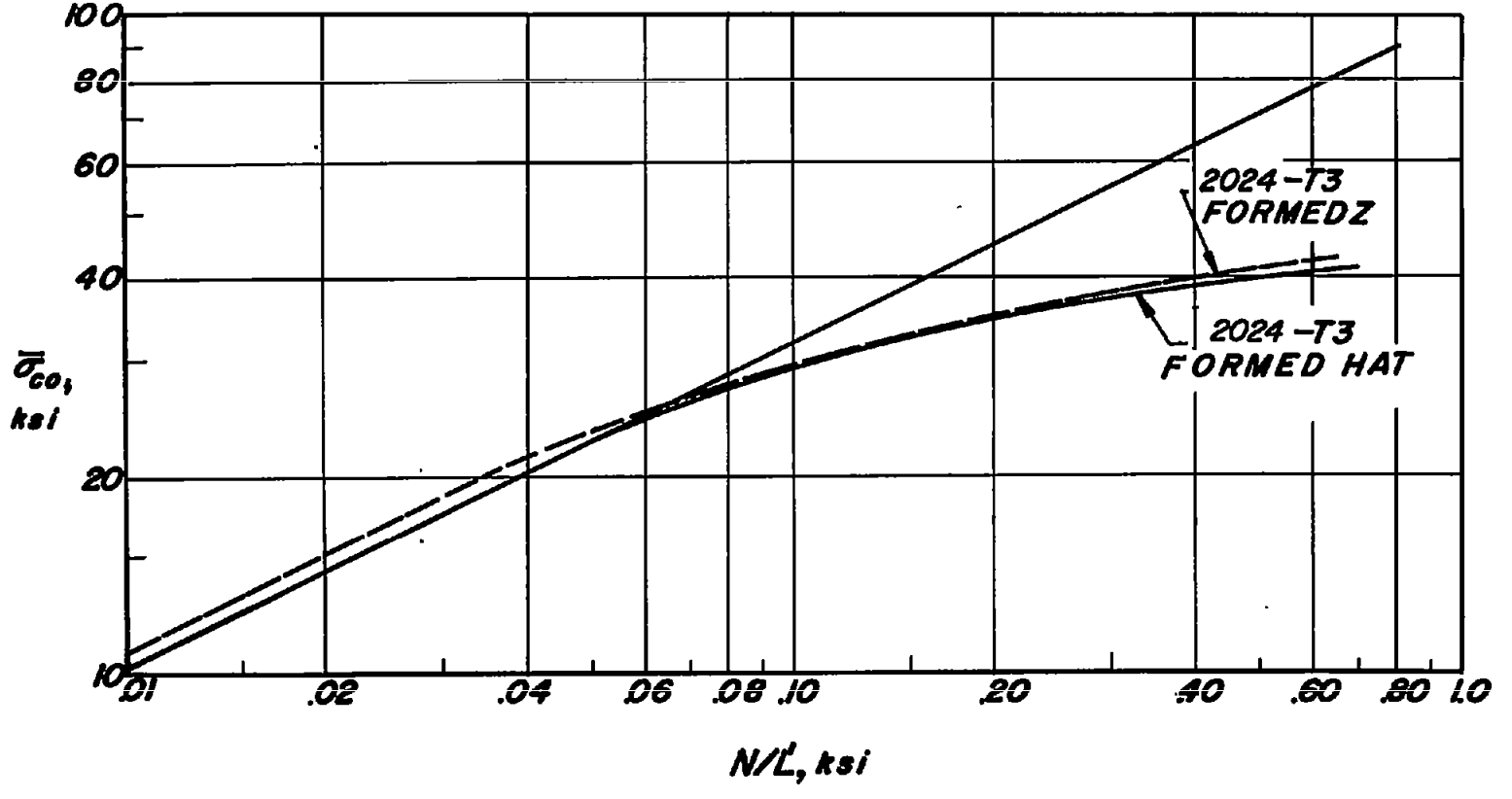


(b) Hat-stiffened panels. $E = 10.5 \times 10^6$ psi.

Figure 20.- Continued.

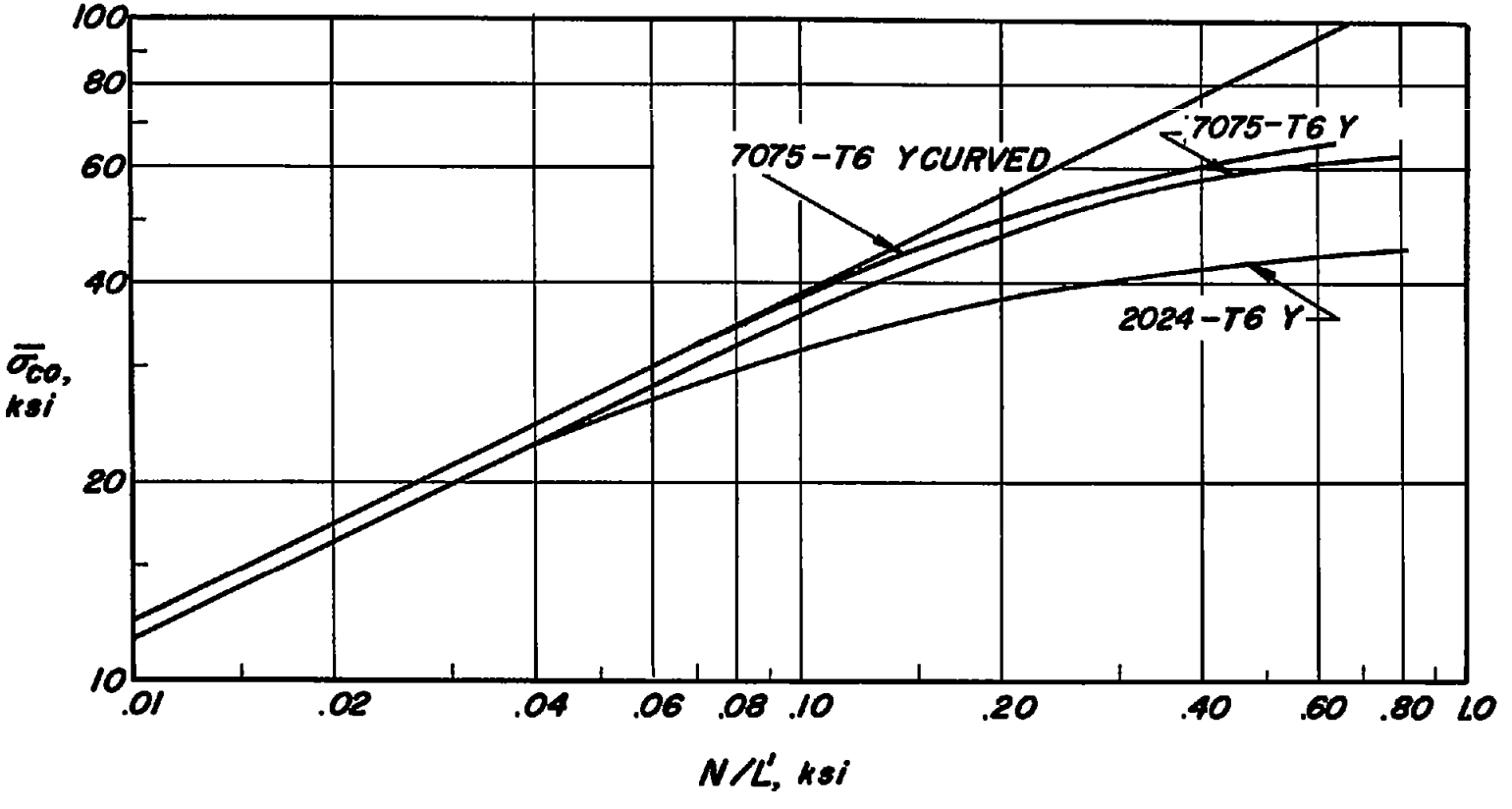


(c) Y-stiffened panels. $E = 10.0 \times 10^6$ psi.

Figure 20.- Concluded.

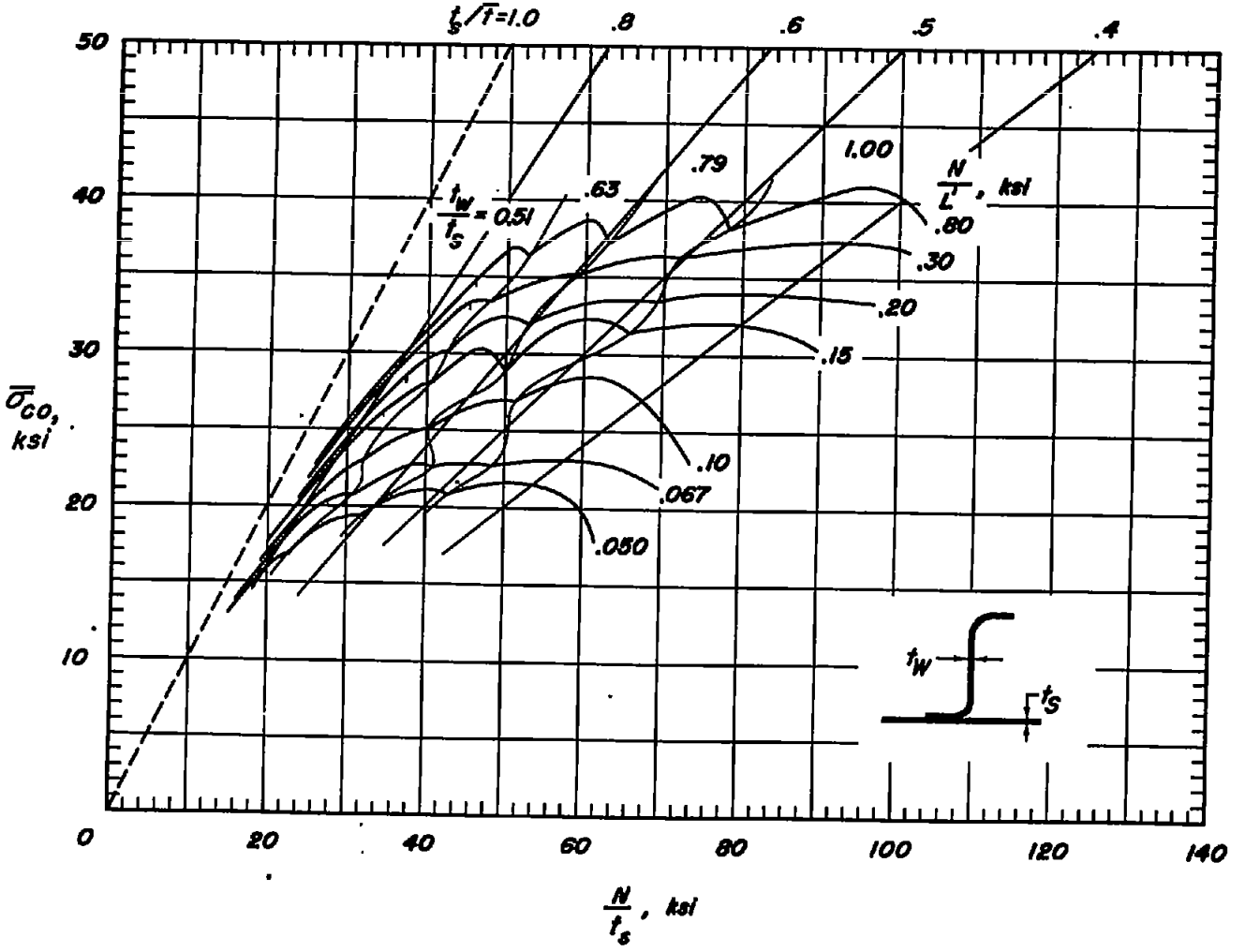


(a) Z-stiffened panels of 2024-T3 aluminum alloy.

Figure 21.- Minimum-weight charts for stiffened panels with specified skin thickness.

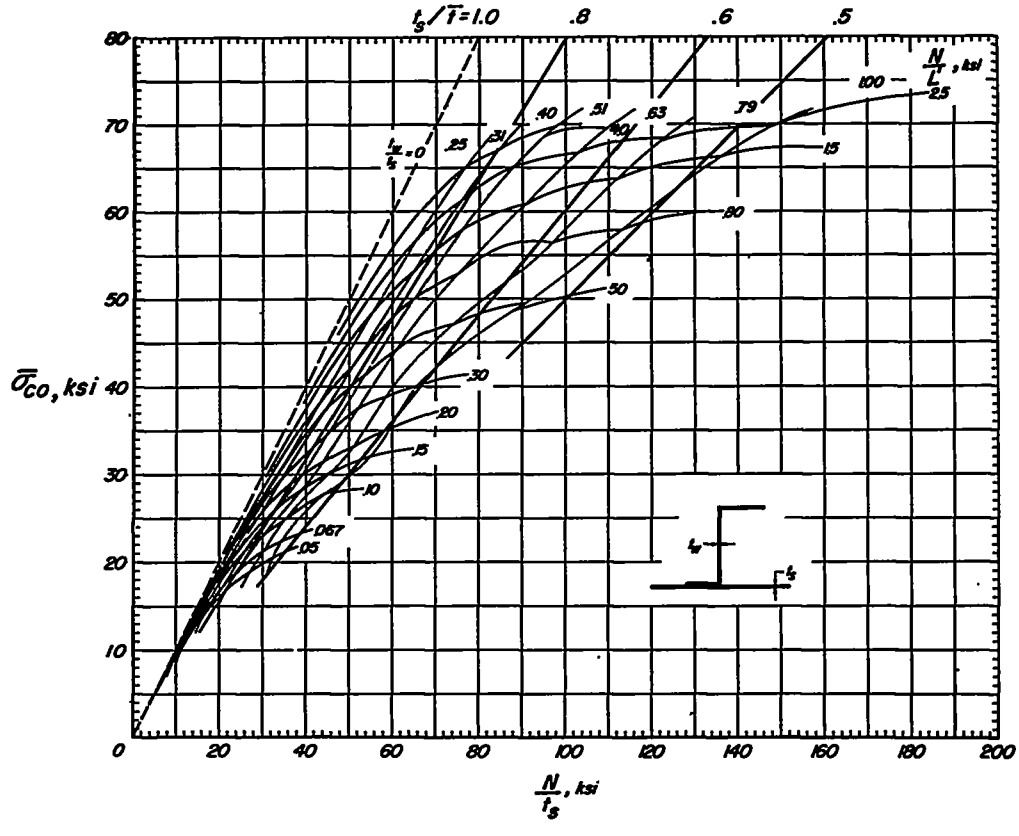


(b) Z-stiffened panels of 7075-T6 aluminum alloy.

Figure 21.- Continued.

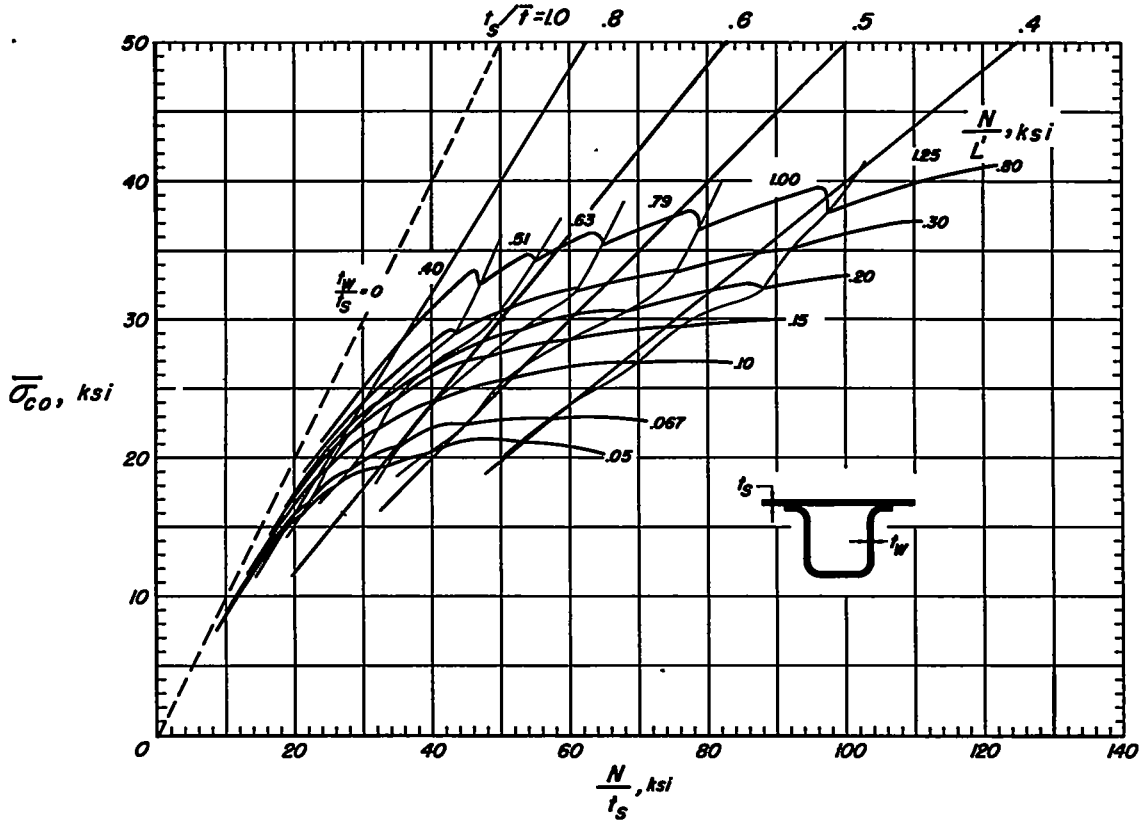


(c) Hat-stiffened panels of 2024-T3 aluminum alloy.

Figure 21.- Continued.

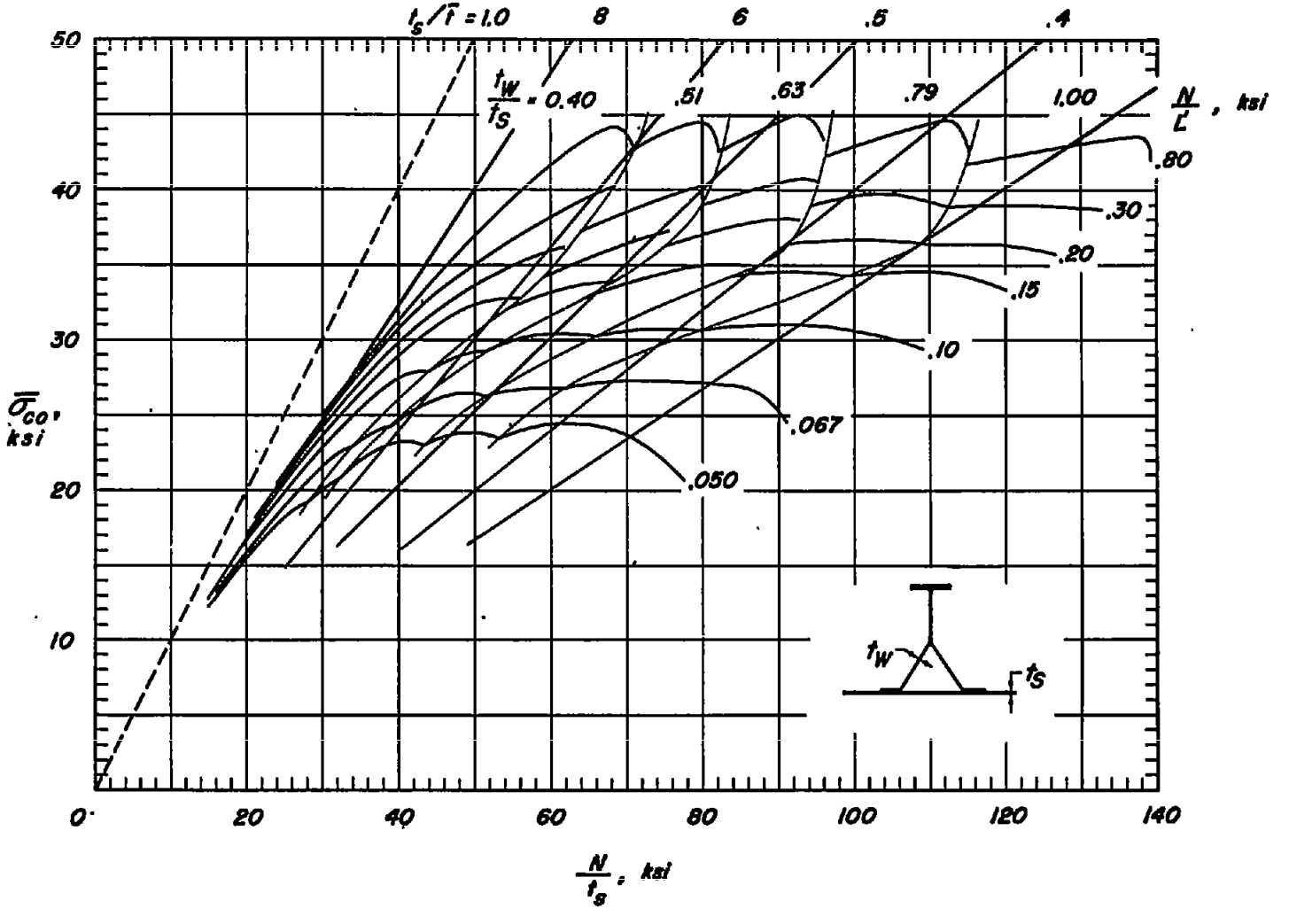


(d) Y-stiffened panels of 2024-T3 aluminum alloy.

Figure 21.- Continued.

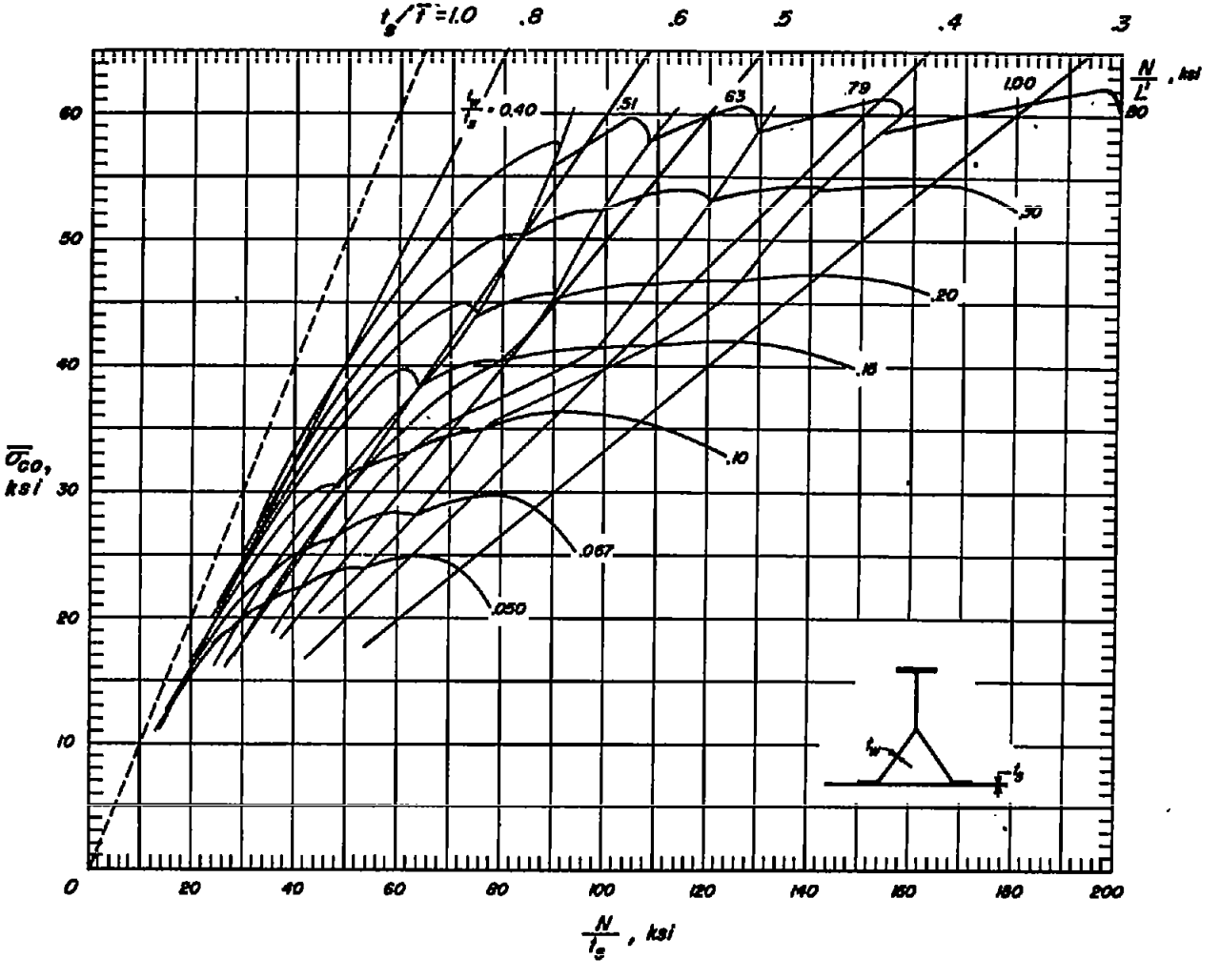


(e) Y-stiffened panels of 7075-T6 aluminum alloy.

Figure 21.- Concluded.

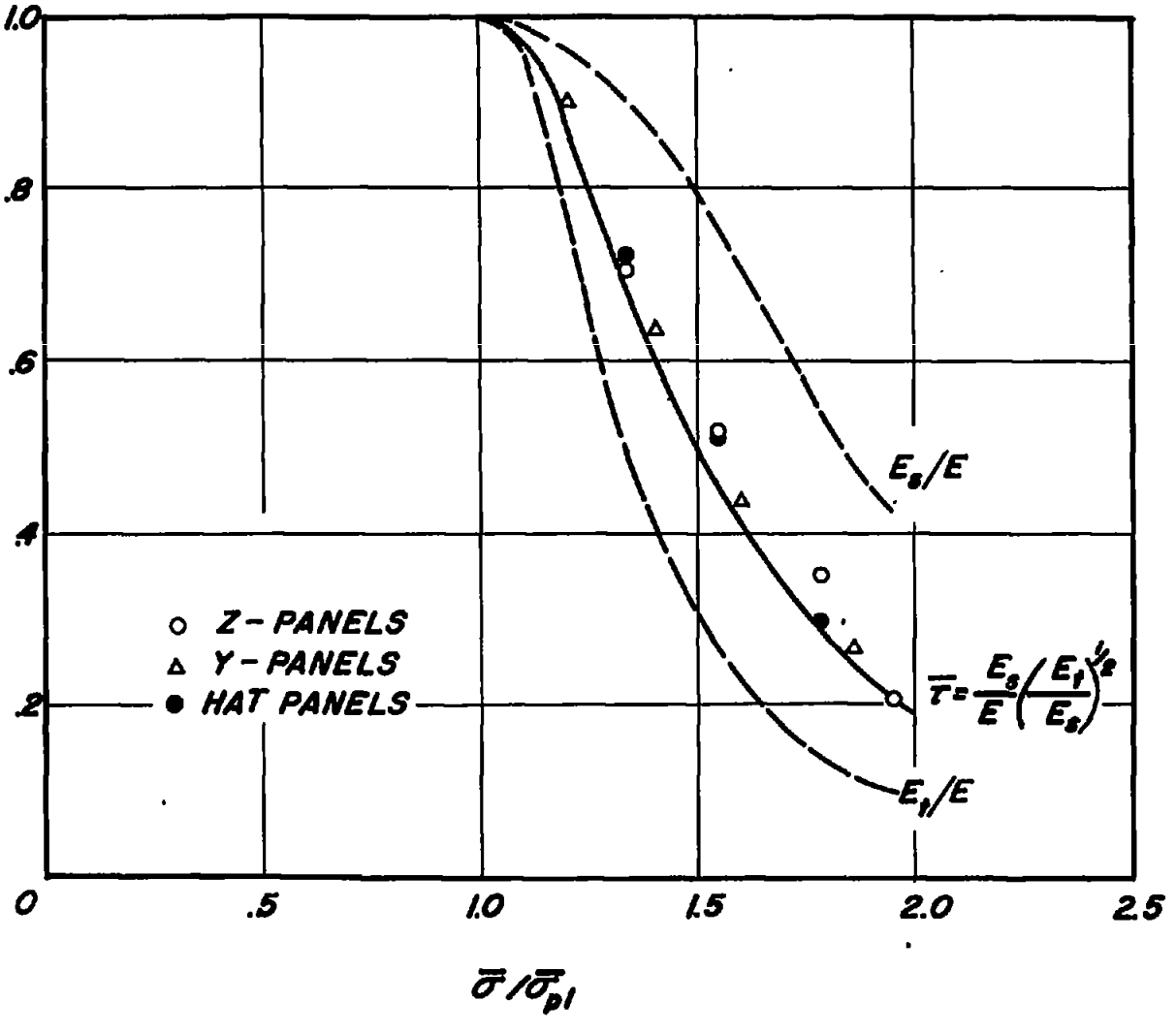


Figure 22.- Plasticity-reduction factor for optimum stiffened panels of 2024-T3 aluminum alloy. Data taken from reference 26.

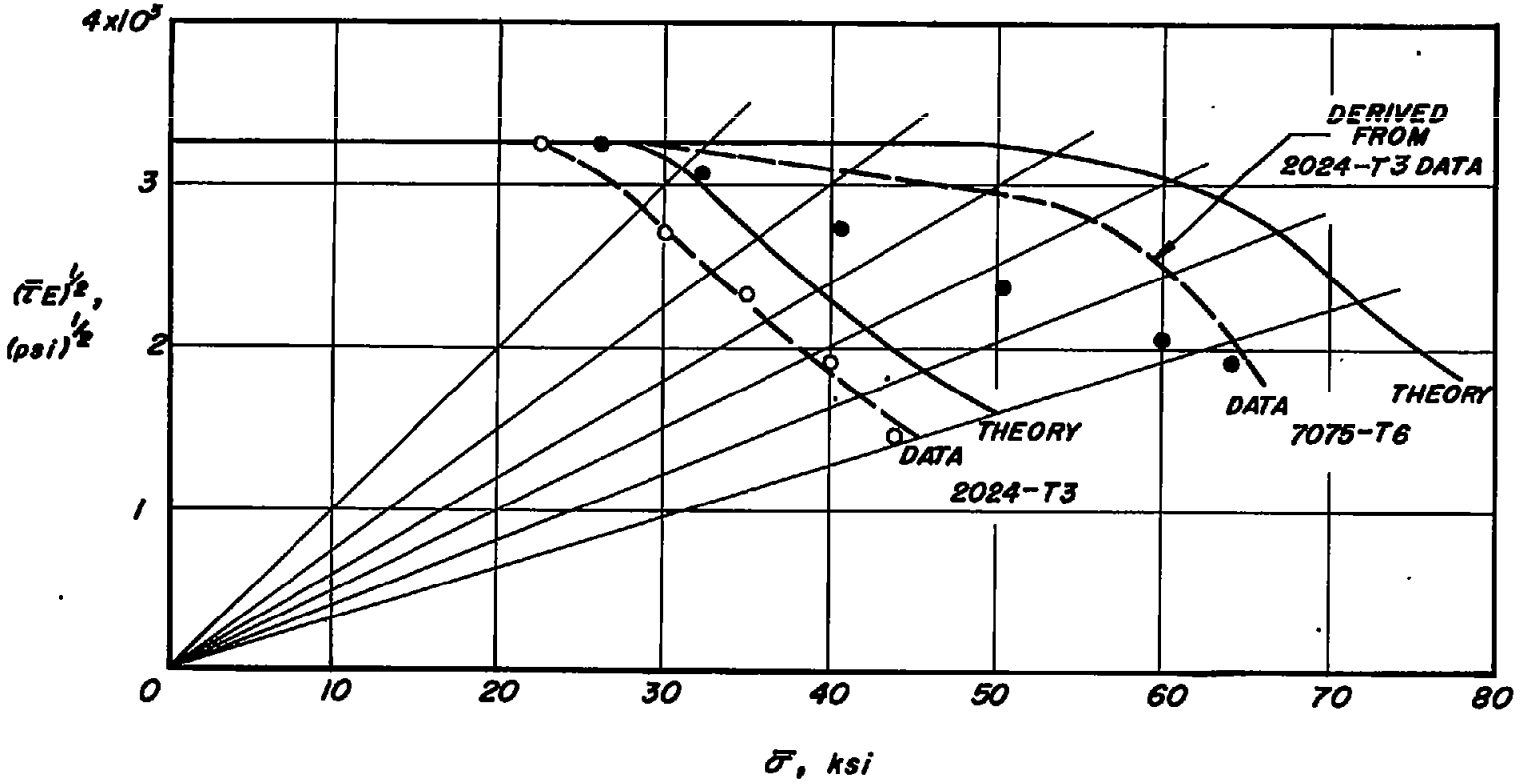


(a) Z-stiffened panels.

Figure 23.- Use of buckling similitude to derive optimum-panel data for stiffened panels.

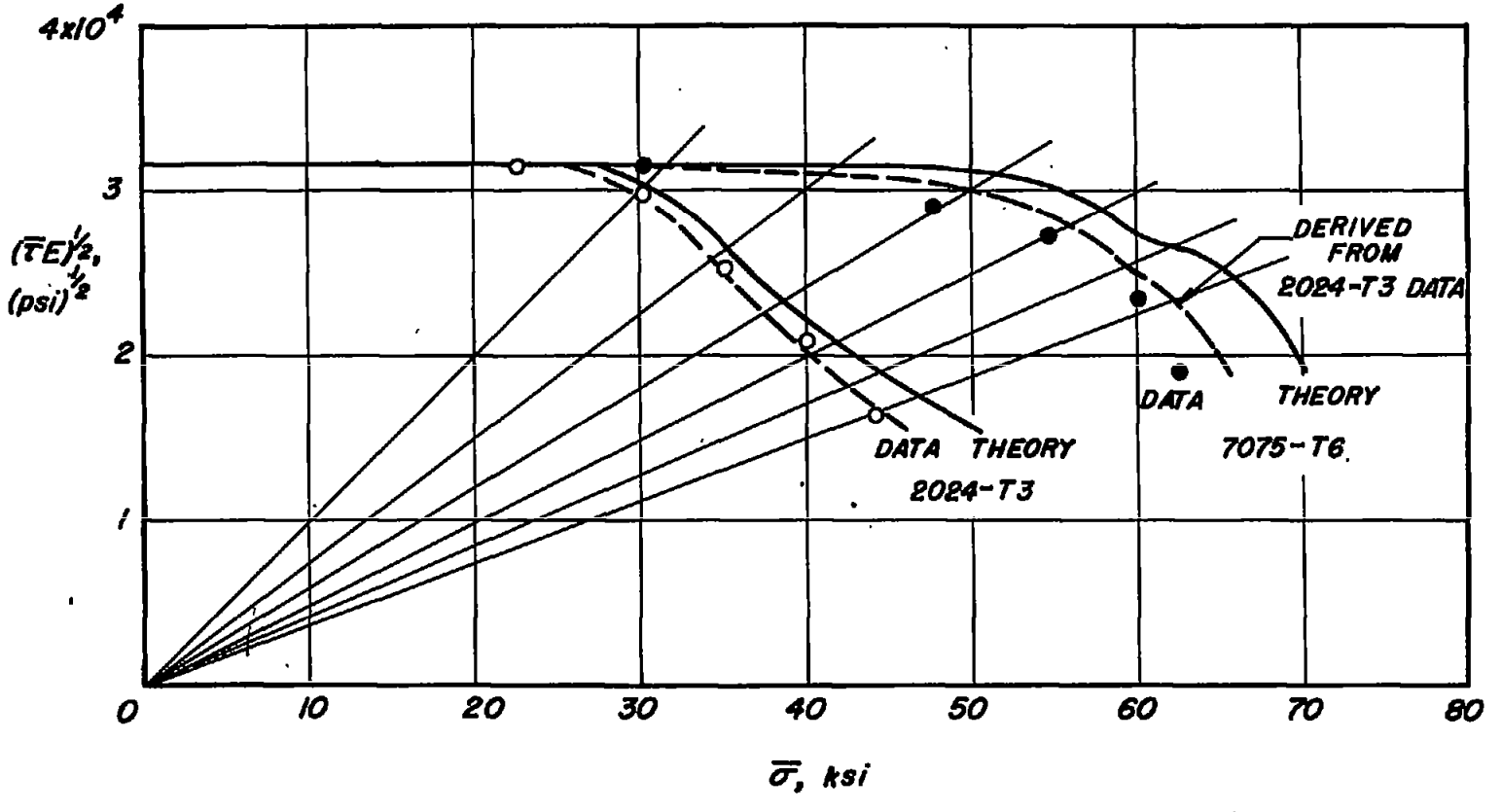


(b) Y-stiffened panels.

Figure 23.- Concluded.

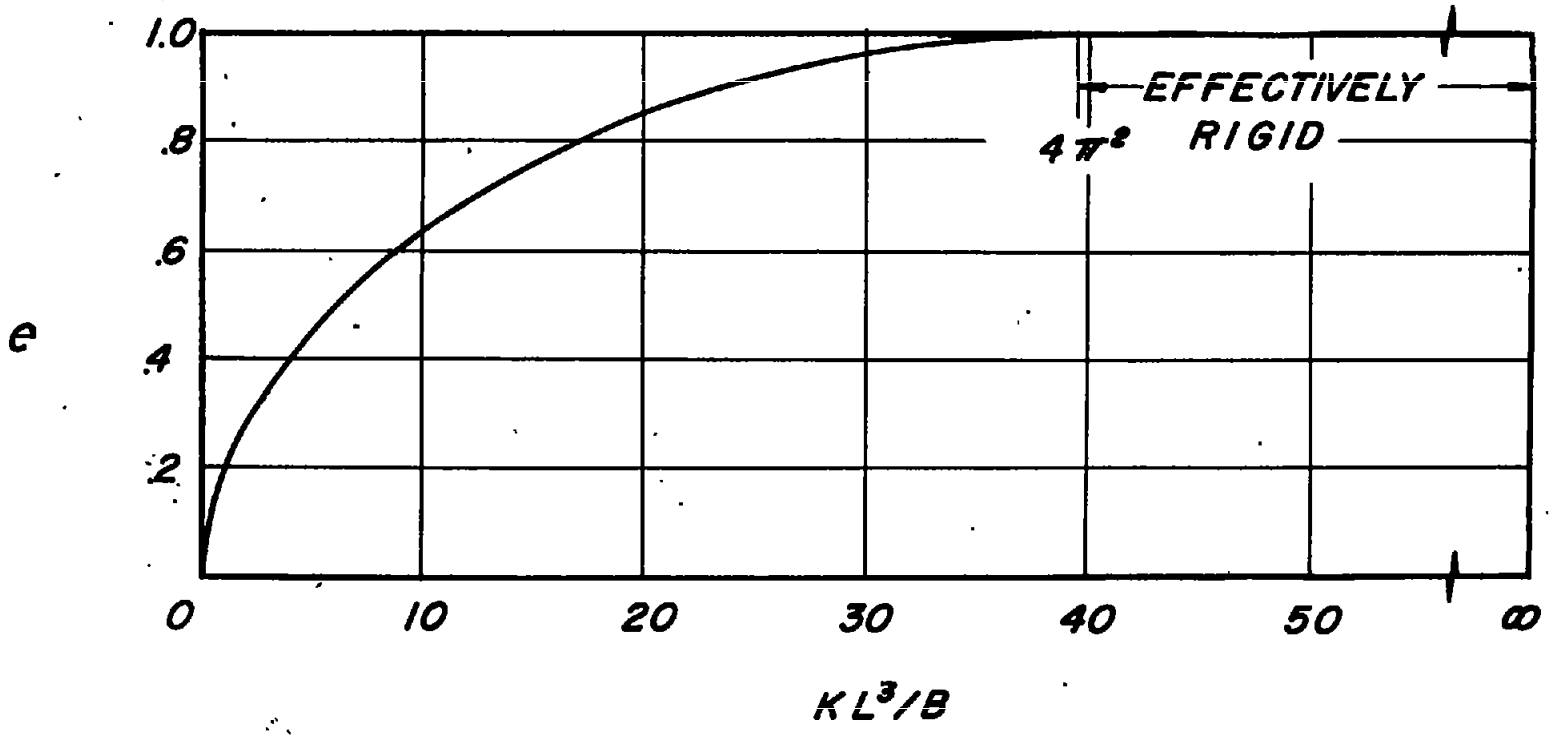


(a) e as a function of $KL^3/B$. Supports of zero rotational restraint.

Figure 24.- End fixity of continuous panels over many deflectional supports. $L/w < 0.2$.

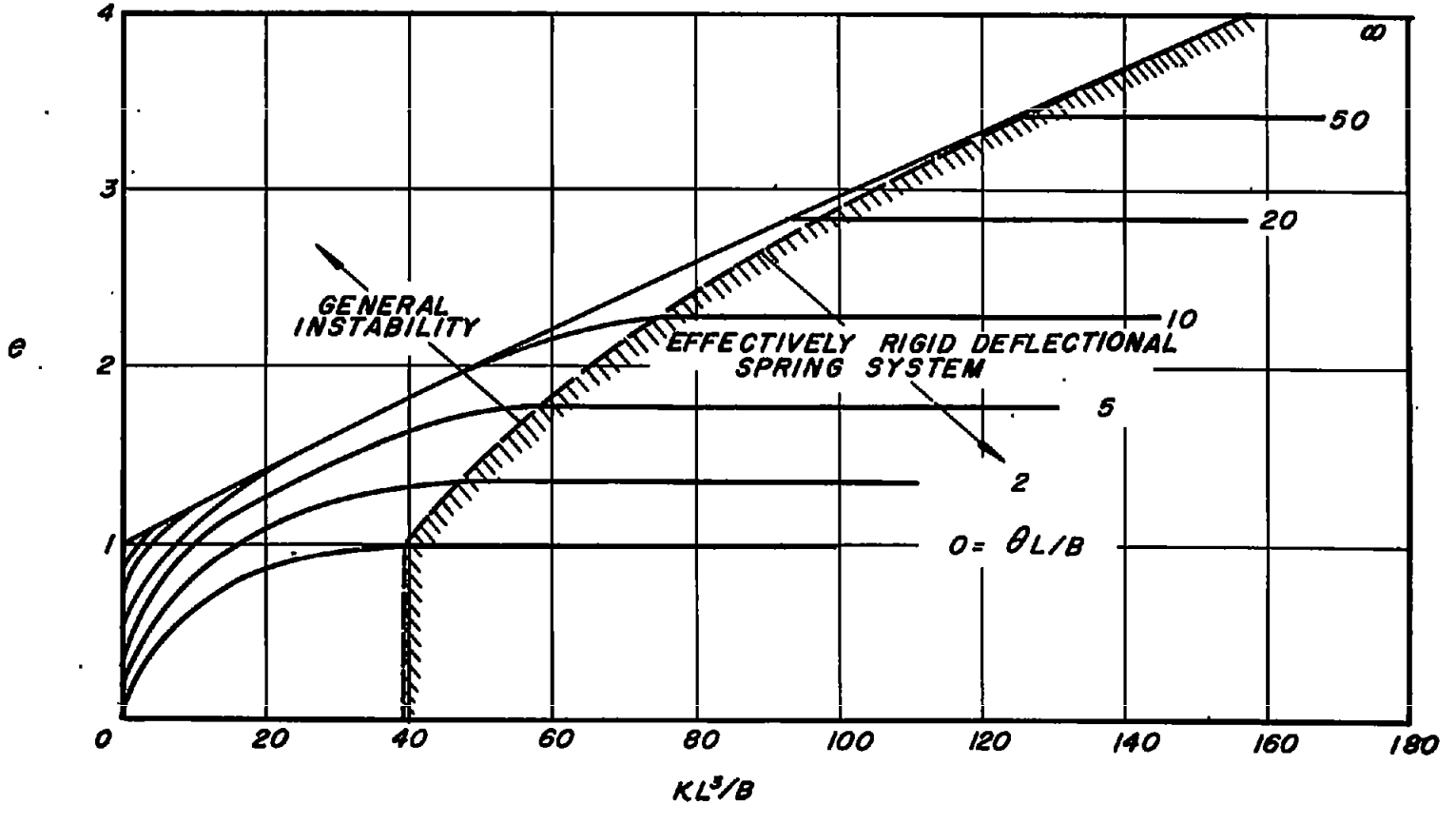


(b) e as a function of $KL^3/B$ and $\theta L/B$.

Figure 24.- Concluded.

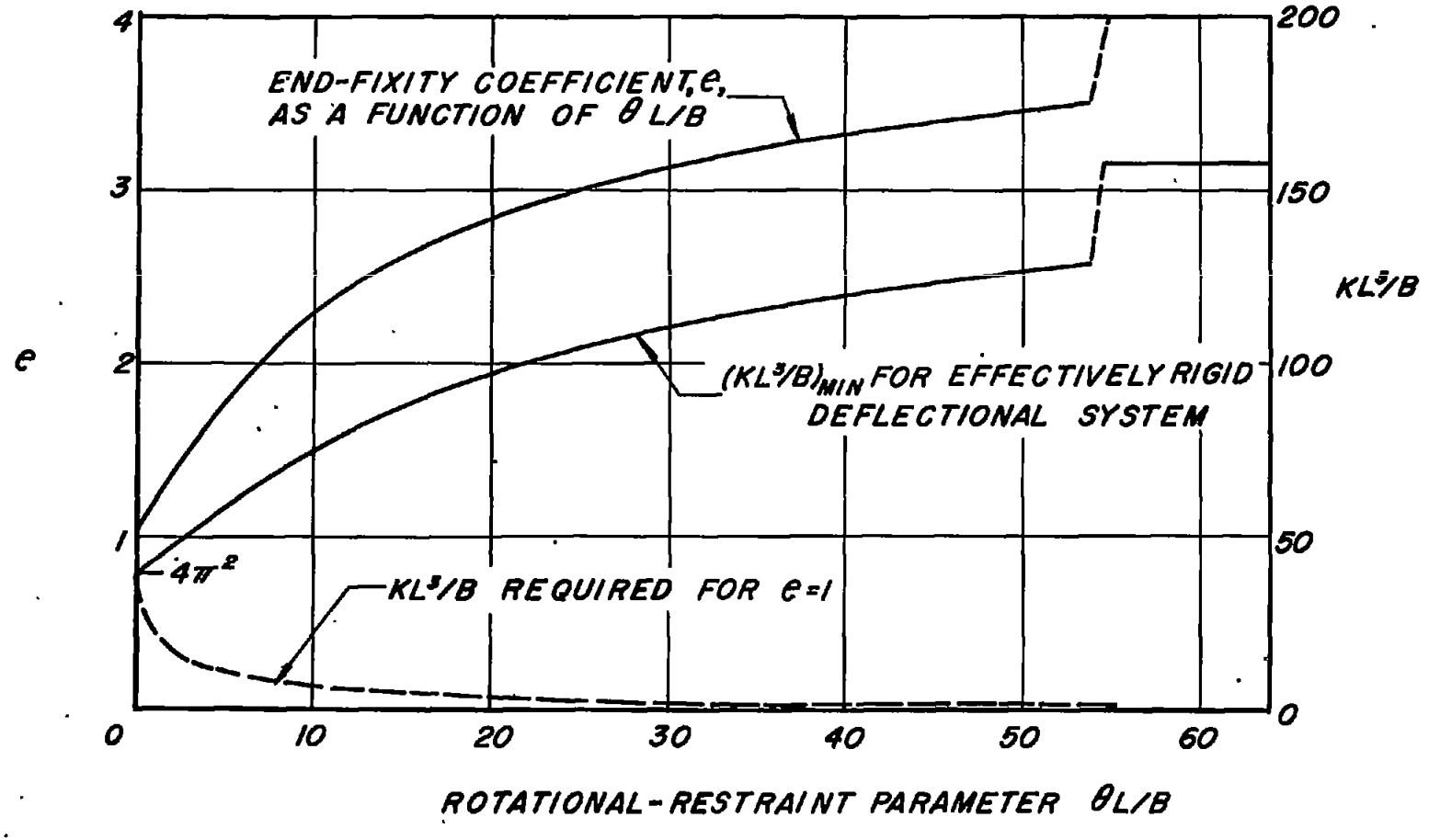


Figure 25.- Minimum deflectional stiffness for effectively rigid deflectional system. Continuous panel over many supports; L/w < 0.2.